

ABSTRACT

SAURABH CHHAPARWAL. Fiber Surface Modification by Particle Coating.

(Under the guidance of Dr. Tushar K. Ghosh, Dr. Behnam Pourdeyhimi, Dr. Richard Kotek)

Functionalities like anti-static, anti-bacterial, anti-odor, soil-resistance, biocompatibility etc. are function of fiber surface properties independent of characteristics of the fiber bulk. Development of processes for imparting these functionalities to the textile substrates is of prime importance.

Current research is one such effort to develop a 'single step' process to dry-coat meltblown webs with functional nano particles. Driven by the ecological and economic advantages, electrostatic spraying technique was integrated with meltblow process to impart ultraviolet shielding properties by coating titanium dioxide to the meltblown web. Various process parameters like carrying air pressure, electrostatic charging voltage, spraying distance etc. were studied to maximize the amount of particle coating for least amount of particle loss in the environment. It was found that particle loading percentage increased linearly with carrying air pressures. Final weight loading of 90-94wt% was achieved for 0.8 bars of carrying air pressures. Electrostatic charging voltage played critical role in capturing the charged particles that were not deposited on to the meltblown web. Point of spray of particles in the web was of critical importance to ensure good bonding of particles.

Motivated by the objective to control the heavy loss of particles while spraying, particle filled polymer was also spun in various bicomponent configuration. Bicomponent sheath-core, side-by-side and biconstituent web with particle filled polymer as one of the component were meltblown. Highest particle loading of 0.7wt% was achieved for the biconstituent webs.

All the samples made were characterized for ultraviolet transmission testing, mechanical properties like tensile stress and strain % at failure and bending length. Thermo gravimetric analysis and differential scanning calorimetry was also done for the bicomponent samples to study the effect of particle loading on thermal decomposition temperature and crystallinity. Samples made by electrostatic spraying showed the excellent ultraviolet protection factor while the samples made by bicomponent spinning had improved thermal stability along with ultraviolet rays blocking characteristics.

FIBER SURFACE MODIFICATION BY PARTICLE COATING

By

SAURABH CHHAPARWAL

A thesis submitted to the Graduate Faculty of

North Carolina State University

In partial fulfillment of the

Requirements for the degree of 'Master of Science'

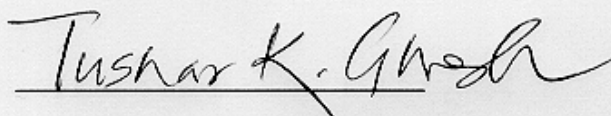
In

TEXTILE TECHNOLOGY AND MANAGEMENT

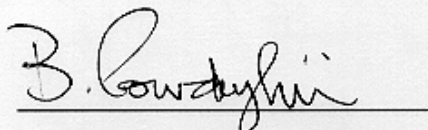
Raleigh, NC

DECEMBER 2005

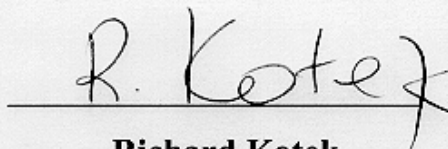
Approved by:



Tushar K. Ghosh
Chair of Advisory Committee



Behnam Pourdeyhimi
Co-Chair of Advisory Committee



Richard Kotek
Member of Advisory Committee

DEDICATION

I dedicate this thesis to my family, grandfather Late. Murlidhar Chhaparwal, grandmother Yashoda Chhaparwal, parents Mrs. Gayatri Chhaparwal and Mr. Suraj Karan Chhaparwal, and brother Gaurav Chhaparwal. It's the smile of their face that has driven me to where I am today.

BIOGRAPHY

Saurabh Chhapparwal was born on 3rd July 1980 in a small town, Kekri, in Rajasthan, India. He has been living in Kota, Rajasthan (India) since 1981 where he completed his high school from MODERN SCHOOL, Kota in the year 1998. He pursued his undergraduate degree from one of India's most prestigious institutes of engineering, Indian Institute of Technology (IIT), Delhi. He completed his Bachelor of Technology degree in Textile Technology from IIT in May 2002. After the graduation he worked as a Quality Assurance Engineer at Auro Weaving Mills, Baddi (a weaving subsidiary of Vardhman Spinning and General Mills, Ludhiana) for almost a year before he joined the masters program in Textile Technology in Fall of 2003 at Philadelphia University. He got transferred to master's program in Textile Apparel, Technology and Management Department at North Carolina State University. He graduated in December with Master of Science Degree in December 2005 with additional diploma in Nonwoven Science and Technology.

ACKNOWLEDGEMENT

I would like to thank Chair of my advisory committee, Dr. Tushar K. Ghosh for his guidance, support and encouragement during my masters. My learning experiences with him would be the guiding principles for the rest of my life. I would like to express my sincere appreciation to Co-chair of my advisory committee, Dr. Behnam Pourdeyhimi for his support and mentorship. I would also like to thank Dr. Richard Kotek for technical assistance as a member of my advisory committee. I wish to extend my sincere appreciation to Dr. John Hagewood for his time and efforts to guide me to face the technical challenges during the research.

I also wish to thank lab managers of various labs, Stephen Sharp, Birgit Anderson, Rob Byron, Timothy Mumford, Ted Dodson, Jan Pegram, Judy Elson and Terezie Zaplotova for their time and efforts in helping me in fabrication and characterization of the samples.

I wish to thank all my colleagues, especially Sohil Arora, Ravi Shankar Agarwal and Jeessang Hwang for their motivation and help at various times.

I also wish to thank Rob Cooper, Tywana Johnson and all the staff members of College of Textiles for their cooperation during my stay.

TABLE OF CONTENTS

List of Abbreviations.....	vii
List of Symbols.....	ix
List of Tables.....	xi
List of Figures.....	xiii
1 INTRODUCTION.....	1
2 BACKGROUND.....	3
2.1 Dry Particle Coating of Nonwoven Webs.....	3
2.2 Electrostatic Powder Deposition	8
2.3 Meltblowing Process	10
2.4 Particle Filled Fibers.....	12
3 OBJECTIVE.....	25
4 EXPERIMENTAL DESIGN.....	26
4.1 Materials.....	26
4.2 Particle Spray Setup	27
4.3 Bicomponent Web Formation	33
4.4. Web Characterization	33
4.4.1 Percent Particle Loading	33
4.4.2 Ultraviolet Transmission Testing.....	34
4.4.3 Thermal Characterization.....	35
4.4.4 Mechanical Properties.....	35
4.4.5 Surface Characterization.....	36

5	RESULTS AND DISCUSSIONS	40
5.1	Electrostatic Spray Coated Web	40
5.1.1	Effect of carrying air pressure and spray height on loading Percent	40
5.1.2	Particle distribution in web	42
5.1.3	Web Characterization – Spray Coated web	44
5.1.3.1	Percent Particle Loading	44
5.1.3.2	UV- Transmission Testing	46
5.2	Bicomponent Web Structures	48
5.2.1	Characterization of Masterbatch	50
5.2.2	Bi-component and Biconstituent structures	54
6	CONCLUSIONS	73
7	REFERENCES	70
	APPENDIX A : Processing conditions of various samples	76
	APPENDIX B : Summary Tables for Characterization	79
	APPENDIX C : List of figures of setups used for samples fabrication	84

LIST OF ABBREVIATIONS

Al₂O₃: Aluminum Oxide

CaCO₃: Calcium Carbonate

cps: count per seconds

DCD: Die-to-Collector-Distance

DSC: Differential Scanning Calorimetry

EDX: Energy Dispersive X-ray

Fe₂O₃: Iron Oxide

HDPE: High Density Polyethylene

H₂O₂: hydrogen peroxide

LDPE: Low Density Polyethylene

MFR: melt-flow-rate

mm: millimeter

NCRC: Nonwovens Cooperative Research Center's

PA: Poly(acryl amide)

PBT: poly(butylene terephthalate)

PE: Polyethylene

PET: Polyester or Polyethylene terephthalate

PP: Polypropylene

PVC: Poly(vinyl chloride)

SEM: Scanning Electron Microscope

SiO₂: Silicon Dioxide

TGA: Thermogravimetric analysis

TiO₂: Titanium Dioxide

UPF: Ultraviolet Protection Factor

UV: Ultraviolet Violet

WAXS: Wide angle X-ray diffraction

ZnO: Zinc Oxide

LIST OF SYMBOLS

Ag : Silver

Cu : Copper

d: spray distance (inch)

Fe : Iron

h: Height of spray (cm)

Ni : Nickel

Pd : Palladium

Pt : Platinum

T_g : Glass Transition Temperature ($^{\circ}\text{C}$)

ϕ : Diameter of spray attachment (inch)

α : Spray angle or Angle of spray ($^{\circ}$)

μm : micron or micrometer

H_f : Heat of crystallization (J/gms)

η : Viscosity of polymer melt (Pa.s)

ϕ : Volume loading percent

γ : Shear rate

$A_{4\text{mm}}$: Area of opening in attachment #1 with 4mm diameter.

$V_{4\text{mm}}$: Velocity of air and particle mixture to be sprayed by attachment #1.

$A_{25.4\text{mm}}$: Area of opening in attachment #2 with 25.4mm diameter.

$V_{25.4\text{mm}}$: Velocity of air and particle mixture to be sprayed by attachment #2.

AD_{LW} : areal density of the particle loaded web

AD_{BW} : areal density of the base web

λ : wavelength of light.

T_{λ} : spectral transmittance at wavelength (λ).

E_{λ} : relative erythema spectral effectiveness (CIE 1987).

S_{λ} : solar spectral irradiance.

$\Delta\lambda$: wavelength step (1 nm)

UV-A: Ultraviolet radiations from 315-400 nm.

UV-B : Ultraviolet radiations from 280-315 nm.

$T_{(UV-A)av}$: Average A-range ultraviolet transmittance.

$T_{(UV-B)av}$: Average B-range ultraviolet transmittance.

θ_s : static contact angle.

LIST OF TABLES

Table 1.1 List of various nanoparticulates useful in textile applications	02
Table 2.1 Description of polymers and titanium dioxides studied [26]	16
Table 2.2 Classification of melt-spun fibers [31]	19
Table 4.1 Technical specification of polypropylene CP-15000-P [43]	26
Table 4.2: Specification for Desktop Meltblow setup.	27
Table 5.1 Summary of measure particle loading (%) by weight for external coated samples	44
Table 5.2 List of images obtained by optical microscopy in refractive index solution	45
Table 5.3 UPF, %Blocking UV-A and %Blocking UV-B for samples made by modified setup.....	46
Table 5.4 UPF, %Blocking UV-A and %Blocking UV-B for samples made by final setup.....	46
Table 5.5 Summary of UV Transmission testing data for bicomponent samples.....	55
Table A1 Processing conditions of samples made by various setups, initial setup, modified setup and fi.....	76
Table A2 List of bi-component webs prepared in various trials	77
Table A3 List of bi-constituent webs prepared in various trials	78
Table B1.1 Summary of viscosity vs. shear rate at 200 ⁰ C for TiO ₂ loaded polypropylene system.	79
Table B1.2 Viscosity of homo-polypropylene and compounded masterbatch at 20wt% loading	79
Table B2 Summary of thermal decomposition temperature of bicomponent samples, B1 – B15	80
Table B3 Summary of thermal decomposition temperatures of biconstituent samples BC3 – BC5	80

Table B4 Summary of results H_f , onset values for bicomponent samples, B1 – B15.**81**

Table B5 Summary of results H_f , onset and peak temperature for biconstituent samples, BC1 – BC5.**81**

Table B6 Summary of strip test (ASTM D5035-95) for bicomponent samples B1-B14.....**82**

Table B7 Summary of strip test (ASTM D5035-95) for biconstituent samples BC1-BC5...**82**

Table B8 Summary of bending test (ASTMD5732) for biconstituent samples B1-B14**83**

Table B9 Summary of bending test (ASTMD5732) for biconstituent samples BC1-BC5...**83**

Table B10 Summary of UV Transmission testing data for biconstituent samples BC1-BC5 and BC1-2L – BC5-2L.**83**

LIST OF FIGURES

Figure 2.1 Schematic diagram of apparatus used in making web by 3M [3].	04
Figure 2.2 Enlarged cross-sectional view of a portion of a sheet product [3].	04
Figure 2.3 Schematics of Coform set up [4].	05
Figure 2.4 Schematic diagram of particle coating as post treatment – electrostatic method [6].	06
Figure 2.5 Schematic diagram of particle coating as post treatment – hot air stream [9].	07
Figure 2.6 Mechanism of dry-mechanical particle coating process [68].	07
Figure 2.7 Schematic diagram of fluidization hopper [10].	09
Figure 2.8 Schematic diagram of (a) corona charging powder gun; (b) tribo charging powder gun [10].	10
Figure 2.9 Schematic diagram of melt-blowing manufacturing equipment [12].	10
Figure 2.10 (a) Side by Side (b) Sheath/Core (c) Sheath/Core Eccentric (d) Segmented Pie (e) Island in the Sea (f) Tipped Trilobal [14].	11
Figure 2.11 Displacement of interface due to viscosity difference a) for Side-by-Side cross section; b) Sheath-Core cross-section [15].	12
Figure 2.12 Variation of melt viscosity as a function of shear stress at 473K for PP/Ag fiber composite at varying Ag content (vol%) (O) 0;(□)0.43;(◊) 1.3; (˜)2.4; (P)4.1; (*)5.6; [28].	14
Figure 2.13 Variation of melt viscosity composition of PP/Ag fiber composites at 473K at constant shear rates (s ⁻¹): (a) 2*10 ³ ; (b) 3*10 ³ ;(c) 5*10 ³ [28].	14
Figure 2.14 Effect of spherical and rod-shaped filler particles on the viscous flow of a polymer melts as a function of shear rate (concentration of spheres is higher than that of rods) [30].	15
Figure 2.15 Effect of filler particle shape on the viscosity of polypropylene (PP) at 200 ⁰ C: (Δ) neat PP; (□) PP containing 40% by weight glass bead; (O) PP containing 40% by weight talc) [30].	16
Figure 2.16 Viscosity behavior at various shear rates with various levels of TiO ₂ -A at 180 ⁰ C of (a) LDPE-23 [(b) LDPE-5 [26].	17

Figure 2.17 Relative viscosity $\eta(\phi)/\eta(\theta)$ as a function of volumetric loading ϕ [26].	18
Figure 2.18 Interface shape for capillary dies as a function of viscosity ratio (a) $\eta_{\text{filled}} > \eta_{\text{unfilled}}$ (b) $\eta_{\text{filled}} < \eta_{\text{unfilled}}$ [26].	18
Figure 2.19 SEM micrographs of (a) core part, (b) sheath part at the cross-section of PP 3 (c) boundary of the sheath–core at the cross-section of PP 6 [31].	19
Figure 2.20 Differential scanning calorimetry of spun fibers of varying silver concentration; (a) fibers containing silver in core part (b) fibers containing silver in sheath part [31].	20
Figure 2.21 Polarized light microscope micrographs for (a) pure PP and (b) PP toughened with 5wt% DB-70 ENP crystallized at 118 ⁰ C for 5 h [33].	21
Figure 2.22 Filament diameter of the extrudate at 200 ⁰ C for 7nm and 21nm TiO ₂ particle size [34].	21
Figure 2.23 Filament diameter of the extrudate at 200 ⁰ C for 1%, 2% and 3% TiO ₂ loading by weight [34].	22
Figure 2.24 Apparent elongational viscosity of the melt at 200 ⁰ C for 7nm and 21nm TiO ₂ particle size [34].	22
Figure 2.25 Apparent elongational viscosity of the melt at 200 ⁰ C for 1%, 2% and 3% TiO ₂ loading by weight [34].	23
Figure 2.26 Differential scanning calorimetry analysis of the extrudate for 1%, 2% and 3% TiO ₂ loading by weight [34].	23
Figure 2.27 Thermo gravimetric analysis of the extrudate for 1%, 2% and 3% TiO ₂ loading by weight [34].	24
Figure 4.1 Specification and Scanning electron microscopy image of TiO ₂ particles.	27
Figure 4.2 Schematics of side view of the initial setup.	28
Figure 4.3 Schematics of the modified setup (a) side view; (b) front view.	30
Figure 4.4 Particle spraying attachment for modified setup.	31
Figure 4.5 (a) Spraying attachment for final setup; b) particle spray characterization.	31
Figure 4.6 Schematics of side view of the final setup.	32
Figure 4.7 (a) Image by optical microscope; (b) image converted to binary 16 bit	

unsigned format; (c) after applying 5*5 smooth filter; (d) after high pass threshold filtering; (e) after blob analysis (41 blobs with 72.81 % area in image).	38
Figure 4.8(a) SEM image of the same sample A at location 1; (b) SEM image of the same sample A at location 2; (c) Ti detection by X-ray analysis at location 1 (area = 8.58 %); (d) Ti detection by X-ray analysis location 2 (area = 14.51%); (e) Carbon detection by X-ray analysis at location 1(area = 33.56 %); (f) Carbon detection by X-ray analysis at location 2 (area = 21.78%)	39
Figure 5.1 Graph showing effect of carrying air pressure on particle loading %	41
Figure 5.2 SEM images of samples of various loading percent by weight (a) 2%; (b) 8%; (c) 40%; (d) 42%; (e) 90%.	42
Figure 5.3 (a) High particle loading by initial setup at 1200X; (b) high particle loading by initial setup at 7500X; (c) high particle loading by modified setup at 500X; (d) high particle loading by modified setup; (e) high particle loading by final setup at 40X; (f) high particle loading by final setup at 1200X.	43
Figure 5.4 Ultraviolet transmittance for various wavelengths for Samples made by modified setup.....	47
Figure 5.5 Ultraviolet transmittance for various wavelengths for samples by final setup....	48
Figure 5.6 Schematic of various fiber cross-section configuration (a) sheath-core; (b) side-by-side; (c) bi-constituent.....	48
Figure 5.7 (a) Viscosity with shear rate at 200 ⁰ C for TiO ₂ filled polypropylene (PP-1200) melt at various loading percent (5%, 10%, 15% and 20%) by Haake Minimelter; (b) Viscosity vs. shear rate results of masterbatch for various temperatures (190 ⁰ C, 210 ⁰ C, 230 ⁰ C) and loading percent (0%, 20%).	49
Figure 5.8 DSC analysis curves for pure homo-polypropylene and compounded master-batch.	50
Figure 5.9 (a)-(c) Optical micrographs of masterbatch's smear.	51
Figure 5.10 (a)-(d) Scanning electron micrographs of masterbatch's smear (mean particle size = 4 μm).	52
Figure 5.11 (a) – (b) X-ray analysis (EDX) of the smear for carbon and titanium.	53
Figure 5.12 (a) – (b) Scanning electron micrographs of the smear at various magnifications highlighting the TiO ₂ agglomerates in the melt.	53

Figure 5.13 UV transmission graphs of bicomponent samples B1 – B16 for wavelength (a) 700 nm to 280 nm; (b) 400 nm to 280nm.	56
Figure 5.14 UV-transmission graphs for biconstituent samples BC1 – BC5.	56
Figure 5.15 Thermo gravimetric analysis graphs of bicomponent sheath-core fiber structures, B1-B2.	57
Figure 5.16 Thermo gravimetric analysis graphs of bicomponent side-by-size fiber structures, B3 - B8.	58
Figure 5.17 Thermo gravimetric analysis graphs of bi-constituent fiber structures, BC3 – BC5.	58
Figure 5.18 DSC thermographs of bicomponent samples (a) B1-B2; (b) B3 – B15.	60
Figure 5.19 DSC thermograms of biconstituent samples, BC1 (0.0wt%) – BC5 (0.75wt%).	60
Figure 5.20 Graphs summarizing tensile strip test of bicomponent and biconstituent samples.	62
Figure 5.21 Graph summarizing bending length test of bicomponent samples B1 – B14. ...	62
Figure 5.22 Optical micrographs in refractive index solution some of the bicomponent samples at 10X.	63
Figure 5.23 Optical micrographs in refractive index solution by stereoscope microscope at 10X (a) B3; (b) B5; (c) B8.	64
Figure 5.24 SEM micrographs of (a)–(b) Sample B6; (c)–(d) Sample B8 at various magnifications made by side-by-side die-plate configuration.	65
Figure 5.25 (a)-(b) SEM micrographs of bicomponent side-by-side sample, B16 showing drips.	65
Figure 5.26 Optical micrographs at 10X in refractive index solution a) BC3; b) BC4; c) BC5.	66
Figure 5.27 SEM micrographs of biconstituent samples (a) BC3 (0.2%); (b) BC4 (0.4%); (c) BC5 (0.7%); (d) BC6 (1.0%).	67
Figure C1 3” laboratory scale meltblown setup.	84
Figure C2 Schematics of bicomponent meltblown setup at NCRC Partner’s Lab.	84

Figure C3 Cross laid web (IX) made by perpendicularly orienting particle loaded meltblown webs by thermal point bonding.85

Figure C4 Electrostatic spray gun.85

1 INTRODUCTION

Polymeric fibers are generally used to create a textile structure (e.g., yarns, fabrics, etc.) or used as such in reinforcement of composites. Fibers are somewhat unique in that they offer very high specific surface and are often used in applications where the high surface area is of value. The motivation for fiber surface modification is to introduce one or more specific properties required for specific applications. The desired properties may range from improved adhesion to response to stimuli in environment.

The suitability of fibers for a given end-use application depends on several factors including mechanical behavior, chemical resistance, dimensions, and surface characteristics. Fiber surface modification has been one of the main areas of research in the development of functional fibers. In addition to research in developing/synthesizing new fiber forming polymers with specialized properties, surface modification offers many new opportunities. Properties of fibers such as anti-microbial, anti-odor, anti-fungal, anti-static, wicking, soil resistance, adhesion, and biocompatibility, etc. are all function of fiber surface properties.

Various techniques available for surface modification includes hot and cold plasma irradiation [66], enzyme treatment [73], chemical finish [74], metal vapor deposition [71-72] and coating of various polymers and additives by wet and dry methods. Among various surface modification techniques, dry powder coating techniques are attractive to study for ecological and economic reasons. Being solvent free, the high cost of drying along with air and water pollution is virtually eliminated in a dry process.

In dry processing efforts are being done for reduction in overall solid content without compromising the uniformity of coating. Development in nanotechnology and hence, nano-particulate materials is a major break thorough in this regard. A unique value of nano-particulates is their extremely high surface area [65]. Thus, their application induce many more active sites for imparting desired property making nano-particulates, ideal to be used as dispersions and coatings for a wide variety of applications. Some of the nano-coatings are self-healing ensuring longer coating life. But most of the methods of nano coating are either wet methods or are high temperature methods like flame hydrolysis, sol spraying, metal vapor deposition etc thus, useful mainly for metals or ceramics as a substrate [56-58].

In the recent past large number of nanoparticulates have been developed and efforts have been done to incorporate these nanoparticulates as fillers or as surface modifiers in polymer

to impart various unique and important mechanical [59], thermal [60], physical and chemical barrier [61-62], optical, electrical and magnetic properties [63-64]. Some of the nanoparticles used for textile applications are summarized in **Table 1.1**.

Table 1.1 List of various nanoparticles useful in textile applications

Metals	Compounds	
	Organic	Inorganic
Pd/Pt	Vitamins	TiO ₂
Ag	DNA	ZnO
Fe	Hydroxylapatite	Fe ₂ O ₃
Ni	Color Pigments	Al ₂ O ₃ ,
Cu		SiO ₂ , CaCO ₃

The current research is one such effort to develop a process for modification of fiber surface in nonwoven webs, preferably meltblown webs, by coating or incorporating titanium dioxide (TiO₂) micro and nano particles on or in the polymeric matrices. Titanium dioxide (TiO₂), in micro and nano form, has many interesting applications like ultraviolet shielding, disinfectant, super hydrophobic surfaces [1], super hydrophilic surfaces [2], self cleaning surfaces by 'lotus effect' [1], high dielectric constant surfaces and many more.

2 BACKGROUND

Surface of fibers in fabrics or various other textiles like surfaces, for example, paper and polymeric films can be modified by various wet and dry methods. The scope of the present research is to study the methods for dry coating of nonwoven webs by particles. Many such methods have been reported in the published literature. In order to obtain good functional characteristics through particle coating, most of the methods are directed toward covering most of the available fiber surface uniformly and thereby create large number of active sites. In a fiberweb the desired functionality by particle coating can be enhanced by introducing finer fibers and hence, higher available fiber surface area for activation. In that vein, meltblowing process is ideal because it produces some of the finest fibers (1- 10 μm). Various methods of dry particle coating are discussed in **section 2.1**. Electrostatic deposition of particles is discussed in **section 2.2**. The meltblowing process is discussed in **section 2.3**. One shortcoming of the dry coating process is potential particle escape in the environment. To eliminate this problem, incorporating particles in polymer melt before extrusion has also been looked at and presented in **section 2.4**.

2.1 Dry Particle Coating of Nonwoven Webs

One of the early methods of incorporating particles in a nonwoven web was revealed in 1976 by Minnesota Mining and Manufacturing Company (3M) [3]. The patent described addition of activated carbon particles into meltblown webs to make respirators. Details of the process are discussed in later sections. Since then several companies have proposed other ways for incorporating particles to make products ranging from respirators, filters to diapers and sanitary napkins. In what follows, some of these methods are described in details:

Insitu Dry Particle Coating

Insitu coating of the webs with the particles implies attachment of particles to the web while the web is being made. In fact, the particles are sprayed or attached by various means on the fibers before they become part of the web.

One of the early reported methods to incorporate particles in nonwoven web especially meltblown web consists of mixing of particulate in the hot air stream used to draw extruded fibers in the meltblowing process [3]. The particles incorporated were activated

carbon of 2 μm - 2mm in diameter. They were incorporated by mixing with an additional air stream projected on the merging air/fiber stream of a pair of meltblowing dies placed at an angle to each other, at the point where fibers in the web becomes non-tacky, see **Figure 2.1**. Thus, particles trapped between two layers of fibers formed from the two meltblown dies are collected on a screen. The particles though entrapped between the two layers of fibers, has only point contact with the fibers, **Figure 2.2**, thus the products made from this web had serious problem of “dusting” during use.

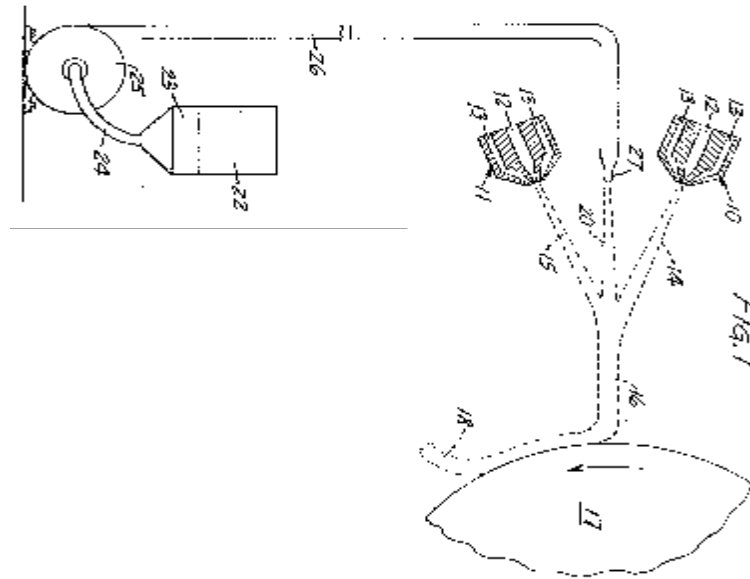


Figure 2.1 Schematic diagram of apparatus used in making web by 3M [3].

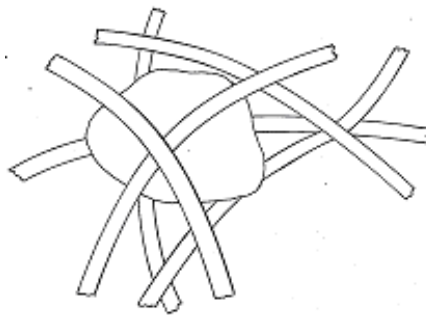


Figure 2.2 Enlarged cross-sectional view of a portion of a sheet product [3].

Coforming technique, a patented technology by Kimberly Clark [4] used for coating fiberwebs by pulp fibers and super absorbent particles is claimed to be capable of evenly distributing particles and holding them without “dusting”. In coforming process particles were incorporated in meltblown webs, made from polyolefins and elastomers, at the point where the web is still tacky, see **Figure 2.3**. This process was further improved by heating

the particles before being sprayed [5], thus further reducing the dusting, as the heated particles were better attached to the fiber surface.

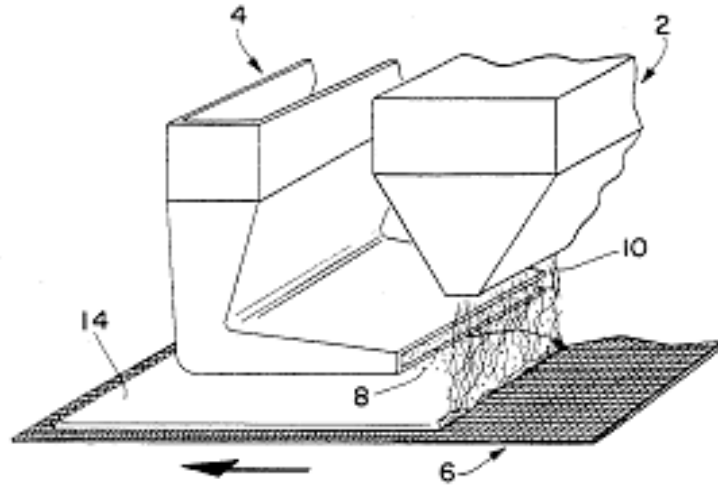


Figure 2.3: Schematics of Coform setup [4]

Particle Coating as Post Treatment

Particle coating as a post treatment obviously requires an additional processing step. There are a number of methods that could fall under this classification, however, for the purpose of this review only dry coating methods are studied.

Cohen et. al. [6] developed a method to coat nonwoven fiberwebs with particles by electrostatic charging of the web. In this method, the web is electrically charged uniformly and the charged web is passed through a fluidized bed of particulates so that at least some particulates adhere at the charged sites, see **Figure 2.4**. Particles may or may not be charged in the polarity opposite to that of web before being applied. Thus, particles either adhere to points of opposite charge on the web or induced charge of opposite polarity and then got adhered to the web. Fiberweb made from thermoplastic fibers and filaments like polyolefins, polyamides and polyesters, could be charged by various ways like corona discharge method [7] and between the surface of a grounded metal electrode and a series of discharge electrodes [8]. These particle-loaded webs were than bonded thermally. The uniformity of the particle distribution on the web depends greatly on distribution of the charge on the web; hence, method to be used for charging of web is critical.

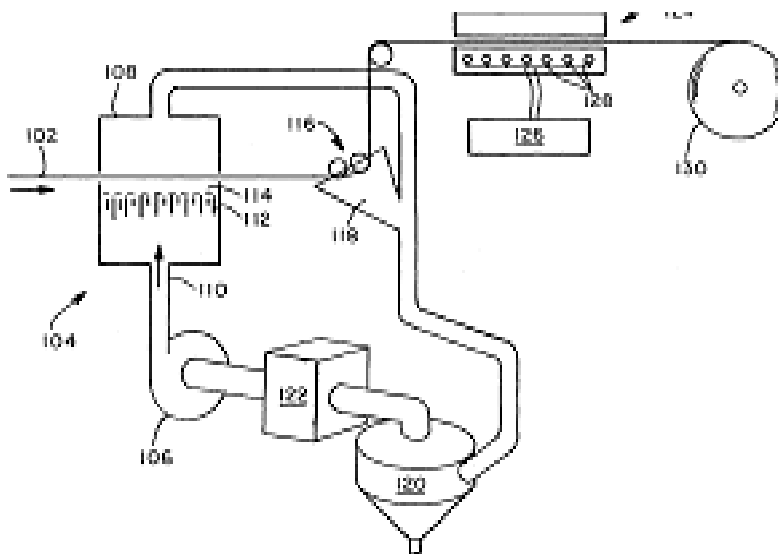


Figure 2.4 Schematic diagram of particle coating as post treatment – electrostatic method [6].

Tatsuo et. al disclosed [9] a number of new methods of coating bicomponent thermoplastic nonwoven fiberwebs solid particles like activated carbon, zeolite, titanium oxide, water absorption resins, ion exchange resins, metal particles, calcium carbonate etc.

The patent describes 3 methods of incorporating particles to the fiberweb. The first method disclosed by Tatsuo et. al., involves spraying of heated particles (temperature of particle at least 50⁰C above the melting point of the fiber) on the web with the help of preheated air stream. Due to high airflow volume and speed of the carrying air, particles impact the fiber surface with high kinetic energy resulting in maximum bonding to the fiber surface. However, the method has a disadvantage of web shrinkage due to high air stream temperature. The process is presented schematically in **Figure 2.5**. In the second method disclosed by Tatsuo et. al. [9] heated particles (particle temperature at least 50⁰C above the melting point of fiber surface) are dropped onto the fiberweb placed on heat resistant moving conveyor. The heated particles melt the fiber surface at the point of contact forming a good bond. The fiberweb could be subsequently calendared to enhance the bonding. To finish the process, the loose particles can be blown away by air stream or by shaking the conveyor-carrying particle loaded web. Tatsuo et. al [9] also disclosed a method in which the web is passed through a closed chamber containing heated particles. The chamber has particles suspended in air by the shaking action of the chamber, and as the web passes through the chamber the heated particles get deposited on the web, which is then quickly cooled.

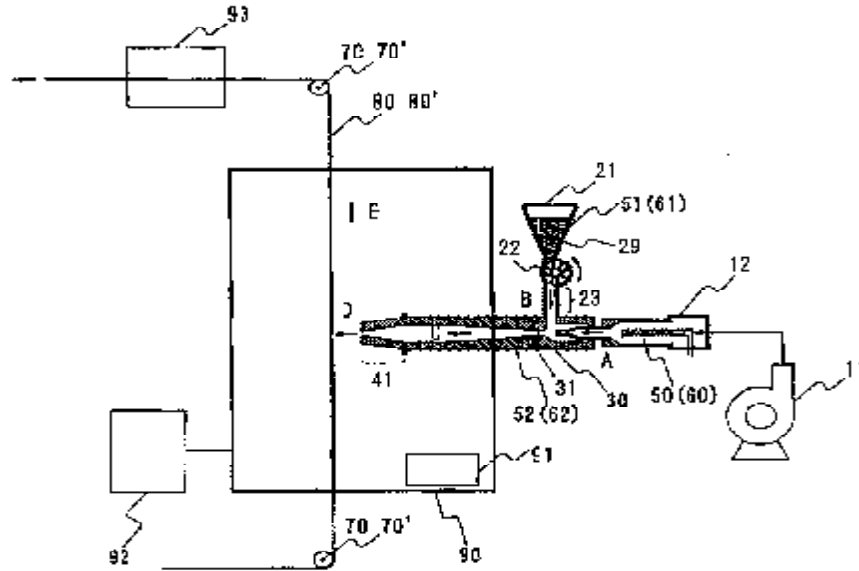


Figure 2.5 Schematic diagram of particle coating as post treatment – hot air stream [9].

Dry-Mechanical Coating

Dry-mechanical coating technique is generally used for coating soft metals with wax [67], ceramics [68] etc. In this method the additive and the substrate are fed to a closed vessel having elliptical rotor in the center. Vessel and rotor rotate in opposite direction forcing particles and substrates to pass through narrow gaps between rotor tip and vessel as shown **Figure 2.6**. The high shear and compression force results in coating of particles on the substrate. But this process is also limited by type of substrate, as most of the textile surfaces are very soft to handle the high shear and compressive forces. Nowarat and co-workers [69] have successfully used it for coating Al_2O_3 fibers with nano Al_2O_3 and CuO particles.

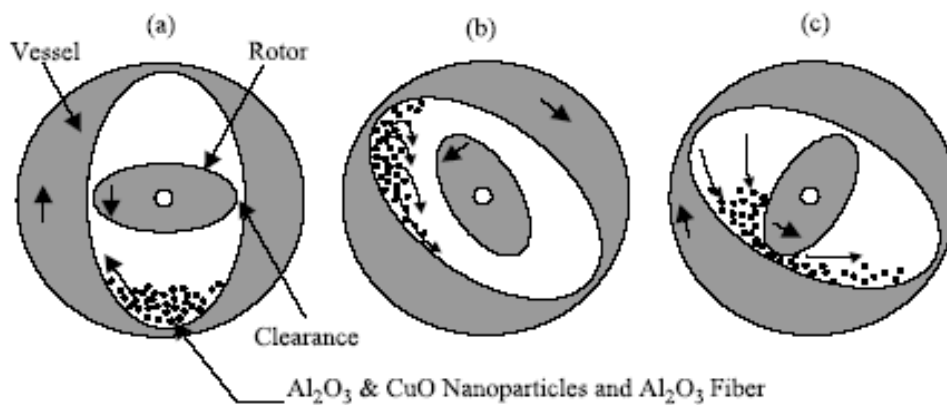


Figure 2.6: Mechanism of dry-mechanical particle coating process [68]

Metal Vapor Deposition

Metal vapor deposition is yet another method for coating mainly low emissivity metals or alloys on fibers, fiberwebs and films [70-72]. In this method, metallized coatings ranging between 5 nm to 5 micron are deposited on the substrate. The process can impart excellent properties without any change in bending rigidity but is limited only to metallic coatings and relatively thin webs.

To summarize the dry coating methods reported in literature suggest that particle coating of fibers during fiber formation while the fibers are still tacky results in improved adhesion and less dusting off. Also meltblowing fiber forming process seems to be more appropriate for fiber surface modification because of the relatively larger specific surface area of meltblown fibers. Electrostatic powder deposition technique with heated particles is a convenient way to spray particles and enhances potential for bonding. These processes are discussed in more details in **section 2.2** and **section 2.3**.

2.2 Electrostatic Powder Deposition

Electrostatic powder deposition is a process of spraying mixture of charged powder particles and air towards a grounded target surface so that the charged particles are deposited on the grounded target due to electrostatic force of attraction. The process has various steps beginning with fluidization followed by charging of powder particles. The charged particles are then transferred to the spraying guns to be sprayed on target.

Process Description

Fluidization is the process of mixing powder or suspending powder particles in compressed air. The purpose of fluidization is twofold; firstly, it allows the particles to be easily transported from the fluidizing hopper to the spray gun with a high degree of uniformity and consistency. Secondly, fluidization also serves to precondition the powder, breaking up agglomerations by removing adsorbed moisture and thereby, improving handling and flow-ability of the material.

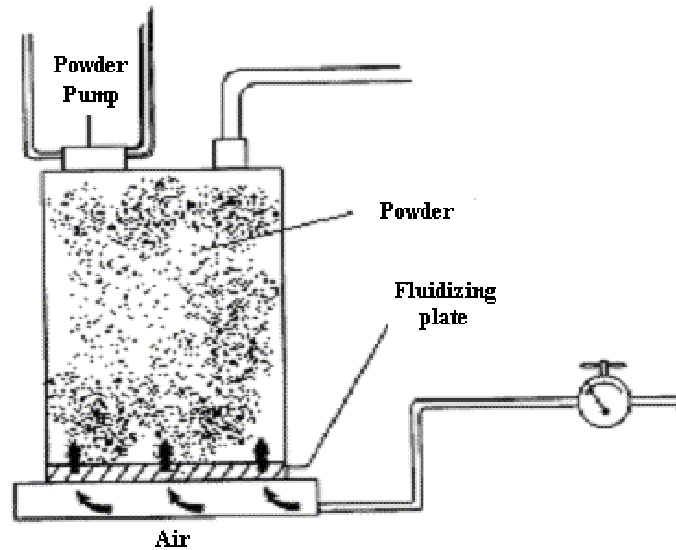
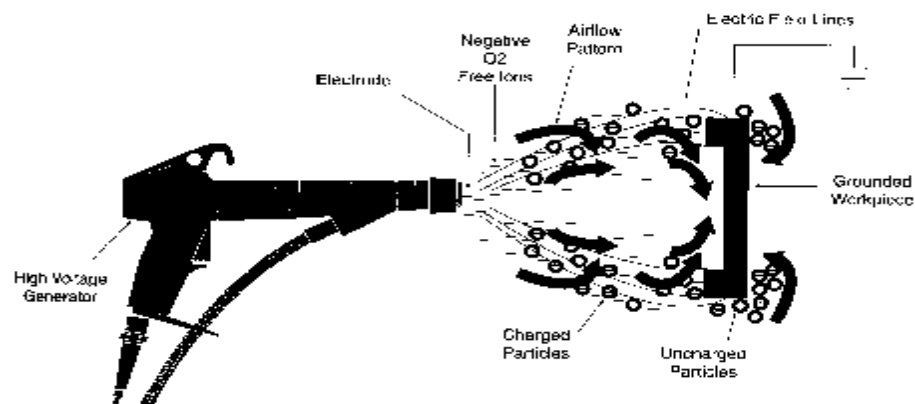
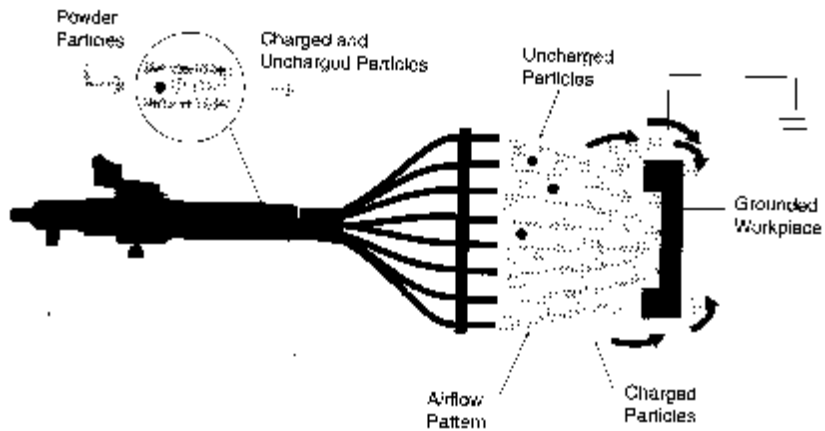


Figure 2.7 Schematic diagram of fluidization hopper [10].

In the process of fluidization, air is introduced into the powder through porous floor of fluidization hopper as shown in **Figure 2.7**. As the air moves upward through powder, individual particles are suspended in air. The particle containing air stream could then be pumped like a liquid. Uniformity of electrostatic spray is dependent on charging of the individual powder particles. Two primary methods of charging are corona charging and tribo charging. In the corona charging, electrons are transferred to or from powder particle by air ions, see **Figure 2.8(a)**. Tribo charging is generated by friction of one material on another. In tribo charging gun as shown in **Figure 2.8(b)**, the powder particles get charged due to rubbing on specifically formulated and shaped surface. These charged particles are then sprayed towards the grounded target where they get deposited due to electrostatic force of attraction.



(a)



(b)

Figure 2.8 Schematic diagram of (a) corona charging powder gun (b) tribo charging gun[10].

2.3 Meltblowing Process

Melt blowing is a one step process where molten polymer, generally thermoplastic resin, is extruded through one or more rows of orifices of a die, drawn by converging sheets of hot air and thereby forms a plurality of micro-sized fibers [11]. **Figure 2.9** shows schematic diagrams of the melt-blowing process.

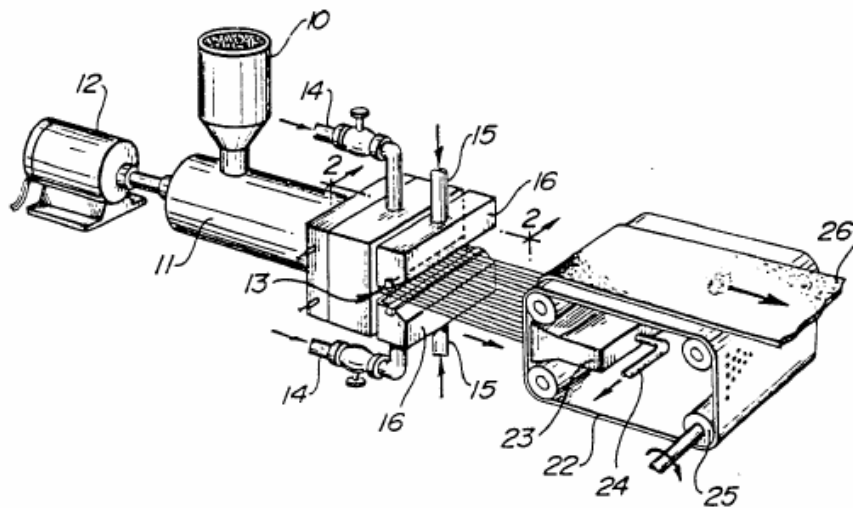


Figure 2.9 Schematic diagram of melt-blowing manufacturing equipment [12].

To form meltblow fibers, polymer chips or pellets are fed to the feeder (10 in **Figure 2.9**), which are then forced to the heating zone (11 in **Figure 2.9**) by the screw motor (12 in **Figure 2.9**). In the extruder the polymer is exposed to incrementally increasing temperatures

in consecutive heating zones. The polymer subsequently enters the “die” (shown as 2 in **Figure 2.9**), which is heated to the desired temperature [12]. From the die, molten polymer stream is extruded through a row of orifices into hot compressed air or gas streams flowing at sonic velocities. The polymer elongates to form fine filaments, which are deposited on a continuously moving collecting surface. Because of the fineness and large number of fibers, meltblown webs can develop significant bonding strength through fiber entanglement engendered by the turbulence in the air-stream. Additionally, the distance between die and collection surface (Die-to-Collector-Distance/DCD), determines if the fibers are still tacky as they are deposited on the collector. With shorter DCD’s meltblown fibers are deposited in a tacky state allowing in-situ autogenously bonding to take place without requiring further bonding steps [13].

In general, most meltblown fibers are formed from single type of polymer. However, recent developments in bicomponent fiber formation allows for use of two (or more) polymer types, extruded and distributed in the fiber cross-section precisely. This capability opens up many possibilities of functionalizing fibers for specific usage.

Bi-component Fiber Formation

Bi-component fibers are defined as fibers obtained by extruding two polymers simultaneously from the same spinneret and are contained in the same filament or fiber [14]. In bi-component structure the two constituents could be arranged in many configurations and geometries some of which are shown in **Figure 2.10a-f**, as follows;



Figure 2.10 (a) Side by Side (b) Sheath/Core (c) Sheath/Core Eccentric (d) Segmented Pie (e) Island in the Sea (f) Tipped Trilobal [14].

The bi-component meltblowing process is principally same as the single component fiber formation described. The primary difference between them is that instead of one polymer stream, two separate polymer streams are extruded through the same die. The die spinnerets are designed to position the different polymers as they are desired in the fiber cross-section. In forming bicomponent fibers, component polymer characteristics such as,

thermal behavior, elongational viscosity, etc. must be compatible. Incompatibilities may lead to crimping due to unequal shrinking as well as, inadequate adhesion between the two polymer surfaces, unless of course these are particularly desirable as in the case of crimped and splittable fibers. As an example, large elongational and shear viscosity difference between the constituents greatly affect the spinnability of the polymer systems and may have direct impact on the cross-section of the fiber as demonstrated by Han [15]. In case of side-by-side configuration, component with lower viscosity tends to wrap around component with higher viscosity, see **Figure 2.11.a** [15]. Similar are trends in sheath core structures i.e. the higher viscosity core component tends to push the sheath out while if it is in sheath than it compresses the core in spite of same volume ratio, see **Figure 2.11 b**.



Figure 2.11 Displacement of interface due to viscosity difference a) for Side-by-Side cross section; b) Sheath-Core cross-section [15].

Bi-component meltblowing has come a long way from 1970's when Buntin and Lohkamp disclosed a process for making meltblown fibermats made from two or more materials in single feed [16-17]. Now they are being used in many diverse applications as abrasive wipes [18], filter rods [19], respirators [20], heat and moisture exchangers [21], artificial leather and many more.

2.4 Particle Filled Fibers

Bi-component fibers formation technology has been used in a number of applications where one of the component polymer systems has been used to incorporate particles in the fiber. Typically sheath-core bicomponent configuration, see **Figure 2.11(b)** has been used to incorporate particles either in the sheath or in the core. Particle fillers may be added to polymers for the purposes of providing reinforcement for improved mechanical properties, anti-bacterial and anti-microbial activities, anti-flammability and sometime simply to fill the fiber volume cheaply. Variety of fillers and polymers have been used commercially including calcium carbonate in poly(vinyl chloride) (PVC) as a cheap filler [22], mica & talc in

polypropylene for improved stiffness, glass fiber for significant improvement in strength, stiffness including heat distortion. Carbon black to make rubber conducting, silver as antibacterial and antimicrobial agents [24], antimony oxide as flame retardant, TiO₂ for enhanced mechanical properties and optical covering (opacity) [25-26] are some other applications. Bond from DuPont has disclosed an invention of making of an antistatic hairbrush having bristles with nylon or polyester as core and compatible sheath (10-40 weight percent) with carbon [27]. The process of adding particles in a polymer system for fiber extrusion involves compounding of the polymer with particles before extrusion. The compounded polymer is likely to have a different melt rheology, therefore it is important to understand the changes.

Melt Rheology of Particle Filled Polymers

Polymer spinnability (ability to form a fiber) is mainly governed by its rheological behavior and adding particles to the polymer melt greatly influences its rheology and hence, its spinning behavior. Therefore influence of solid particles or fillers on the rheological properties of thermoplastic molten polymers is of great scientific interest. Considerable work has been done in understanding the stratified two-phase flow of polymer melts systems because of its relevance to co-extrusion of sheet and film injection molding and bi-component extrusion of fibers. Filler concentration and its surface chemistry greatly affect the rheological behavior of polymer melt. Also applied shear and elongational rate affects the fiber interface shapes, fiber strength and many other physical properties in bi-component fibers. The presence of fillers in visco-elastic polymers is generally considered to reduce melt elasticity and hence influence the phenomena of die swell [23]. Fillers also affect the mechanical properties like breaking strength, breaking elongation and toughness.

Ghosh and Maiti [28] has investigated the melt rheology of polypropylene filled with titanate coupling -agent -treated silver powder (0-5.6 volume % of Ag). Unlike most of the other cases, melt viscosity decreased with an increase in Ag content up to 4.1vol% beyond which it increased, **Figure 2.12**. The viscosity showed linearly decreasing dependence on shear rates for all the volume % ratios for a range of temperature, **Figure 2.13**. It was suggested that the phenomena of decreased viscosity with loading percent is due to increase in heat conductivity making the flow easier. Beyond 4.1% loading, the filler-filler interaction

would have been greater than the effect of increased thermal conductivity increasing the viscosity. The melt viscosity might have reduced due to lubricating/plasticizing effect of the titanate coupling agent but no additional results have been provided for these conclusions.

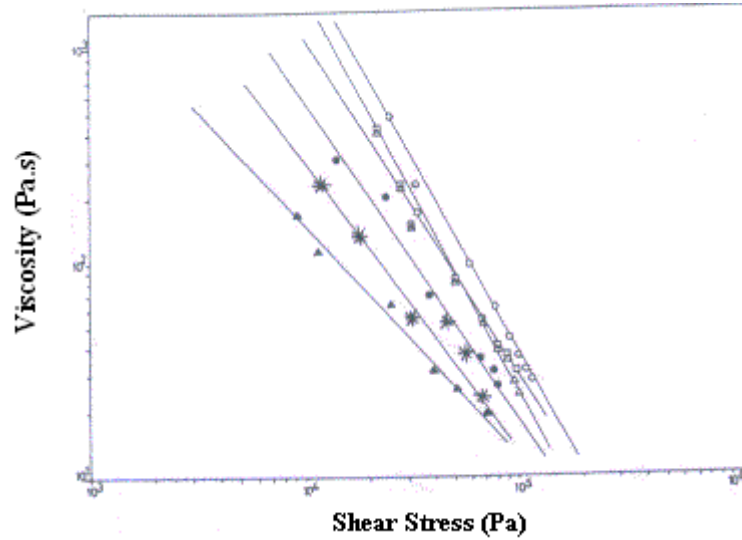


Figure 2.12 Variation of melt viscosity as a function of shear stress at 473K for PP/Ag fiber composite at varying Ag content (vol%) (O) 0;(□)0.43;(○) 1.3; (∩) 2.4; (p) 4.1;(*)5.6; [28].

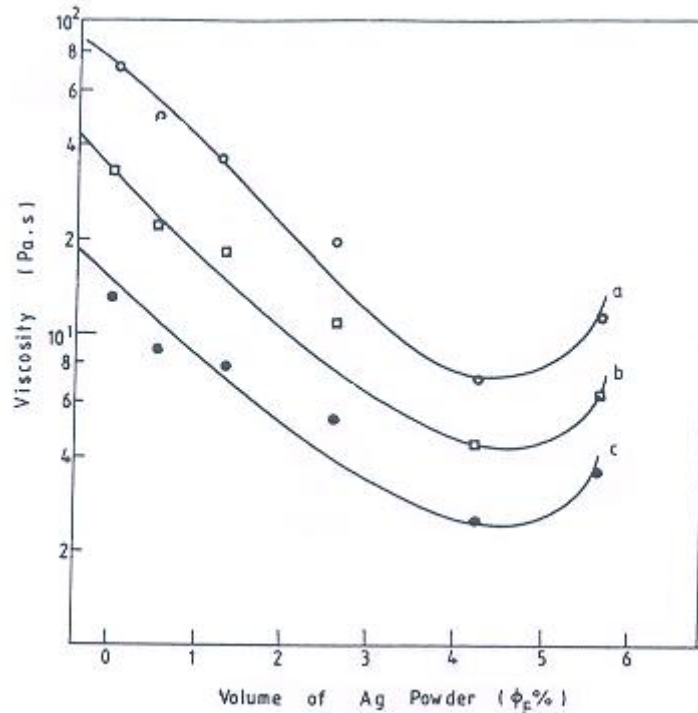


Figure 2.13 Variation of melt viscosity composition of PP/Ag composites at 473K at constant shear rates (s^{-1}): (a) $2 \cdot 10^3$; (b) $3 \cdot 10^3$; (c) $5 \cdot 10^3$ [28].

Lin and Masuda [29] studied the effect of dispersion of $CaCO_3$ particles on viscoelasticity of polypropylene melt for two particle sizes, 0.15 and 4.0 microns. They inferred

that dispersion of the particles greatly influences visco-elastic properties of filled polymers. The system filled with large particles exhibit a relatively stable visco-elastic behavior. Small particles also exhibit similar behavior but only for low loading. It is because of the formation of gel-like structure at low shear stresses, which gets disrupted at high shear stresses.

Shape of particles also affects the rheological behavior of polymer melt. Presence of fillers in viscous polymer melts not only increases their viscosity but also influences their shear rate dependency, especially with non-spherical particles (fibrous or flake-like), which become oriented in flow field [30]. It has been observed, that the particle orientation increases the non-Newtonian behavior especially at lower shear rates, see **Figure 2.14**. **Figure 2.15** show the effect of filler particle shape on viscosity of filled polypropylene melts, containing glass beads and talc particles of similar density, loading and particle size distribution. Talc filled polymer blends show higher viscosity due to increased contact and surface interaction between these irregularly shaped particles [30].

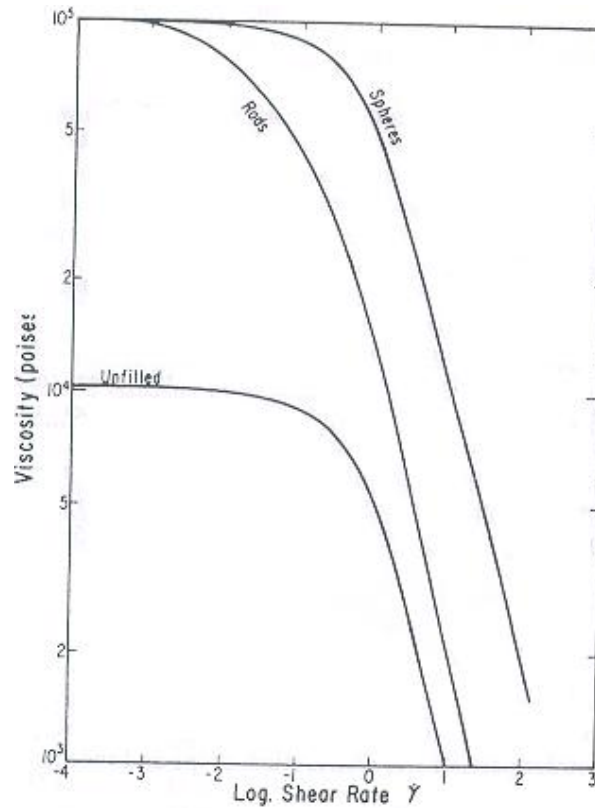


Figure 2.14 Effect of spherical and rod-shaped filler particles on the viscous flow of a polymer melts as a function of shear rate (concentration of spheres is higher than that of rods)[30]

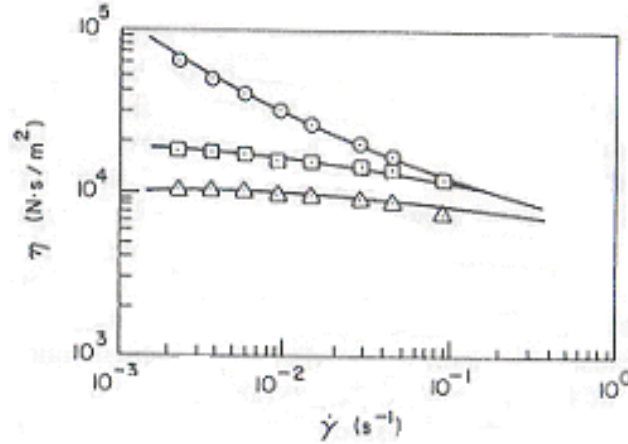
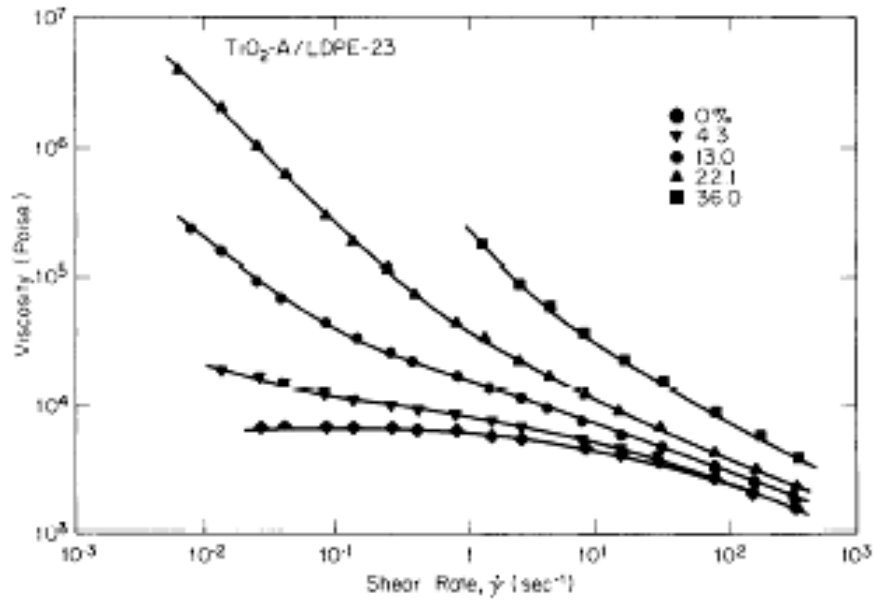


Figure 2.15: Effect of filler particle shape on the viscosity of polypropylene (PP) at 200°C : (D) neat PP; (□) PP containing 40% by weight glass bead; (O) PP containing 40% by weight talc [30]

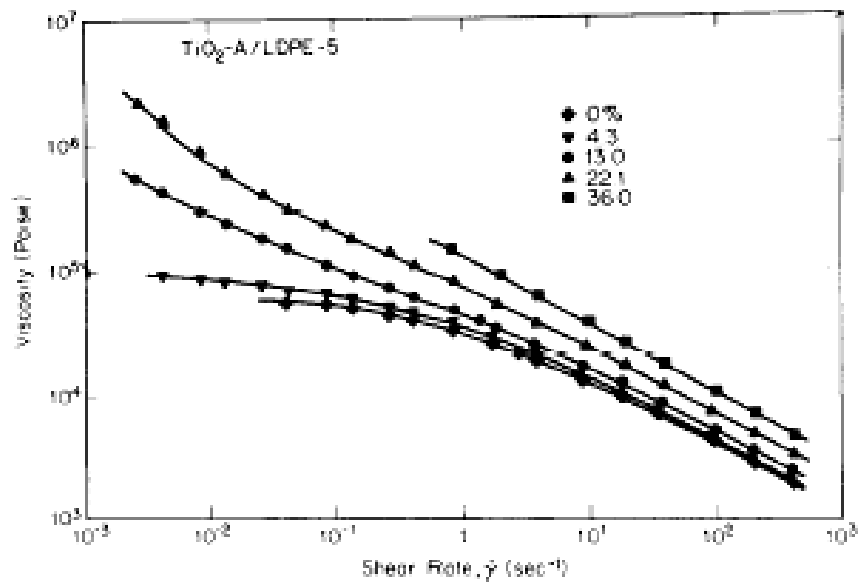
Minagawa and White [26] studied the influence of titanium dioxide (TiO₂) on rheological and extrusion properties of polymer melts like high-density polyethylene (HDPE), high-density polyethylene (LDPE) and polystyrene. They also studied the effect of particle to polymer volume ratio (ϕ) and shear rate (γ), on interface shape and viscosity $\eta(\phi, \gamma)$. **Figure 2.16(a)** and **Figures 2.16(b)** shows the effect of various loading percent of TiO₂ (see **Table 2.1**) on viscosity of LDPE-23 and LDPE-5. **Figure 2.17** shows the effect of various types of TiO₂ on viscosity of HDPE-5 i.e. TiO₂ particles with larger size showed significantly higher increase in viscosity. Also polymer with higher viscosity showed a lower increase in viscosity with shear rate. Similar trends were observed for other polymer too. The presence of TiO₂ filler decreases the extrudate swell due to decreased melt elasticity.

Table 2.1 Description of polymers and titanium dioxides studied [26]

Polymer type	Material	Melt Index	Particle Type	Particle Size, μ	TiO ₂ %	Modification
HDPE – 0.1	High Density Polyethylene	0.1	TiO ₂ – A	0.18	97	Al ₂ O ₃
HDPE – 5.0	High Density Polyethylene	5.0	TiO ₂ – B	0.24	97	Al ₂ O ₃
LDPE – 5	Low density Polyethylene	5.0	TiO ₂ – C	0.25	90	Al ₂ O ₃ , SiO ₂
LDPE – 23	Low Density Polyethylene	23.0				
PS	Polystyrene	--				



(a)



(b)

Figure 2.16 Viscosity behavior at various shear rates with various levels of TiO₂-A at 180°C of (a) LDPE-23 (b) LDPE-5 [26].

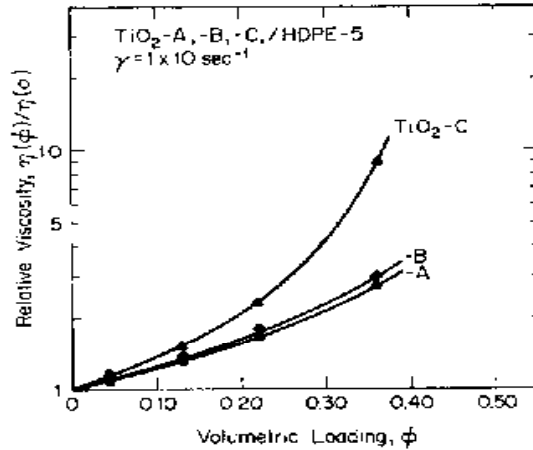


Figure 2.17 Relative viscosity $\eta(\phi)/\eta(0)$ as a function of volumetric loading ϕ [26].

Minagawa and White [26] has also studied filled and unfilled side-by-side structures. They inferred that the final cross-section of fiber depends on viscosity ratio of components, length/diameter (L/D) ratio of die and dwell time in capillary of die. Increasing viscosity ratios, extrusion time and die L/D ratio increases the overlapping of lower viscosity component over higher viscosity component making it more of a partially covered sheath core structure rather than side-by-side structure, see **Figure 2.18**.

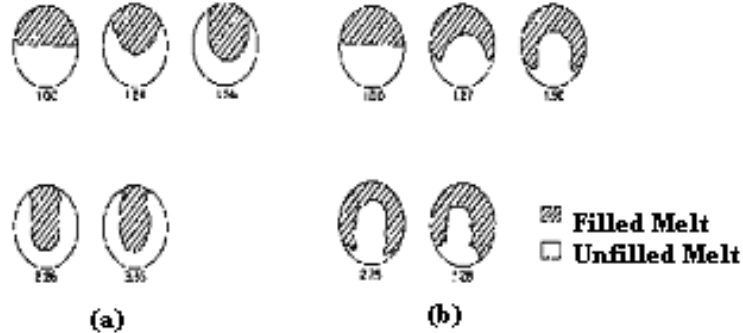


Figure 2.18 Interface shape for capillary dies as a function of viscosity ratio (a) $h_{\text{filled}} > h_{\text{unfilled}}$ (b) $h_{\text{filled}} < h_{\text{unfilled}}$ [26].

Based on the study by Minagawa and White [26] it can be inferred that for making good sheath-core structures, sheath polymer needs to have lower viscosity than core. Adhesion between core-sheath is likely to be higher if the core polymer has higher elasticity (hence, higher die swell for the given shear rate). This is so because higher die-swell would cause the core to penetrate more into the sheath and hence, more adhesion along with thinner sheath.

Sang and Sung [31] studied sheath-core fibers with various levels of silver nanoparticle content in either sheath or core, **Figure 2.19**. They examined various sheath core combinations with particle loaded PP-master batches as either sheath or core was made, see **Table 2.2**. Sang and Sung reported reduction in crystallinity of PP with addition of nano silver as shown in **Figure 2.20**. They also noted anti-microbial activity only in the samples having nano silver in sheath (PP5, PP6 and PP7 in **Table 2.2**) even for low particle loading. Samples containing particles in core did not demonstrate any anti-microbial effect at any loading. It implies that some of the nano silver particles are exposed to the fiber surface when loaded in sheath even for loading as low as 0.3wt%.

Table 2.2: Classification of melt-spun fibers [31].

Sample	Component (sheath/core)	Extruding ratio (sheath/core)	Silver content (wt%)	Melt flow rate (g min ⁻¹)	Nozzle diameter (mm)
PP 1	PP/PP	50/50	0	3.0	0.5
PP 2	PP/M1 ^a	50/50	1.5	3.0	0.5
PP 3	PP/M2 ^b	50/50	5.0	3.0	0.5
PP 4	PP/PP	50/50	0	4.0	1.0
PP 5	M1 ^a /PP	10/90	0.3	4.0	1.0
PP 6	M1 ^a /PP	30/70	0.9	4.0	1.0
PP 7	M1 ^a /PP	50/50	1.5	4.0	1.0

^a M1 is master-batch type1, which contains 3wt% nano silver.
^b M2 is master-batch type2, which contains 10wt% nano silver.

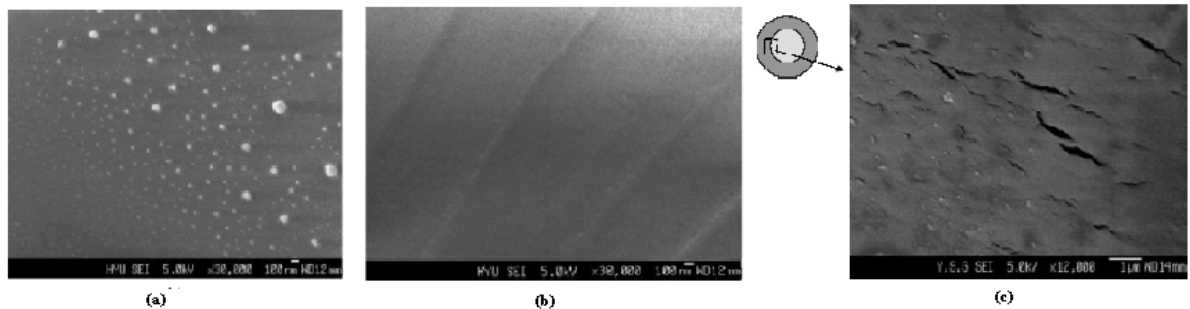


Figure 2.19 SEM micrographs of (a) core part, (b) sheath part at the cross-section of PP 3 (c) boundary of the sheath-core at the cross-section of PP 6 [31].

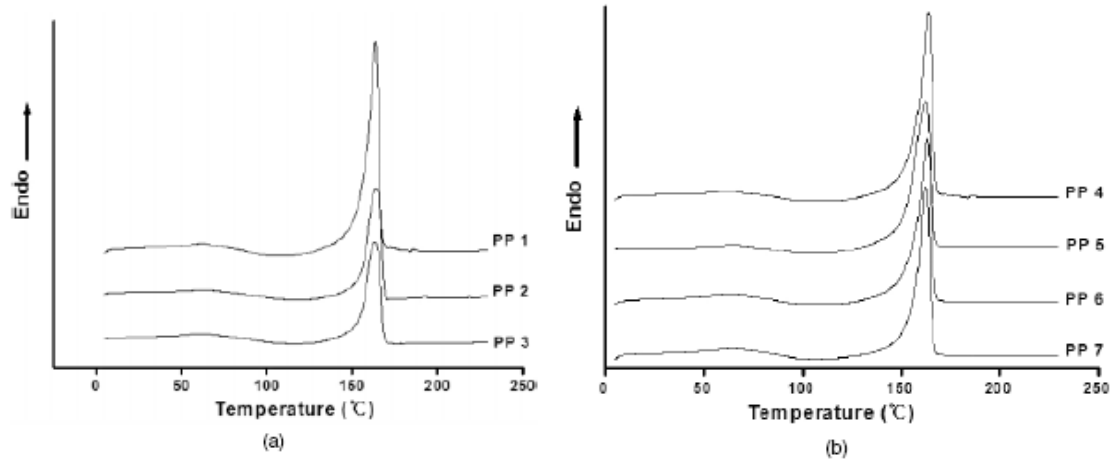


Figure 2.20 Differential scanning calorimetry of spun fibers of varying silver concentration; (a) fibers containing silver in core part (b) fibers containing silver in sheath part [31].

Liu and Lai [32] studied the antimicrobial effect of adding nano zinc oxide in the sheath of polyester sheath core fibers. The fibers studied included 300, 500 and 1000 ppm master batch of Polyester as sheath and another polyester of higher intrinsic viscosity as core. Liu and Lai [32] examined the spinning processes as well as the fiber physical and anti-bacterial properties. Spinning failures were reported for drawing speed of 500m/min at draw ratios of 1.8 for 1000 ppm loading. Decreasing the spinning temperature from 288⁰C to 285⁰C made the spinning feasible. All the samples showed high anti-bacterial and anti-fungal activity implying the presence of particles on the surface of the fiber.

Zang and Liu et. al. [33] investigated the effect of blending isotactic PP with three types of elastomeric nano-particles (ENP): styrene–butadiene DB-70 with 70 wt% butadiene, DB-50 with 50 wt% butadiene, and modified DB-50 ENP by spray drying DB-50 rubber latex together with dissolved sodium benzoate (10 phr based on dry latex). They reported slight enhancement of mechanical properties of the extrudate. Zang and Liu postulated that the increase may be due to increase in nucleation density of the blends, while the crystallization kinetics of the blends becomes faster compared to pure PP samples. This was supported by the fact that spherulitic size in the blend was found to be much smaller than that of pure PP, see **Figure 2.21**.

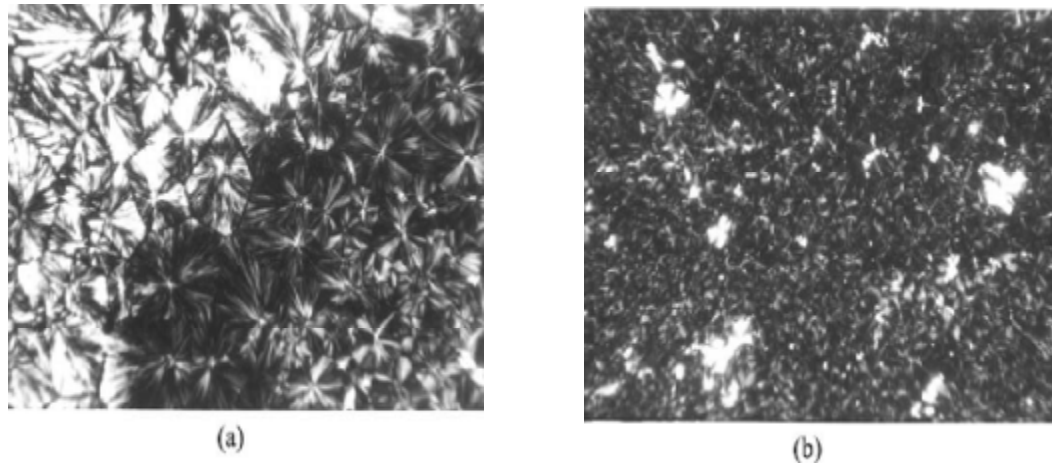


Figure 2.21 Polarized light microscope micrographs for (a) pure PP and (b) PP toughened with 5wt% DB-70 ENP crystallized at 118°C for 5 h [33].

Chiu [34] studied the spinning and elongational flow behavior of polypropylene blended with nanoscale TiO₂ of average size of 7 nm and 21 nm at 1, 2 and 3% weight ratios. It was observed that for the given process parameters, diameter of the filament made with 7 nm particles is significantly higher than that of filament containing 21 nm particles implying higher die swell ratios and hence, higher elasticity for 7 nm particle-polymer system than 21 nm particle-polymer system, see **Figure 2.22**. They also observed that the increase in particle loading ratio by weight, it takes longer to solidify due to increased thermal capacity of the melt hence, was drawn more for the given drawing ratios, as a result the filament diameter decreased with increased particle loading (**Figure 2.23**).

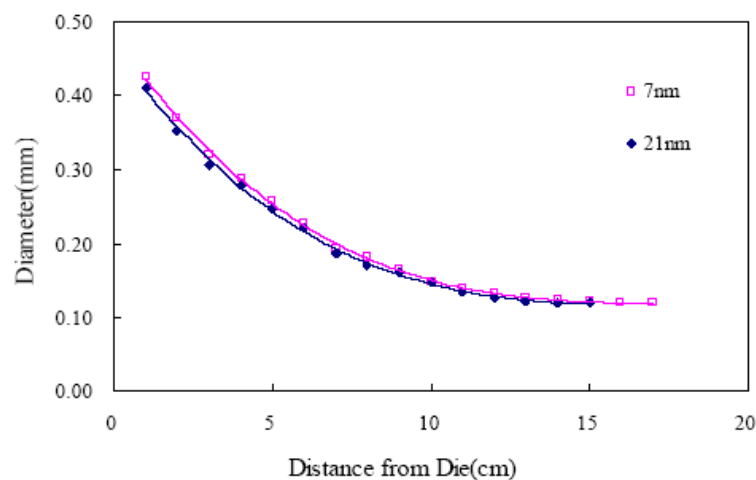


Figure 2.22 Filament diameter of the extrudate at 200°C for 7nm and 21nm TiO₂ particle size [34].

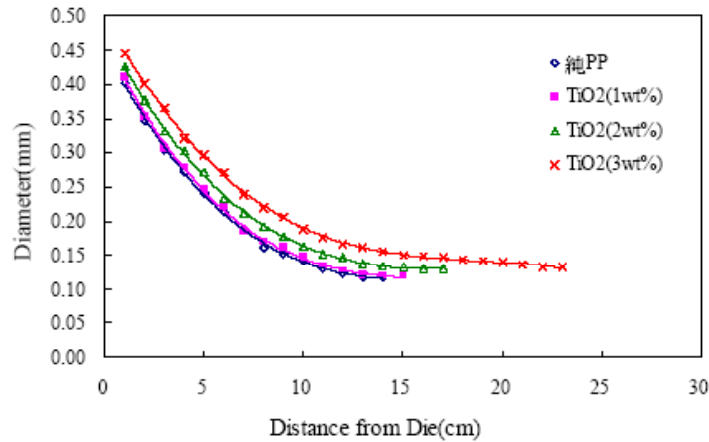


Figure 2.23 Filament diameter of the extrudate at 200°C for 1%, 2% and 3% TiO₂ loading by weight [34].

Chiu [34] also reported higher increase in apparent elongational viscosity for 7nm particle-polymer system than 21 nm particle-polymer systems, with increase in elongational rate. Also the increase was higher for higher shear rates (**Figure 2.24**).

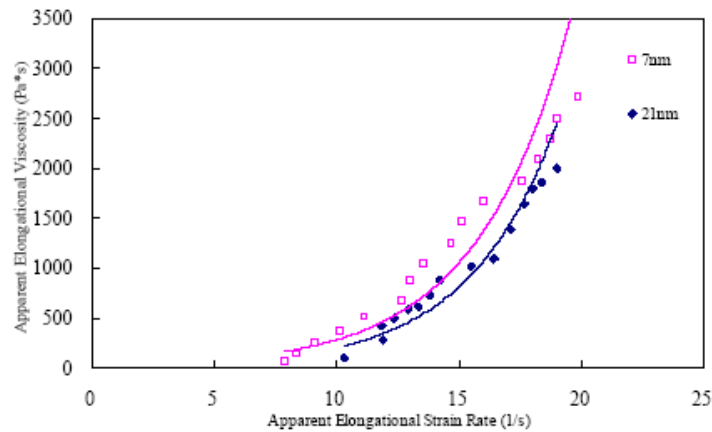


Figure 2.24 Apparent elongational viscosity of the melt at 200°C for 7nm and 21nm TiO₂ particle size [34].

Chiu [34] also reported an increase in apparent viscosity with increasing particle-loading ratios. As explained, for a given weight loading total surface area of particles having 7nm diameter is much more than that of 21 nm diameter, hence higher polymer particle interaction and hence, higher viscosity. Also at higher apparent elongational strains, the increase was higher for higher weight ratio (**Figure 2.25**).

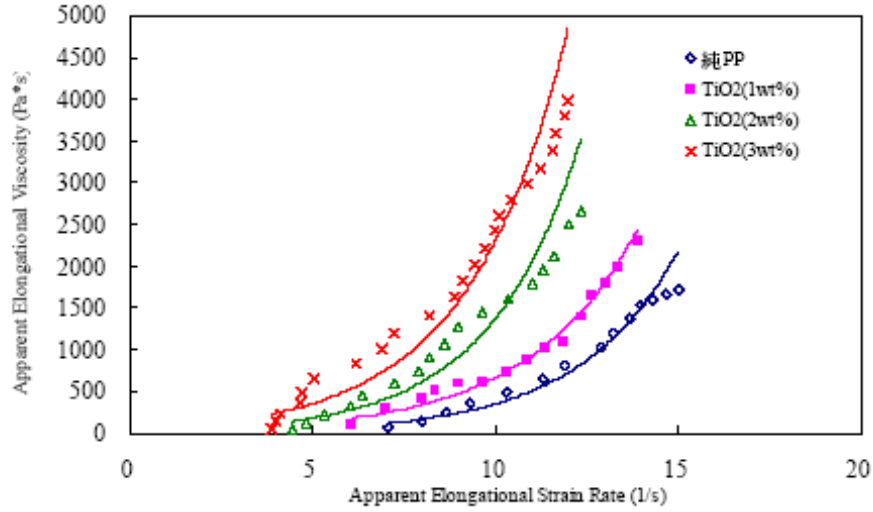


Figure 2.25 Apparent elongational viscosity of the melt at 200⁰C for 1%, 2% and 3% TiO₂ loading by weight [34].

Chiu [34] also reported that melting temperature did not changed with loading ratios, see Figure 2.26 but the onset temperature for decomposition increased significantly with loading percent as TiO₂ absorbed most of the energy while heating see Figure 2.27.

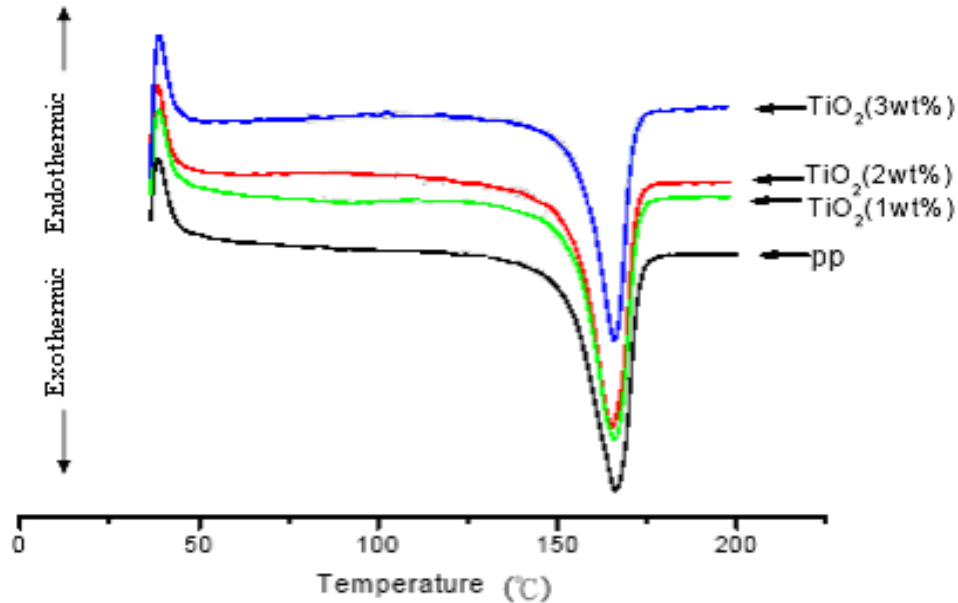


Figure 2.26 Differential scanning calorimetry analysis of the extrudate for 1%, 2% and 3% TiO₂ loading by weight [34].

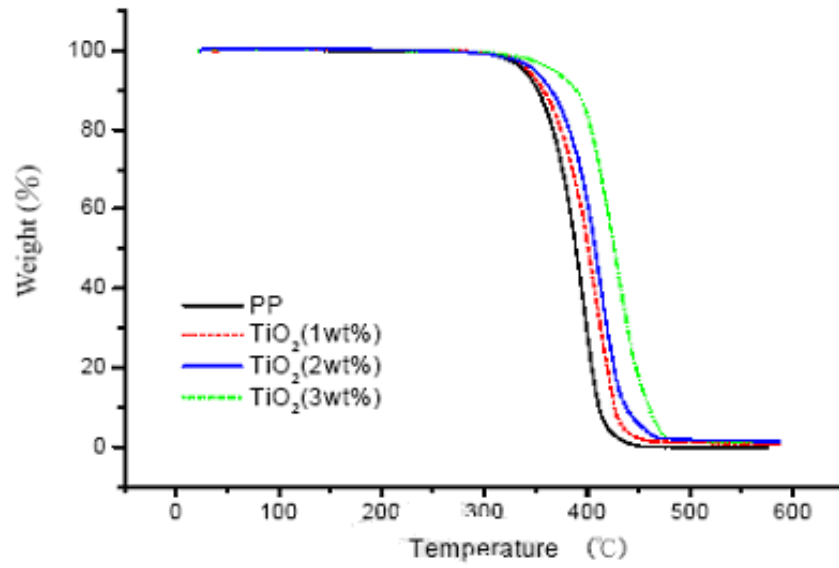


Figure 2.27 Thermo gravimetric analysis of the extrudate for 1%, 2% and 3% TiO₂ loading by weight [34].

3 OBJECTIVE

Major objective of the current research is to develop a process for fiber surface modification of meltblown fiberweb by incorporating nanoparticles on the fiber surface. This entails surface characterization of fibers as a function of percent particle loading as well as the distribution of the particles on the fiber surface.

In order to obtain uniform powder-coated fiber surface 2 potential methods will be examined: 1) Extrusion of powder-polymer compound in a bicomponent fiber structure. 2) Spraying of powder particles to the fiber surface while the fibers are being formed.

In the later sections, the first method will be described as bicomponent extrusion method and the second method as powder spray method. Various process parameters will be studied to maximize the particle loading for both methods. Fibers will be characterized for various properties like ultra-violet transmission, thermal behavior, mechanical properties and fiber surface characterization.

4 EXPERIMENTAL DESIGN

The implementation of the powder spray method requires development of an experimental set up combining meltblown fiber formation and electrostatic powder spray methods. The bicomponent fiber extrusion using nano particles in one of the components involve compounding of polymer with particles and subsequent extrusion. In both cases choice of materials is critical.

4.1 Materials

To validate the concepts polypropylene (PP) is chosen as the fiber forming polymer. The choice is based on the availability of wide variety of PP types in terms of their melt flow rate (MFR), etc. as well as ease of processability in meltblowing. Two separate polypropylene (PP) resins were used for extruding meltblown webs for powder spray and bicomponent extrusion. Polypropylene¹ processed on 3” slot-die laboratory scale meltblowing unit, (further described in **section 4.2**) had a nominal melt-flow-rate (MFR) of 1200 gm/10min. Polypropylene² processed on bi-component meltblowing also had a melt-flow-rate of 1200 gm/10min. Since viscosity of the polymer increases significantly with addition of TiO₂ thus, it was desired to start with very low viscosity polymer hence, we choose the 1200 MFR resin. **Table 4.1** shows the specification of the polypropylene². Also it was compounded with NanoActive™ TiO₂ to prepare the masterbatch. The TiO₂ particles had the mean particle size of 100nm but the mean aggregate size was 5 micron. Summary of the properties of TiO₂ particles³ used in the research are mentioned in **Figure 4.1**.

Table 4.1 Technical specification of polypropylene CP-15000-P [43]

TECHNICAL DATA			
Property	Unit	Typical Value (1)	ASTM Method
Nominal Melt Flow (2)	g/10 min	1200	D1238
Density (3)	g/cm ³	0.905	D792
Melting Point (4)	°F	327	Sunoco
	°C	163	Chemicals
Pellet Size	Pellets/Gram	55	Sunoco Chemicals

- (1) Injection molded specimens where applicable
- (2) 230 °C / 2.16 kg
- (3) at 23 °C (73 °F)
- (4) by DSC

¹ courtesy of Montell USA Inc.

² courtesy of SUNOCO Chemicals Polymer Division.

³ NanoActive™ Titanium Dioxide from NanoScale Materials, Inc.

The TiO₂ powder need to be mechanically agitated or milled to break down the agglomerates before being used for coating or spinning. Also the powder turns yellow when left in open atmosphere for substantial 2-3 days. Reasons of yellowing are not known.

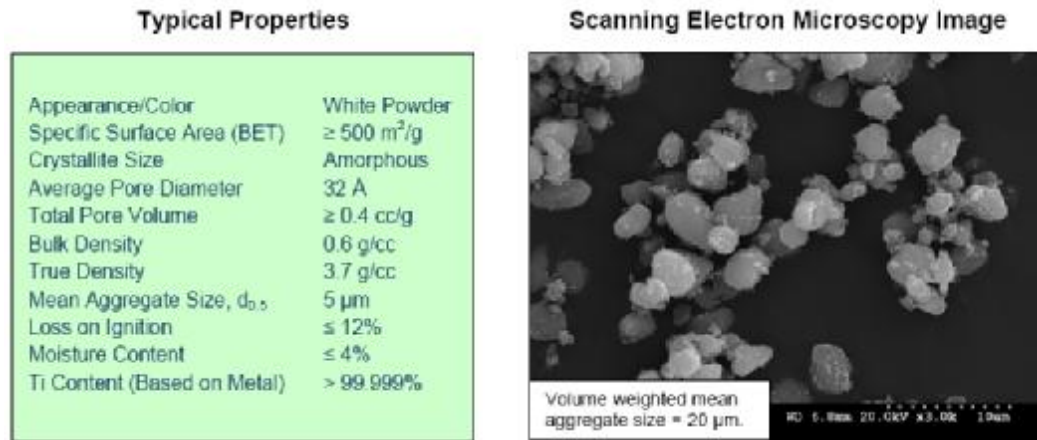


Figure 4.1 Specification and Scanning electron microscopy image of TiO₂ particles.

4.2 Particle Spray Method

One of the major objectives of the research was to develop a novel process for surface modification of fibers in nonwoven web by insitu coating of particles before the web is being collected. Thus, final setup as shown in **Figure 4.6** was designed after stages of development in initial setup.

Desktop meltblow setup, see **Appendix C, Figure C1**, is used to extrude meltblow fibers. It has an active spray width of 3” and can process polymer with maximum melt temperature of 280⁰C. The extruded fibers could be collected on a porous drum followed by a winder to be wound as fabric. Further details of the system are mentioned in **Table 4.2**.

Table 4.2: Specification for Desktop Meltblow setup.

Extuder

Max. Temperature: 280 °C; 1.9 cm (¾”) Single Screw, 24:1 L/D Extruder

Air Heating Assembly

1.8 m (6’) Melt Transfer Hose (170 °C); 1.8 m (6’) Air Transfer Hose (= air temp.);

Meltblowing Die

Max. Die Temperature: 280 °C; 7.6 cm (3”) Active Spray Width; 90⁰ Sharp-Tip Nosepiece
 12 Holes/cm (30 Holes/in.), 0.4 mm (0.016”) Hole-Diameter; Air Gap via Shims, 0.254 mm (0.010”) Shim Thickness; Positive Setback: 0.8 mm (1/32”)

Electrostatic spray setup⁴ (see **Appendix C, Figure C4**) was used for charging and spraying TiO₂ particles on the meltblown web. It could spray the particles with pressures up to 4 bar with maximum volume of 8m³/h. The maximum charging potential of the gun is 100kV with maximum fluidization pressures of 6 bars. Powder coated samples of 2"-3" were made on the meltblow setup, which were then consolidated by thermal point bonding into 8"-10" wide samples by layering them as shown in **Appendix C - Figure C3**.

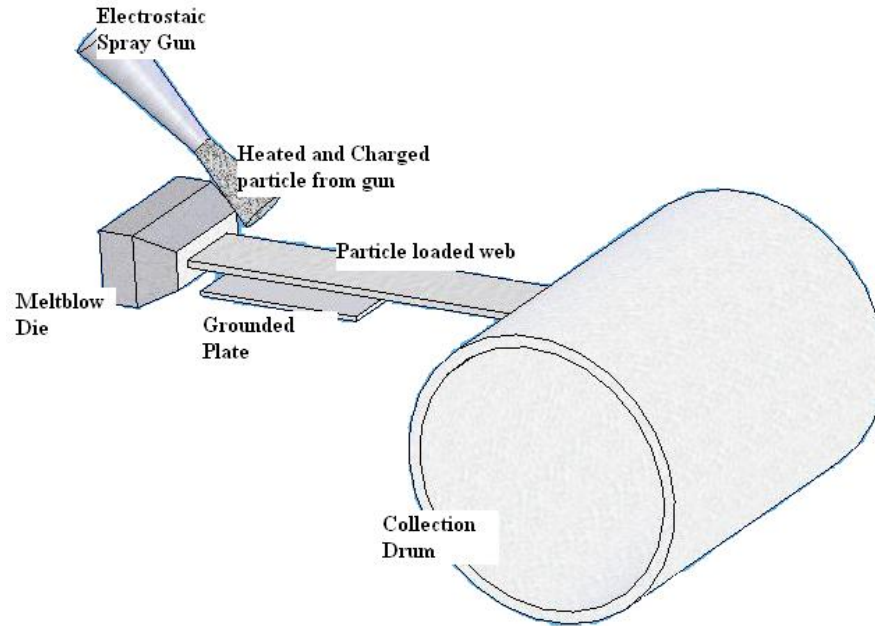


Figure 4.2 Schematics of side view of the initial setup.

Figure 4.2 shows schematic of the preliminary integrated design of the setup used to make the first batch of the samples. The initial setup is principally the same as that of the Coform technique [4] as in both the cases the particles are sprayed at the point where the web is tacky, i.e. 1"-2" from the meltblow die. But unlike Coform technique the present system is integrated horizontally with the meltblown die being in the horizontal plane extruding fibers in horizontal direction. In coform technology only compressed air is used to spray particles on the meltblow web but in this research, particles were charged and then sprayed onto the meltblown web. Theoretically charging of the particles improves the control on particle flow as the electrostatic force of attraction between the particles and the grounded target governs their flow. The electrostatic gun is placed at 45⁰ to the plane of the fiber path from the die to

⁴ PG1 from ITW GEMA

the collection drum. Electrostatic gun sprayed the charged (Electrostatic gun potential – 30-40kV) and heated particles (Heater temperature 300-350⁰C) towards a grounded metallic surface (referred as grounded shield later in the sections). The particle flow is intercepted by the fibers moving in between the spray gun and the grounded plate, see **Figure 4.2**. Since the fibers are still supposed to be tacky (semi-molten state with fiber surface temperature to be above T_g) at the spray distance of ~2” – 4”, the particles tend to adhere to the fiberweb.

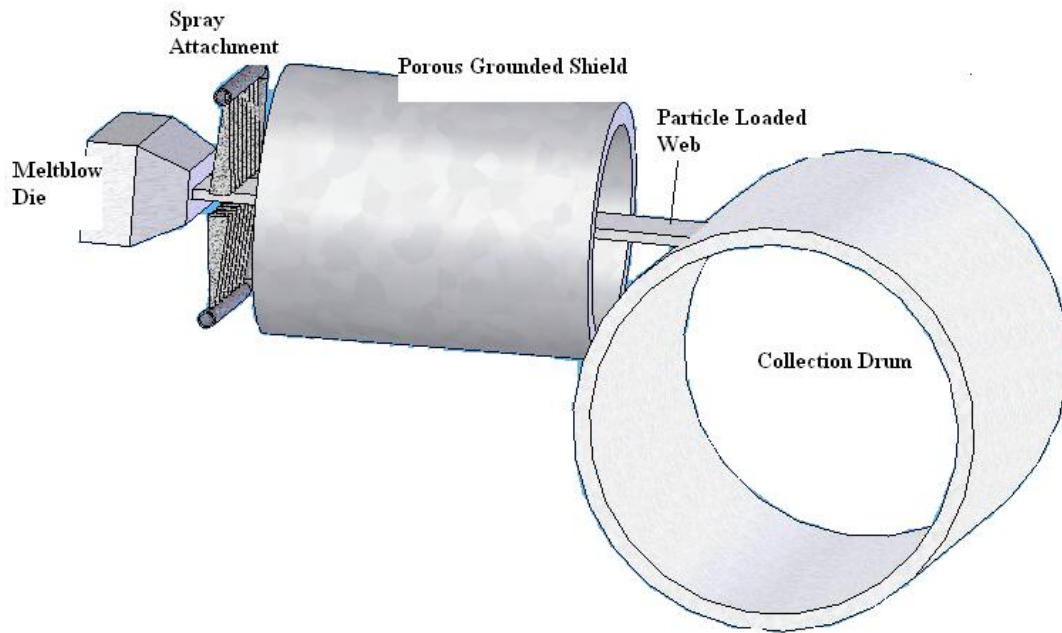
The initial setup has severe limitation of significant particle loss into the environment. The loss was observed even for very low carrying air spray pressures of about 0.2 bars, making this process uneconomical and partly ineffective. Increasing the electrostatic gun’s charging potential didn’t improve the situation much as spray pressure was still high enough to carry the particles in all directions overcoming the forces of electrostatic attraction.

It was observed that the spray air (or particle carrying air) pressure determined the amount and direction in which the powder particles were sprayed more than the electrostatic forces of attraction between the particles and the grounded target. The amount of powder particles sprayed by the gun increased with the carrying air pressure, but it also increased the spray width to be greater than 3 inches. . It is important to recall that the fiber web extruded by the die is also 3 inches wide. Thus, the spread of particles becomes greater than the web width at the point of particle impact leading to greater loss of particles into the environment. Thus, in order to get higher particle loading on web there was a need to increase spray pressures as well as change the spray system to have better control over escaping particles.

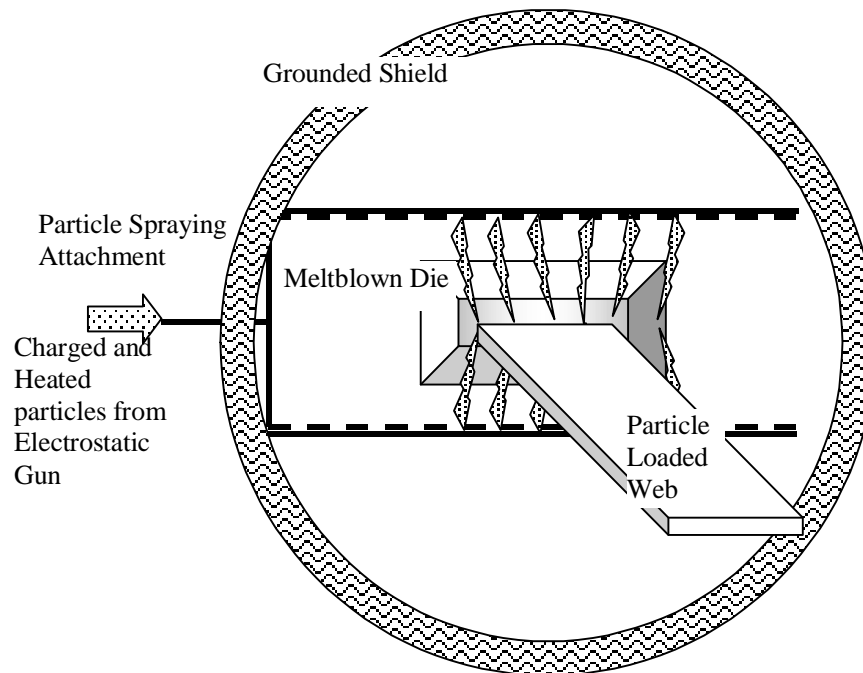
In light of these observations, the system was modified as follows:

1. Spray width, see **Figure 4.5(b)** was controlled by feeding the output of the electrostatic gun to an external attachment having an array of holes slightly more than the width of the web. The attachment sprayed the particles much closer to the web thus, reducing the chances of particles escape into environment.
2. Particles were sprayed from both sides of the web to have higher fiber surface coating even for small increase in spray pressures.
3. Larger grounded surface was used to trap higher amount of lost powder particles, see **Figure 4.3(a)-(b)**.

4. Higher particle charging potentials were tried to increase the particle charge, and hence the attraction towards grounded plate.



(a)



(b)

Figure 4.3 Schematics of the modified setup (a) side view; (b) front view.

In the modified set up the particle spray attachment orifices (see Figure 4.4) being small (4mm diameter holes), caused high air velocities for a given carrying air spray

pressure. This increased the chances of particle loss into environment. Also, the spray was not uniform as the holes closer to the feed side ejected more powders than the others. To alleviate the problem a larger diameter tube was used instead as shown in **Figure 4.5(a)** to make a final setup shown in **Figure 4.6**. The change resulted in substantial improvement in powder delivery and improved particle loading of the web. The larger orifices decreased the particle velocity and lower loss of particles was observed.

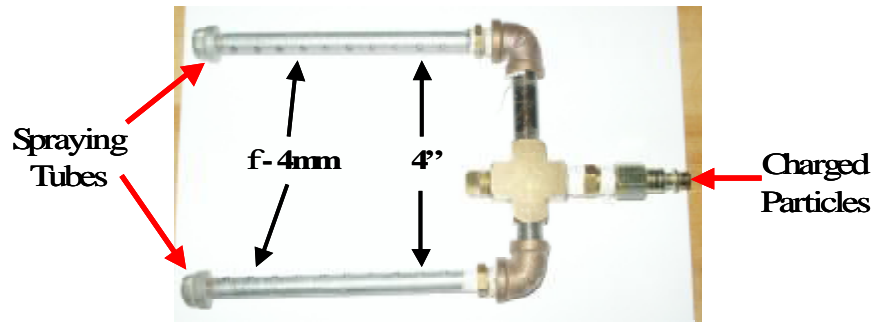


Figure 4.4 Particle spraying attachment for modified setup.

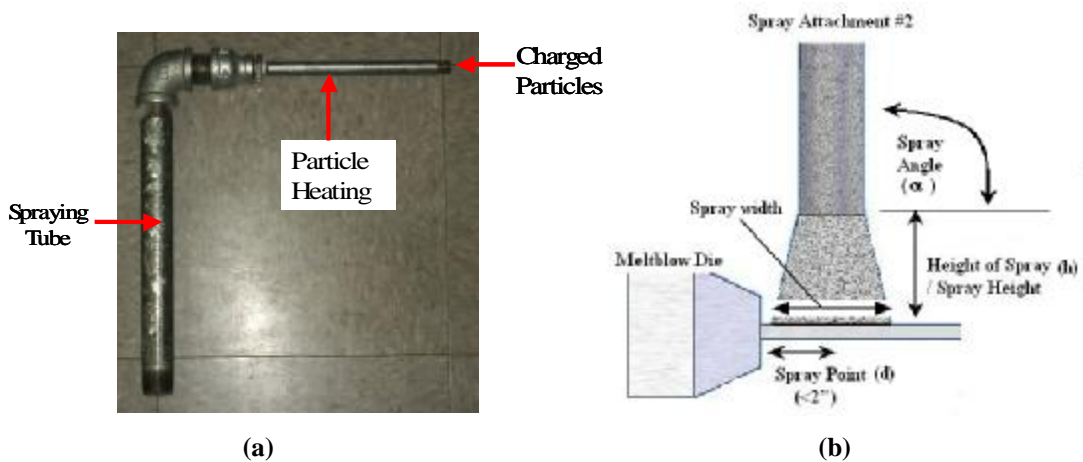


Figure 4.5 (a) Spraying attachment for final setup; (b) particle spray characterization.

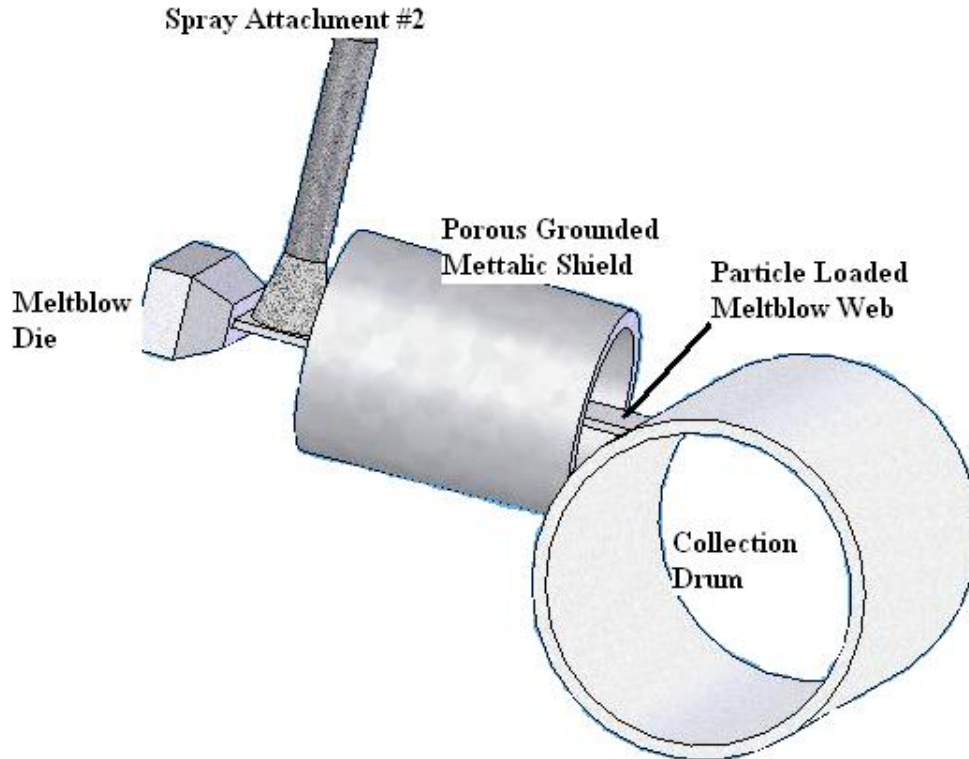


Figure 4.6 Schematics of side view of the final setup.

Particle Spraying Attachments

Attachments used to spray the charged and heated powder particles from the electrostatic gun onto meltblown web at a point where the web is still assumed to be tacky (< 2 inch from the die exit), are called as ‘particle spraying attachments’. The two spraying attachments used in modified setup and final setup are discussed in details as follows:

Attachment for modified setup

Attachment for modified setup consists mainly of 2 metallic tubes (diameter = 0.25 inch) having array of 8 holes (diameter = 4mm) placed at 1 inch spacing from each other (**Figure 4.4**). The tubes are connected to each other in ‘U’ shape configuration and are then connected to the electrostatic gun through flexible tubing. Array of holes of the metallic tubes are facing towards the web spraying the particles at an angle of 45° . The tubes were also electrically insulated from the rest of the system (grounded shield and meltblown die) to prevent the deposition of particles within the tube due to electrostatic force of attraction.

Attachment for final setup

Attachment for final setup consists of metallic tube (inner diameter, $\phi = 1''$; length = 12'') attached to a slider so as to adjust the point of spray at variable distance from the die ("d" in **Figure 4.5.b**). Also the tube can be adjusted to have variable spraying height ("h" in **Figure 4.5.b**) along with variable spray angle (" α " in **Figure 4.5.b**) to have better control over particle velocity and profile for various meltblown-processing parameters. This setup has the advantage of low particle velocity over attachment for modified setup even for high carrying air pressures.

4.3 Bicomponent Web Formation

As described earlier in sections 2.3 and 2.4, in order to incorporate particles on fiber surface one of the component polymers should be a particle polymer compound. Generally, when particles are introduced in a polymer system the composite behavior including its rheological as well as thermal characteristics is altered significantly. The compounded masterbatch of TiO₂ filled polypropylene resin was prepared based on the rheological studies described in Section 5.3. The compounding was done at Polymer Center of Excellence, Charlotte, NC. In the process of compounding, the polymer-particle mix was processed on a 21 mm co-rotating twin-screw extruder (36:1 L/D) at 380⁰F at a pressure of 30 psi and torque of 32 (residence time – 30-40 seconds). The melt was extruded in the form of strand thorough 1 hole die and was cut by air-knife to form pellets. Bicomponent sheath-core, side-by-side and biconstituent webs were then made on a meltblown pilot line at Partner's Laboratory, North Carolina State University. Schematic of the setup is shown in **Figure C2**.

4.4 Web Characterization

The bicomponent/biconstituent fiberwebs made were characterized for basis weight, percent particle loading, ultraviolet transmission, mechanical and thermal properties, as well as surface characteristics using various microscopy techniques.

4.4.1 Percent Particle Loading

Percent particle loading by weight is defined as the amount of particles in grams present on the web per unit weight of the control web. It can be calculated as the difference

in aerial density of the samples with particles (loaded web) and without particles (base web or control web) for the given meltblown conditions, see **equation 4.1**.

% wt particle loading = (AD_{LW} – AD_{BW})*100 / AD_{BW} Equation 4.1

Where, **AD_{LW}**: aerial density of the particle loaded web

AD_{BW}: aerial density of the base web (i.e. the plain web made at same meltblowing condition but without any particle spray)

To determine the aerial densities, seven 1 in² samples of each web were weighed and the average determined.

4.4.2 UV- Transmission Testing

To determine the UV transmittance of the fiberwebs a Varian Cary 3E spectrophotometer equipped with an integrating sphere was used in accordance with a standard test method (AATCC-Test Method 183-2004 [37]). The transmittance (%) for wavelengths from 280-700 nm was measured at an interval of 1 nm. Three measurements of UV Transmittance were performed for each sample at 0⁰, 45⁰ and 90⁰ (0⁰ referring to machine direction) and average of these values is reported. Ultraviolet Protection Factor (UPF) values were then calculated by the **Equation 4.2**.

$$UPF = \frac{E_{eff}}{E'} = \frac{\sum_{290}^{400} E_{\lambda} \times S_{\lambda} \times \Delta\lambda}{\sum_{290}^{400} E_{\lambda} \times S_{\lambda} \times T_{\lambda} \times \Delta\lambda} \dots\dots\dots\text{Equation 4.2.}$$

Where, T_λ, spectral transmittance, is the ratio of the transmitted irradiance to the source irradiance at the wavelength λ.

E_λ is the relative erythema spectral effectiveness (CIE 1987),

S_λ is the solar spectral irradiance,

Δλ is the wavelength step.

Average A-range ultraviolet transmittance (T_{(UV-A)av}) and blocking, and B-range transmittance (T_{(UV-B)av}) and blocking by **Equations 4.3 – 4.6**.

$$T_{(UV-A)av} = \frac{\sum_{315}^{400} T_{\lambda} \Delta\lambda}{\sum_{315}^{400} \Delta\lambda} \dots\dots\dots\text{Equation 4.3.}$$

% Blocking UV-A = 100% - T_{(UV-A)av}.....Equation 4.4.

$$T_{(UV-B)av} = \frac{\sum_{290}^{315} T_{\lambda} \Delta\lambda}{\sum_{290}^{315} \Delta\lambda} \dots\dots\dots\text{Equation 4.5.}$$

% Blocking UV-A = 100% - T_{(UV-B)av}.....Equation 4.6.

UV-A refers to the Ultraviolet radiations from 315-400 nm while UV-B refers to radiations from 280-315 nm. T_{(UV-A)av} and T_{(UV-B)av} are expressed as a percentage.

4.4.3 Thermal Characterization

Thermo Gravimetric Analysis (TGA) of the fiberweb samples was performed by Pyris 1 TGA instrument. Average of two scans per sample type, for temperature ranging from 50⁰C to 550⁰C at 20⁰C/min, is reported to analyze the change in decomposition temperature of the polymer due to addition of fillers (TiO₂ in this case). Decomposition temperature refers to the temperature at which the weight of the sample reduced to half (50%) of the original weight.

Differential Scanning Calorimetry was done on Diamond DSC from Perkin Elmer. Average of two scans per sample type, for temperature range 25⁰C to 210⁰C at 20⁰C/min, is reported to analyze the change in crystallinity as a function of filler content.

4.4.4 Mechanical Properties

To determine the effect of particle loading on tensile behavior of fiberwebs, all of the samples were evaluated on universal testing machine (MTS 30/G) according to ASTM test method D5035-95. In each case seven specimens were tested for analysis. Additionally, bending behavior of the fiberwebs was determined using cantilever method (ASTM D5732) and in each case, seven specimens were tested for further analysis. Flexural rigidity values of

all the samples were calculated from experimentally determined bending length and weight per unit area values using the following equation:

$$G = 9.809 \times 10^6 M_c^3 \dots\dots\dots\text{Equation 4.7.}$$

where: G = flexural rigidity, $\mu\text{N}\cdot\text{m}$, and

M = fabric mass per unit area, g/m^2 .

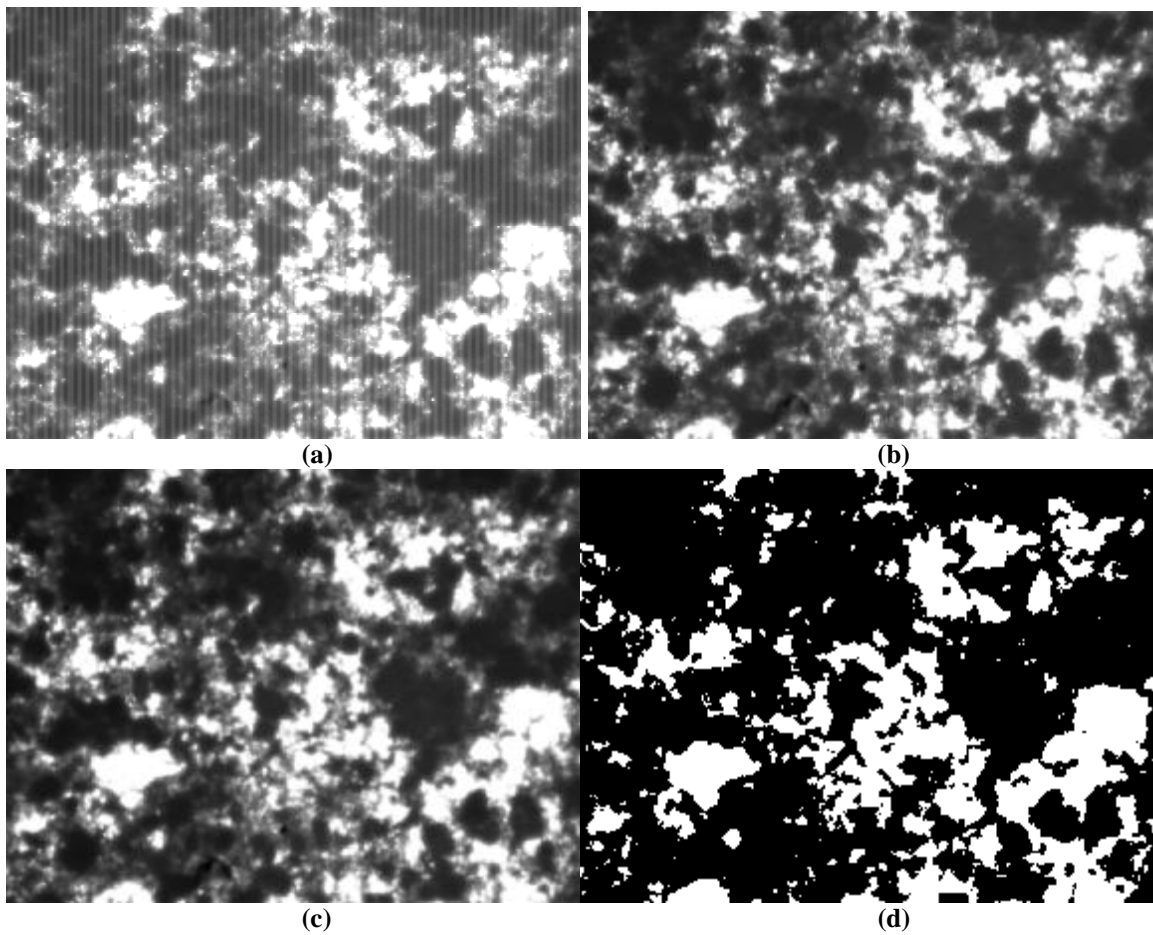
4.4.5 Surface Characterization

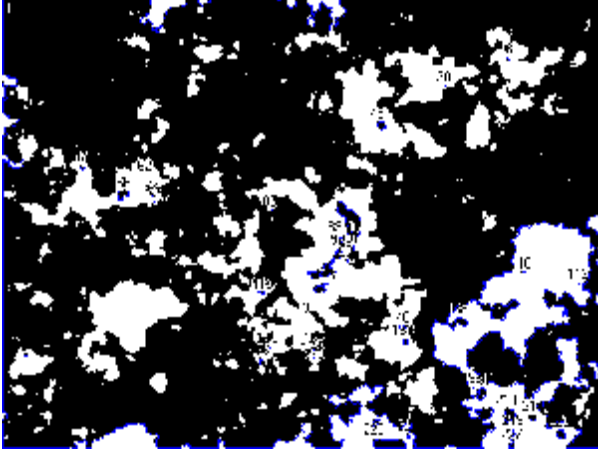
The primary motivation of surface characterization of the fiberwebs is to determine the extent of particle surface loading of the fibers and their distribution. The challenge is to use methods that are able to resolve the very wide distribution of particle size, ranging from 1 to 10 μm used for the study. Various techniques like atomic force microscopy, scanning electron microscopy (SEM), Brunauer, Emmet, and Teller (BET) surface analysis techniques, optical microscopy, laser scanning confocal microscopy, fluorescence microscopy etc were studied to determine the most appropriate method for sample surface characterization. Finally optical microscopy with refractive index solution, scanning electron microscopy and x-ray element analysis (EDX) by SEM were used to determine distribution of the particles. Details of these techniques are described as follows:

Optical Microscopy

Optical microscopy is an effective tool to qualitatively visualize the amount and distribution of particle loading on the fiberweb. Fiberweb images were obtained using a Carl Zeiss Microscope at 10X, 40X and 60X so as to visualize the macro as well as micro distribution of the particles. However, the images obtained were of poor quality due to thickness of the web. Uneven web surface along with particles in the bulk made it difficult to get good images showing particles on fiber surface. Therefore, in order to obtain images showing particles in the fiberweb, polypropylene fibers (Refractive Index – 1.45-1.56) and voids in the web thickness were optically dissolved by immersing the sample in an appropriate refractive index solution. The image so obtained showed particles as dark or opaque regions with rest of the sample (fibers and voids) as light or transparent regions (**Figure 4.7(a)**). The images were than processed by image analysis software (Matrox Inspector 4.1) to obtain an estimate of particle content:

The image (**Figure 4.7(a)**) obtained using the optical microscope with sample immersed in refractive index solution was first converted to 16 bit unsigned binary (**Figure 4.7(b)**), which was then smoothed (by 5X5 Smooth Filter) to remove noises from the image (**Figure 4.7(c)**). The filtered image is again filtered by High Pass threshold filtering at the frequencies suggested by the software itself, to differentiate the region containing particle as black while the rest (fibers and voids) as white (**Figure 4.7(d)**). The image is now ready for blob analysis, which gives percent black region in the image i.e. the projection of powder particles present in the web (**Figure 4.7(e)**).





(e)

Figure 4.7 (a) Image by optical microscope; (b) image converted to binary 16 bit unsigned format; (c) after applying 5*5 smooth filter; (d) after high pass threshold filtering; (e) after blob analysis (41 blobs with 72.81 % area in image).

Scanning Electron Microscopy

Scanning Electron Microscope (SEM) is similar to optical microscope except it uses electrons instead of light to form an image. For this research SEM images were taken by a Hitachi S-3200 ESEM at the working distance of 15mm, acceleration voltage of 15 kV and magnification as 40X, 100X, 500X, 1200X for most of the samples. In order to calculate the surface area of fiber covered, Energy Dispersive X-Ray (EDX) analysis of the samples was also done. The data was gathered at medium scanning rate with 15 frames per image to get a nice image, which could be used further for image processing, see **Figure 4.8 (a)-(b)**. Unlike optical microscopy with refractive index solution, this method can differentiate between fiber surface and voids in the web thus, it seemingly gives better approximation for the area of fiber surface covered by particles. However, the method has some limitations such as masking of carbon in the fibers by large TiO₂ particles (as Ti has higher atomic mass). Thus, TiO₂ particles in the scanned image were of larger dimensions than their actual size. Also smaller TiO₂ less than 1micron were not detected. At magnifications more than 500X, the samples with various levels of loadings look alike and cannot be differentiated. Also images showed significant variations in the loading percent for the same sample due to non-uniform particle distribution. Thus, x-ray analysis of the samples was excluded as a possible method for quantitative analysis of the particle loading.

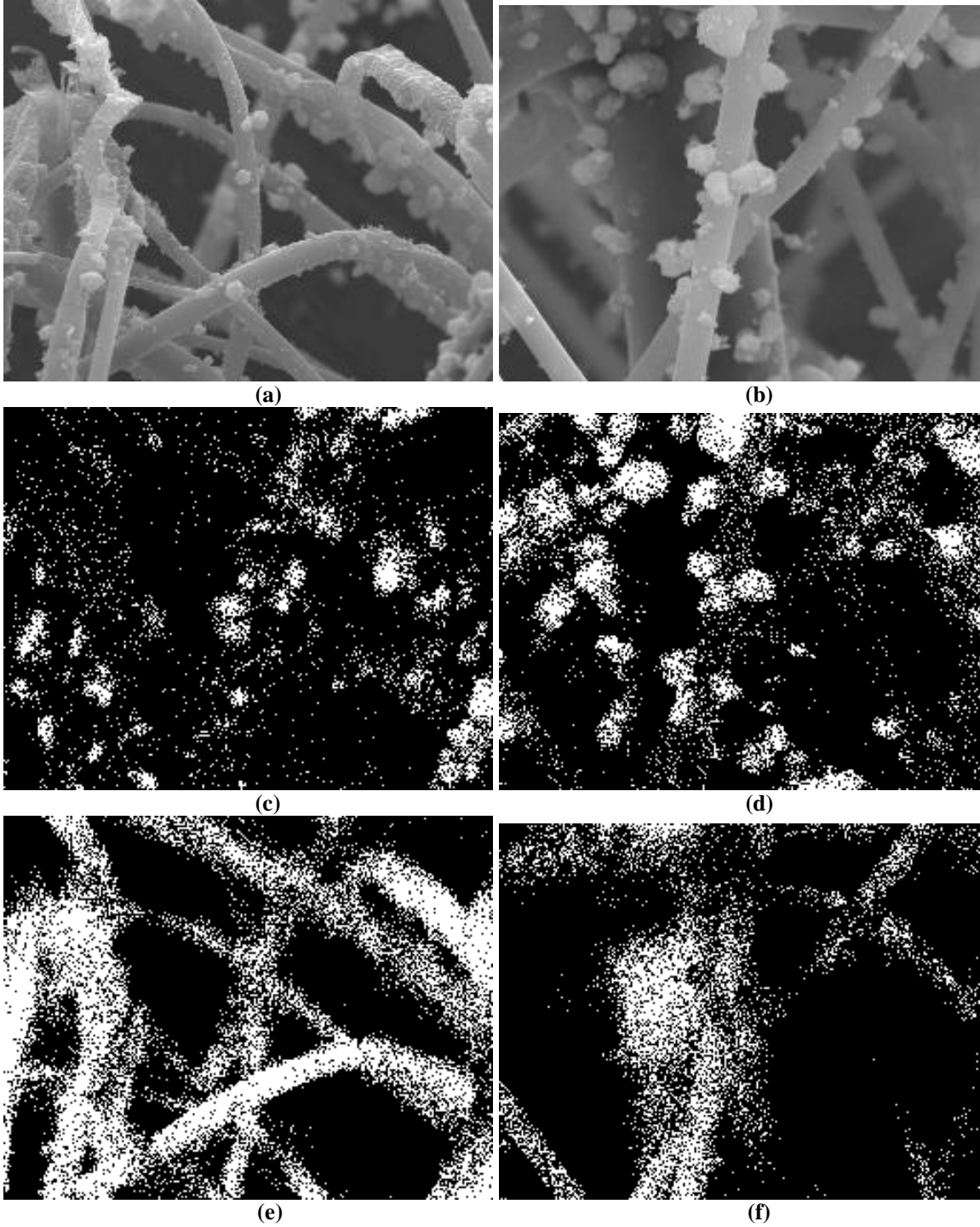


Figure 4.8(a) SEM image of the sample at location 1; (b) SEM image of the sample at location 2; (c) Ti detection by X-ray analysis at location 1 (area = 8.58 %); (d) Ti detection by X-ray analysis location 2 (area = 14.51%); (e) Carbon detection by X-ray analysis at location 1 (area = 33.56 %); (f) Carbon detection by X-ray analysis at location 2 (area = 21.78 %).

5 RESULTS AND DISCUSSIONS

In this section results obtained from experiments using the electrostatic spray system is presented and discussed first. Subsequently, results obtained from extrusion of bicomponent fibers using particle loaded polymer compound in meltblowing are discussed. In all cases the web and fiber characteristics are presented and discussed.

5.1 Electrostatic Spray Coated Web

As mentioned earlier the electrostatic spray system was adapted to the meltblowing system in three stages. To increase the particle loading minimum particle loss the “Initial” setup was modified. For distinction this test setup will be identified as “Modified” set up. The modified setup was further improved and optimized to the “Final” setup. During the various stages of development, test samples were produced and characterized for various properties like loading percent by weight, uniformity of particle distribution and ultraviolet transmission. Also results of studies done to understand the effect of process parameters on the web characteristics are detailed in the following sections.

5.1.1 Effect of carrying air pressure and spray height on loading percent

Carrying air pressure governs the amount of powder particles transferred from fluidization hopper to the gun, for details see **section 2.2**. Thus, higher carrying air pressure should increase the amount of particles sprayed, and therefore should increase the percent particle loading of the web. This phenomenon was studied on the final setup shown in **Figure 4.6**, at various carrying air pressures (0.2, 0.4, 0.6 and 0.8 bar) and height of spray ($h = 2$ and 4 cm). Other processing parameters used on the experimental set up are mentioned in **Table A1** in Appendix A. **Figure 5.1** shows the results of the percent particle loading by weight, calculated by the procedure mentioned in **section 4.4.1**, for various carrying air pressures and spray heights. It shows that by increasing the carrying air pressure from 0.2 bars to 0.8 bars, percent weight loading of the web increased from less than 10wt% to 94wt% for all the spray heights. Increase of carrying air pressures from 0.2 bars to 0.4 bars did not change the loading percent significantly and that must be due to improper functioning of the electrostatic spray gun at very low air pressures.

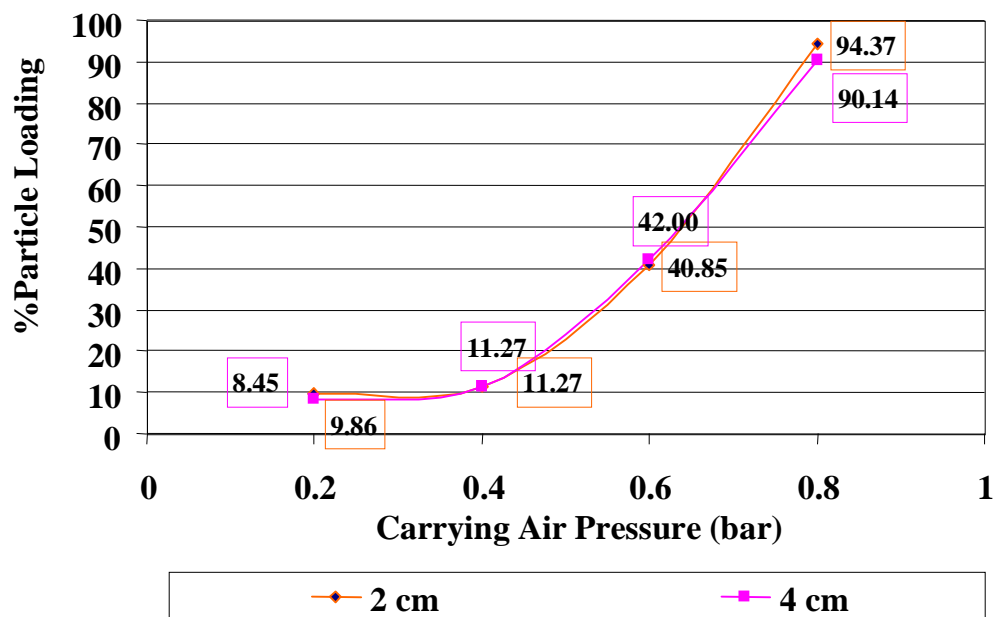
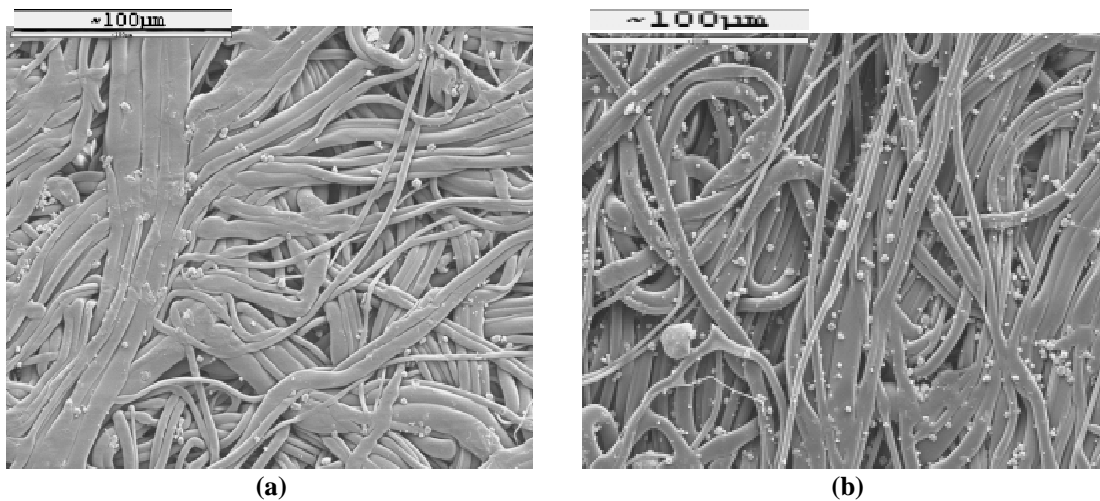


Figure 5.1 Graph showing effect of carrying air pressure on particle loading %.

Scanning Electron Microscopy (SEM) images of the samples listed in **Figure 5.2(a)-(e)** show the difference in particle loading due to variation in carrying air pressures but the difference becomes much less evident for higher loadings and at high magnifications.



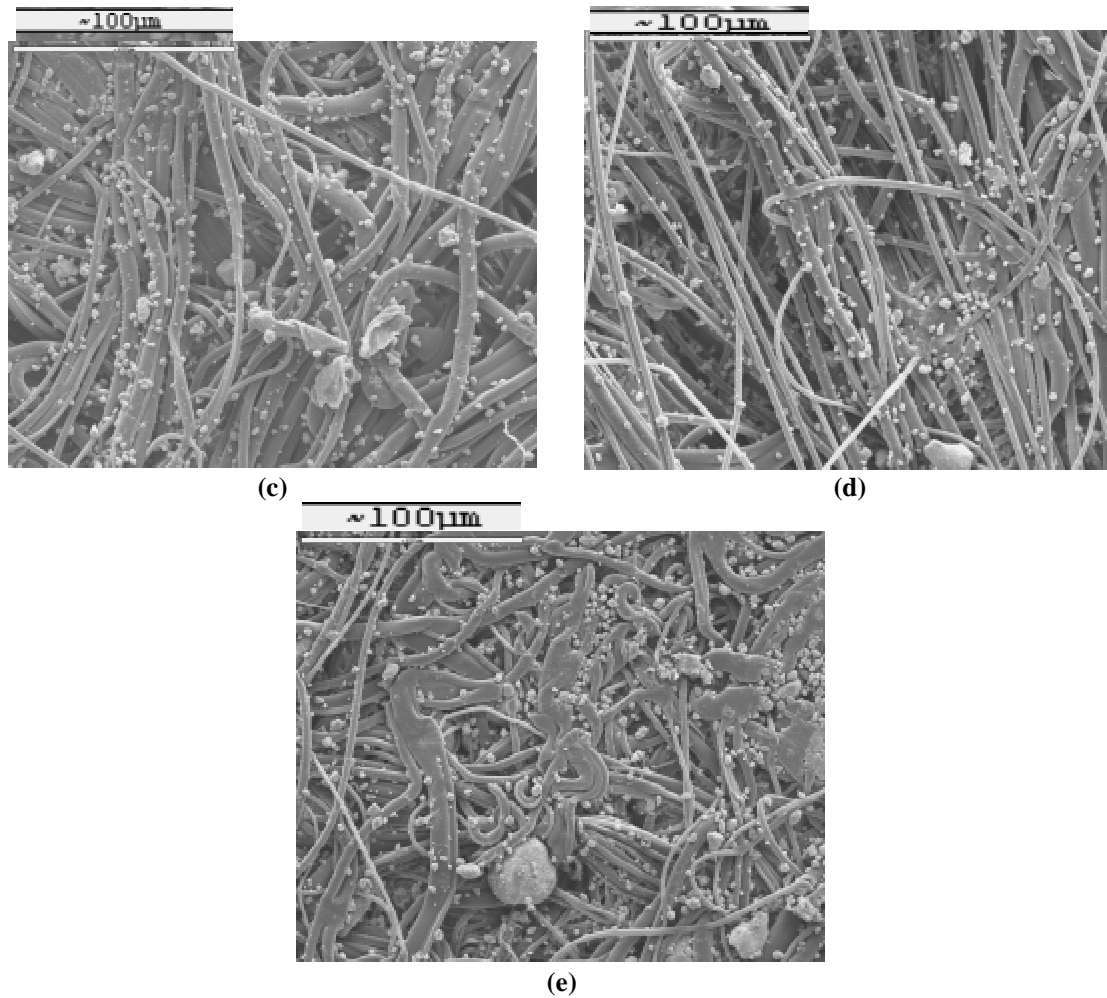


Figure 5.2 SEM images of samples of various loading percent by weight (a) 2%; (b) 8%; (c) 40%; (d) 42%; (e) 90%.

5.1.2 Particle distribution in web

Particle distribution in the web was assumed to be governed by the particle size distribution, carrying air pressure and design of spray attachment. Particle size distribution is affected by fluidization pressure; as at higher fluidization pressure chances of particle deagglomeration is higher and hence, the probability of having finer particles with low variation in size. For all the samples fluidization pressure of 5-6 bars was used thus, effect of fluidization could be considered same for all the samples. Carrying air pressure and design of spray attachment governs the velocity of carrying air stream at exit point of spray and hence, interaction of carrying air with primary air stream. Carrying air pressure and spray attachment's effect on distribution was qualitatively studied through Scanning Electron Microscopy (SEM) micrographs. Some of the SEM micrographs showing particle

distribution at high magnification are shown in **Figures 5.3(a)-(f)**. The figure shows that the best uniformity in particle distribution is obtained for the “final” setup, **Figures 5.3(e)-(f)**. Since “final” setup was designed so as to spray particles with minimum carrying air velocities hence, it can be concluded that the particle distribution uniformity improves significantly with decrease in carrying air velocities.

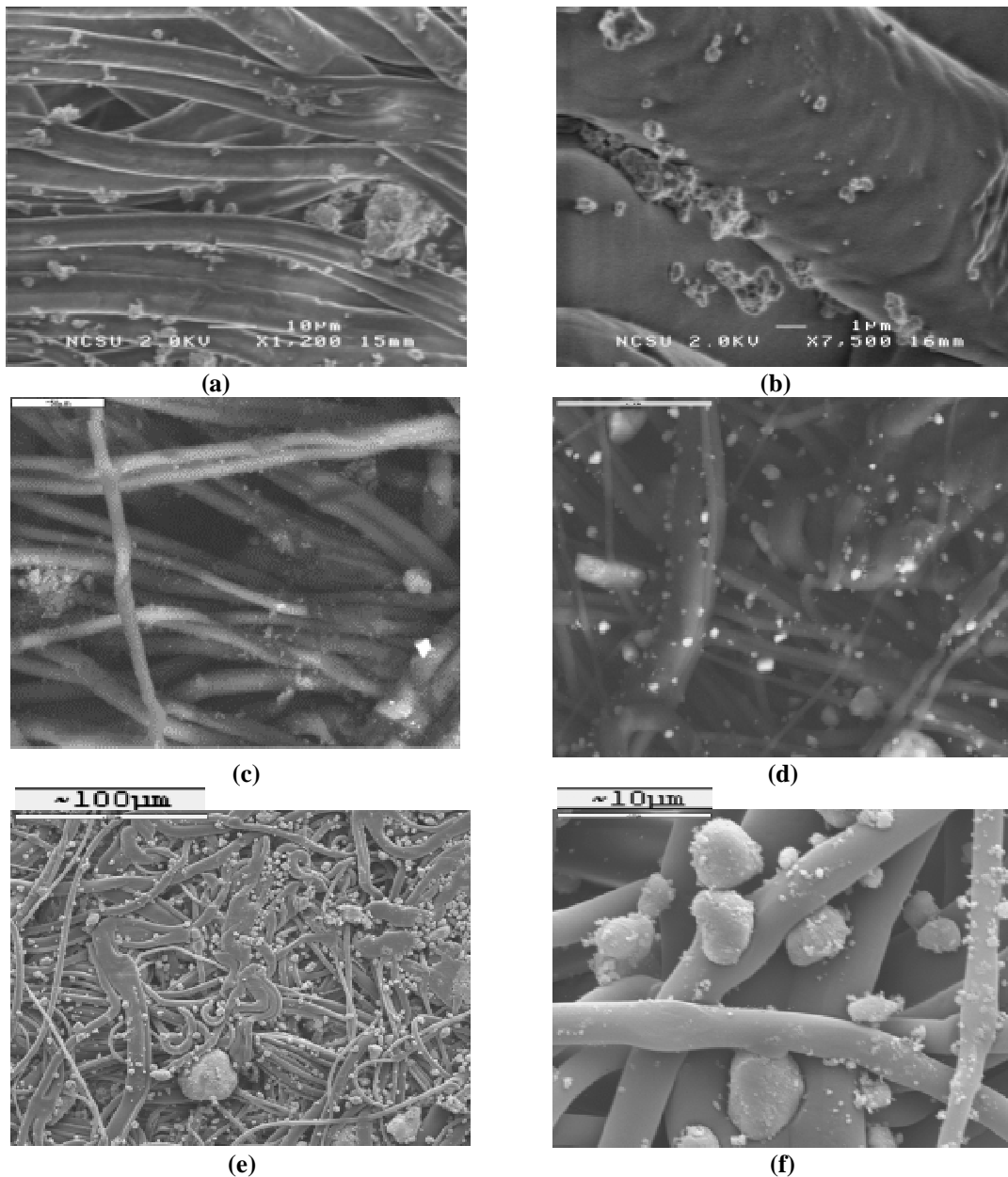


Figure 5.3 (a) High particle loading by initial setup at 1200X; (b) high particle loading by initial setup at 7500X; (c) high particle loading by modified setup at 500X; (d) high particle loading by modified setup; (e) high particle loading by final setup at 40X; (f) high particle loading by final setup at 1200X.

5.1.3 Web Characterization – Spray Coated Web

All of the test samples made by using the different setups are characterized for various properties like aerial density, loading % by weight and UV transmission.

5.1.3.1 Percent Particle Loading

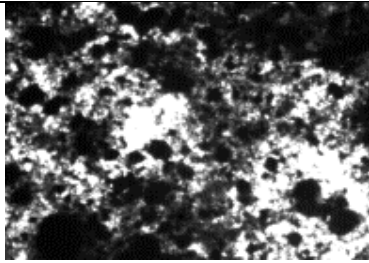
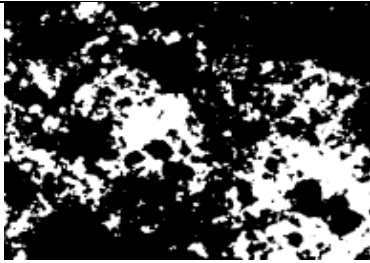
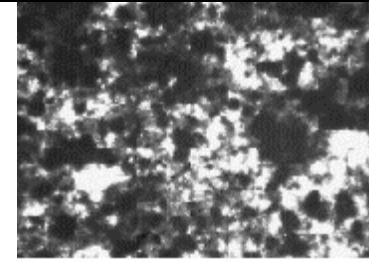
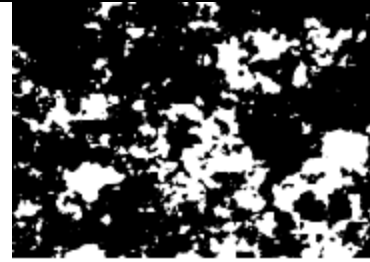
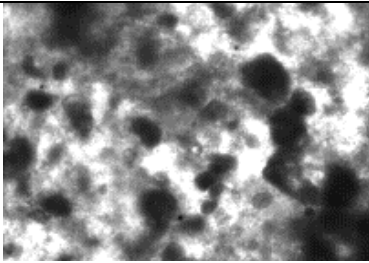
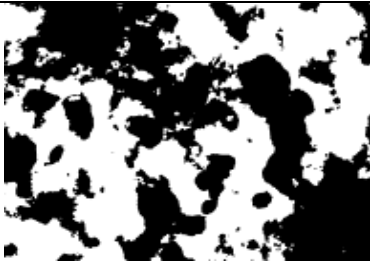
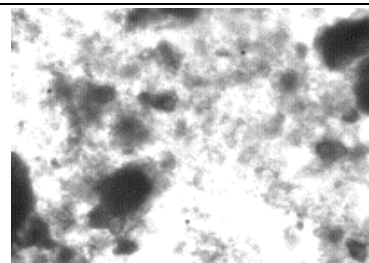

Particle loading by weight and volume of all of the samples was measured by procedures described in **section 4.4.1**. Samples, M1 – M5 made by “modified” setup were than layered into 2 or 4 layer structure (referred as ‘2L’ and ‘4L’ in the **Table 5.1**). Samples, M6 – M9 are made by “final” setup. Loading percent by weight ranges from ~8wt% to 94wt% for the samples made by various setups. The results are summarized in **Table 5.1**.

Table 5.1 Summary of measured particle loading (%) by weight and volume for external coated samples.

Sample #	Aerial Density (gms/m ²)	% Particle Loading	
		(by weight)	(by volume)
M1-2L*	50	32	N.A.
M1-4L*	85	32	N.A.
M2-2L*	54	28	N.A.
M2-4L*	107	28	N.A.
M3-2L*	66	40	N.A.
M3-4L*	113	40	N.A.
M4-2L*	61	25	N.A.
M4-4L*	125	25	N.A.
M5-2L*	61	45	N.A.
M5-4L*	145	45	N.A.
M6**	78	8.4-9.8	15% - 19%
M7**	79	11.2 - 11.4	45% - 49%
M8**	100	40.8 - 42.0	70% - 73%
M9**	138	90.1 - 94.3	78% - 82%
* -2L and 4L refers to 2 layer and 4 layered structure respectively.			
** - % particle loading by weight and volume shows the range for two height of spray 2cm and 4cm resp.			

Samples made by “final” setup are having much higher loading percents as well as distribution uniformity compared to samples made by “initial” or “modified” setups, refer **Table A1** in Appendix A for further details. **Table 5.2** shows the images obtained by optical microscopy in refractive index solution of samples made by “final” setup, and than processed by the procedure mentioned in **section 4.4.5**. It is to be noted that volume loading percent of 70-80% does not imply that 70-80% of the fiber surface is actually covered by particles. It is

due to the fact that all the particles are not present on the fiber surface but also trapped in voids in web. Also images obtained for calculation of particle loading by volume are the 2-dimensional representation of the 3-dimensional arrangement of the particles. Thus a particle present anywhere in the bulk of the web would block the light and appear as dark regions implying that all the fibers in that section of the web are covered by particles, which is actually not the case. Thus, value of volume percent loading obtained by this technique is higher than the actual volume percent loading.

Table 5.2 List of images obtained by optical microscopy in refractive index solution				
S. No.	Loading by Weight %	Optical Image in Refractive Index Solution	Image after processing by Maxtor Image Analysis Software	Loading by Volume %
M9	90 %			78 %
M8	42 %			73 %
M7	15 %			49 %
M6	8 %			19 %

5.1.3.2 UV- Transmission Testing

TiO₂ has been used in sunscreen lotions as ultraviolet (UV) shielding agent since decades. Therefore, TiO₂ loaded samples were tested for UV transmission and shielding by the procedure mentioned in **section 4.4.2**. Test results show that webs made by “modified” setup (M1-M5) and “final” setup (M6-M9) have very low UV transmittance or very high Ultraviolet Protection Factor (UPF) implying that these webs could be used as inner lining fabric for garments meant to provide protection from UV radiations. It is important to note that garments having UPF value greater than 40 could be used for a whole day protection from UV [37].

Table 5.3 UPF, %Blocking UV-A and %Blocking UV-B for samples made by modified setup.

Sample No.*	M1-2L	M2-2L	M3-2L	M4-2L	M5-2L	M1-4L	M2-4L	M3-4L	M4-4L	M5-4L
% Loading (by wt)	32	28	40	25	45	32	28	40	25	45
UPF	29	200	7-16	8-13	465	434	537	76	260	678
Blocking UV-A	90.8	96.2	80-88	81.0	99.3	98.1	98.5	96.8	97.8	99.4
Blocking UV-B	99.7	97.8	88-95	91-93	100.0	99.9	100.0	98.8	99.8	100.0

Table 5.3 shows the UPF values, %Blocking UV-A and % Blocking UV-B for samples made by the modified setup. UPF value is dependent on the amount of TiO₂ loading and its distribution. Therefore, the samples have UPF values ranging from 7 – 500 (for 2L structures) depending upon TiO₂ loading %, see **Table 5.3**. Higher TiO₂ loading gives better UV protection as expected except for M3-2L and M3-4L, which may be due to non-uniform distribution of particles. Comparing 2 layered (2L) and 4 layered (4L) structures; 4L has higher UPF values than 2L as expected. **Figure 5.4** shows the transmittance (%) as a function of wavelength. It is obvious that most of the samples has less than 10% transmittance for most of the UV radiation range.

Table 5.4 UPF, %Blocking UV-A and %Blocking UV-B for samples made by final setup.

Sample No.*	M6	M7	M8	M9
% Loading (by wt)	9.8	11.2	40.8	94.3
UPF	3	14	180	185
Blocking UV-A	65.0	86.0	96.0	96.0
Blocking UV-B	66.0	93.0	99.6	99.6

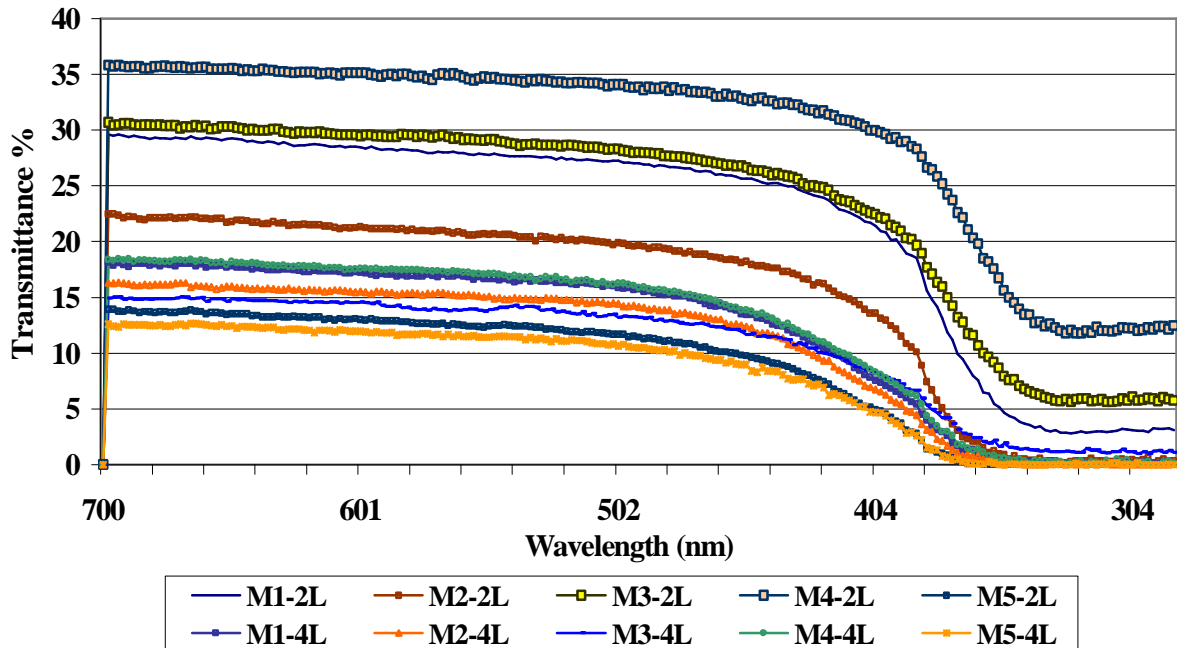


Figure 5.4 Ultraviolet transmittance for various wavelengths for samples made by modified setup.

Table 5.4 shows the UPF values, % Blocking UV-A and % Blocking UV-B for samples made by “final” setup. These samples were not integrated in multi-layered structure by the method described in Section 4.2 and were tested as is, nevertheless the samples (M8 and M9) with high TiO₂ content show high UPF values. Also the distribution of particles for these samples is highly uniform as compared to samples made using the initial setup and modified setup, as seen in Figure 5.2 and Figure 5.3. Therefore, significantly improved loading percent and uniform particle distribution led to high ultraviolet protection factor. Figure 5.5 shows the graphs of UV Transmission testing for 400-280 nm (wavelength range for ultraviolet radiations) for the samples made by “final” setup, M6 – M9. UPF of these samples is comparable to that of samples made by “modified” setup, M1 – M5 despite being monolayer, implying that integrating these samples into multi-layer structure would further enhance their performance as UV protection agent.

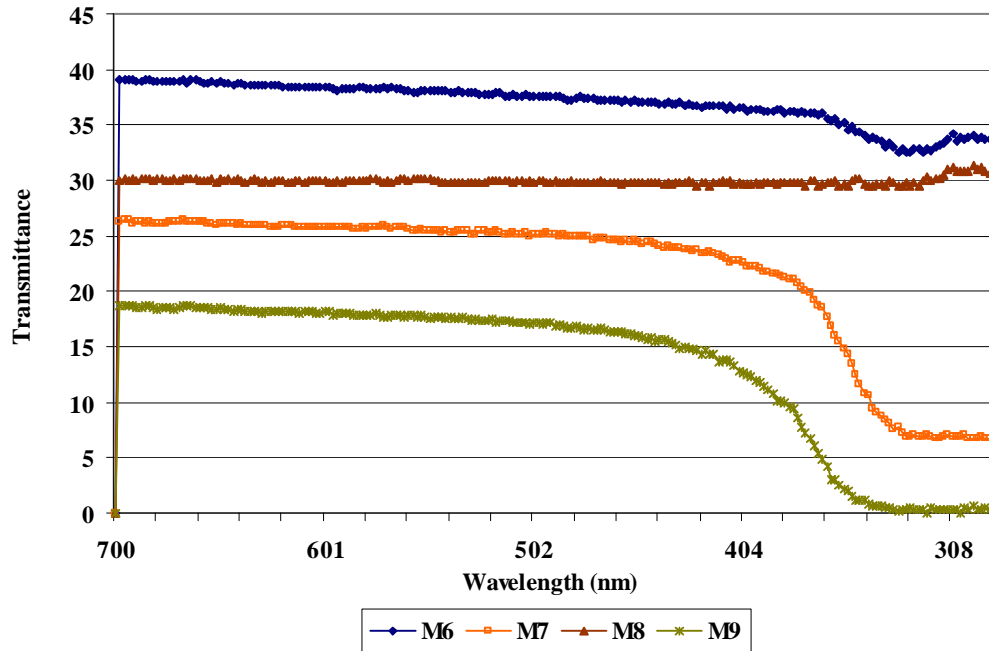


Figure 5.5 Ultraviolet transmittance for various wavelengths for samples made by final setup.

5.2 Bicomponent Web Structures

In spite of high loading and uniform distribution of particles in web made by using the final setup, the problem of heavy loss of particles in atmosphere at carrying air pressure >0.8 bars was of prime concern. Also the particles could subsequently be lost when used, as not all the particles are deeply embedded in fiber surface specially agglomerates that were just entrapped between fibers. Thus, bi-component spinning of sheath-core, side-by-side and biconstituent structures, as shown in **Figure 5.6**, with particle filled polymer as a component was tried.

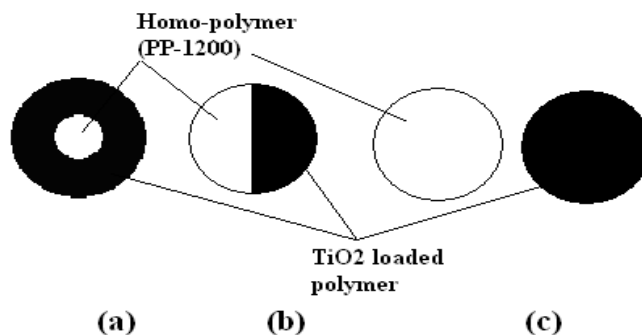


Figure 5.6 Schematic of various fiber cross-section configuration (a) sheath-core; (b) side-by-side; (c) bi-constituent.

There is ample evidence in published literature that addition of TiO₂ is likely to increase the viscosity (or decrease the MFR) of the melt [25-26]. Thus, rheological behavior of compounded polypropylene for various loading percent of TiO₂ (5wt%, 10wt%, 15wt% and 20wt%) was studied using a Minimelter (Haake) and a Rheometer (Advanced Rheometric Expansion System) at various shear rates and temperatures. Variation of melt viscosity as a function of shear rate for compounded polymers with various levels of particle loading is shown in **Figures 5.7(a)-(b)**. The compounded mixture of polypropylene and TiO₂ showed an increase in viscosity with increase in percent particle loading (5wt%, 10wt%, 15wt% and 20wt%) for all the measured shear rates as shown in **Figure 5.7(a)**. Based on this study and requirements for processability on meltblowing, a masterbatch with 20wt% TiO₂ was prepared. It should be noted that higher particle loading may lead to problems like chocking of filters, extruder and die surface abrasion, particle agglomeration in melt, melt rupture etc.

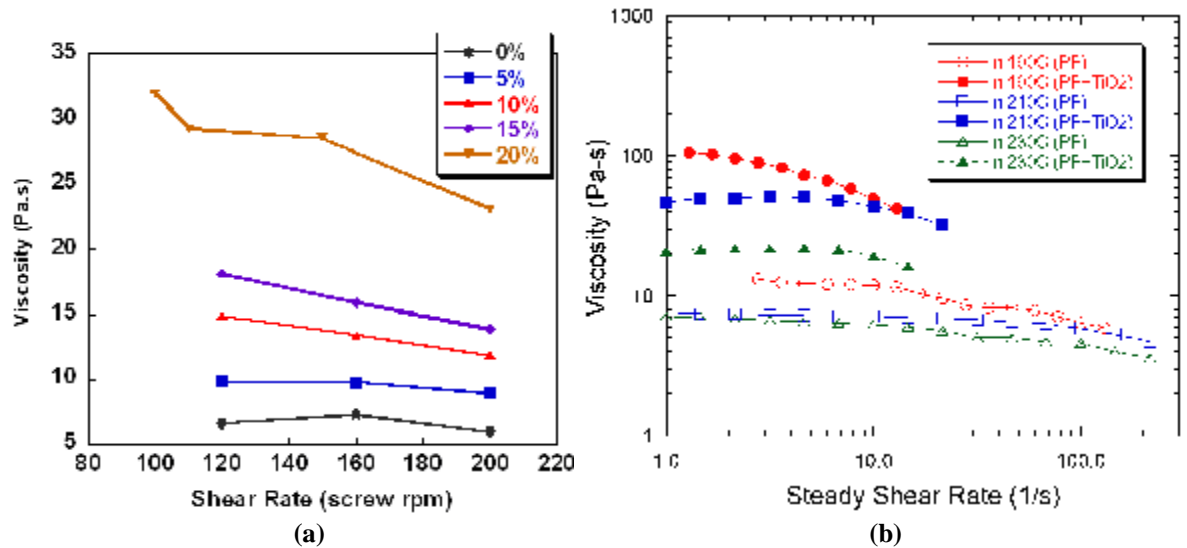


Figure 5.7 (a) Viscosity with shear rate at 200°C for TiO₂ filled polypropylene (PP-1200) melt at various loading percent (5%, 10%, 15% and 20%) by Haake Minimelter; **(b)** Viscosity vs. shear rate results of masterbatch for various temperatures (190°C, 210°C, 230°C) and loading percent (0%, 20%).

Figure 5.7(b) shows viscosity of homo-polypropylene and compounded masterbatch with shear rates at various temperatures of 190°C, 210°C, and 230°C. It can be concluded from the graph that the viscosity of the homopolymer as well as compounded polymer decreases with increase in shear rate, which is in agreement with the expected behavior of shear thinning polymeric system.

5.2.1 Characterization of Masterbatch

In addition to rheological behavior, the compounded masterbatch was characterized for particle loading uniformity, thermal behavior and particle size distribution as these parameters are known to play significant role in deciding spinning parameters and fiber formation.

Thermal Characterization

Particle loading by weight of masterbatch pellets was studied by the ash content of thermo gravimetric analysis (TGA). Five pellets were heated to 650⁰C and average ash content was measured. Ash content was found to be 20%+/-1% implying that the pellets had homogenous particle distribution. Differential scanning calorimetry of the compounded masterbatch showed a decrease in heat of crystallization (H_f) for both heating and cooling curves. Heat of crystallization is directly proportional to crystallinity of the sample. Hence, significant decrease in H_f value of masterbatch (< 80 J/gm) as compared to pure polypropylene (>100 J/gm), implies decrease in % crystallinity of the masterbatch. In other words, crystal formation capacity of the polymer decreased with increase in TiO₂ loading. This could be due to the TiO₂ particles acting as hindrance to chain orientation which is required to form crystals. However, further experimentation like x-ray analysis is required to support this hypothesis. **Figure 5.8** shows the DSC thermograms for the homopolymer polypropylene and compounded masterbatch.

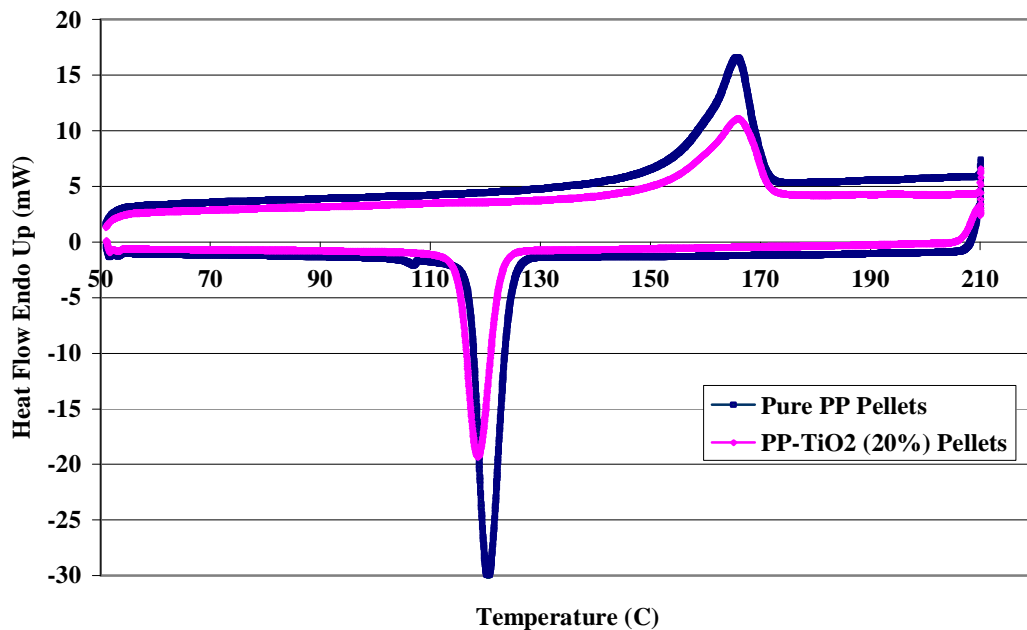


Figure 5.8 DSC analysis curves for pure homo-polypropylene and compounded master-batch.

Particle Size Distribution

Particle shape and size also plays important role in governing the shear viscosity and hence, spinning behavior [30]. Large particle and agglomerates may lead to melt rupture, extruder and die wall abrasion and die-holes clogging eventually leading to spinning failure. Thus, particles size distribution was studied carefully. Films of the masterbatch pellets were made by smearing the pellets on a glass slide at high temperatures, and were observed under optical and scanning electron microscopes at various magnifications.

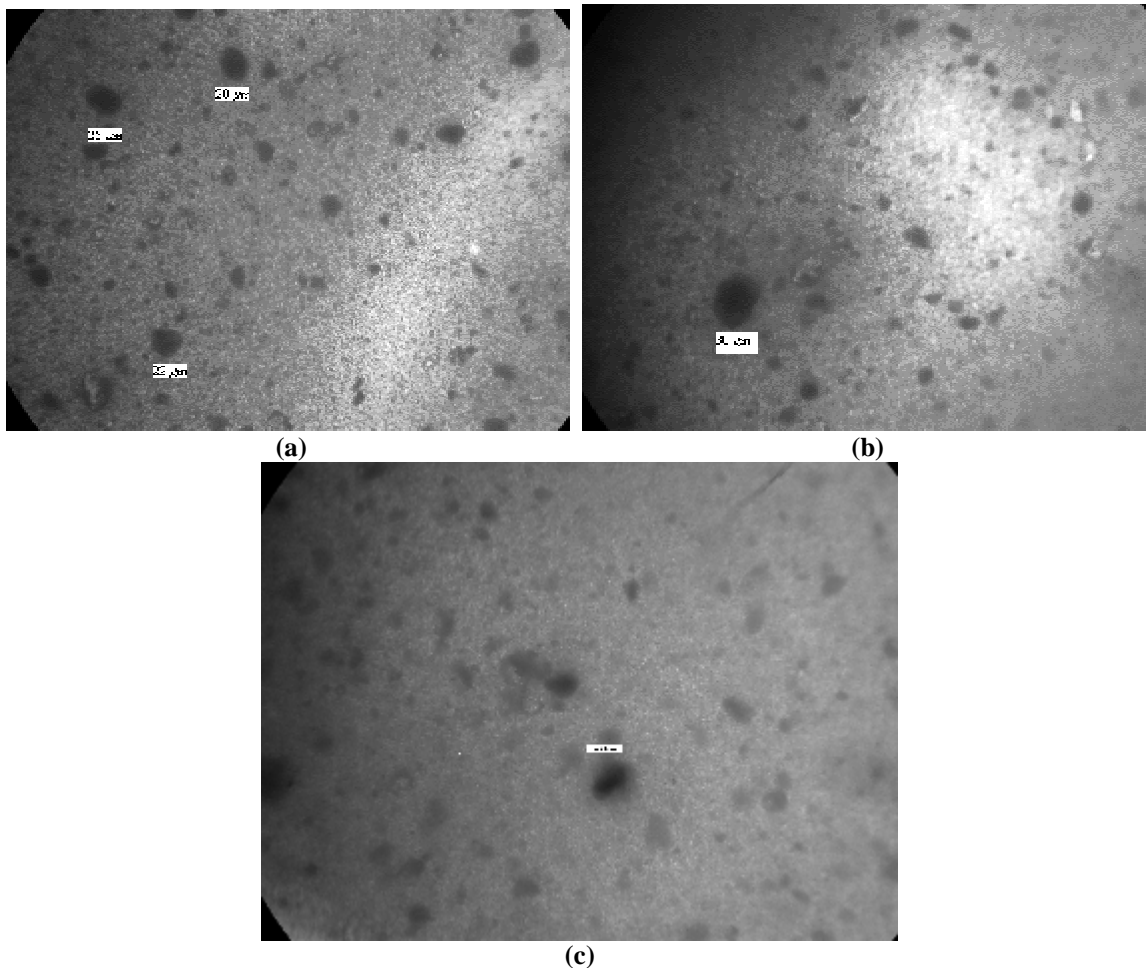


Figure 5.9 (a)-(c) Optical micrographs of masterbatch's smear.

Figure 5.9(a)-(c) and Figure 5.10(a)-(d) shows the optical and scanning electron micrographs of the samples. Though most of the particles in Figure 5.10(a)-(d) are less than 10 μm (mean particle size = 4 μm) some of the scanning electron micrographs and optical micrographs show particles up to 30 μm in dimension. With the possibility of these particles as dust or impurity, Energy Dispersive X-ray (EDX) for elemental analysis was performed. Figures 5.11(a)-(b) show the results of EDX confirming large particles as TiO₂. Though few

in number, these agglomerates could significantly affect the spinning. **Figure 12(a)-(b)** show that some of the seemingly large particles are agglomerates of large number of very small particles held together due to high affinity for themselves. These large agglomerates may or may not brake down due to the high shear force applied on polymer by extruder and walls of flow channels in meltblown die.

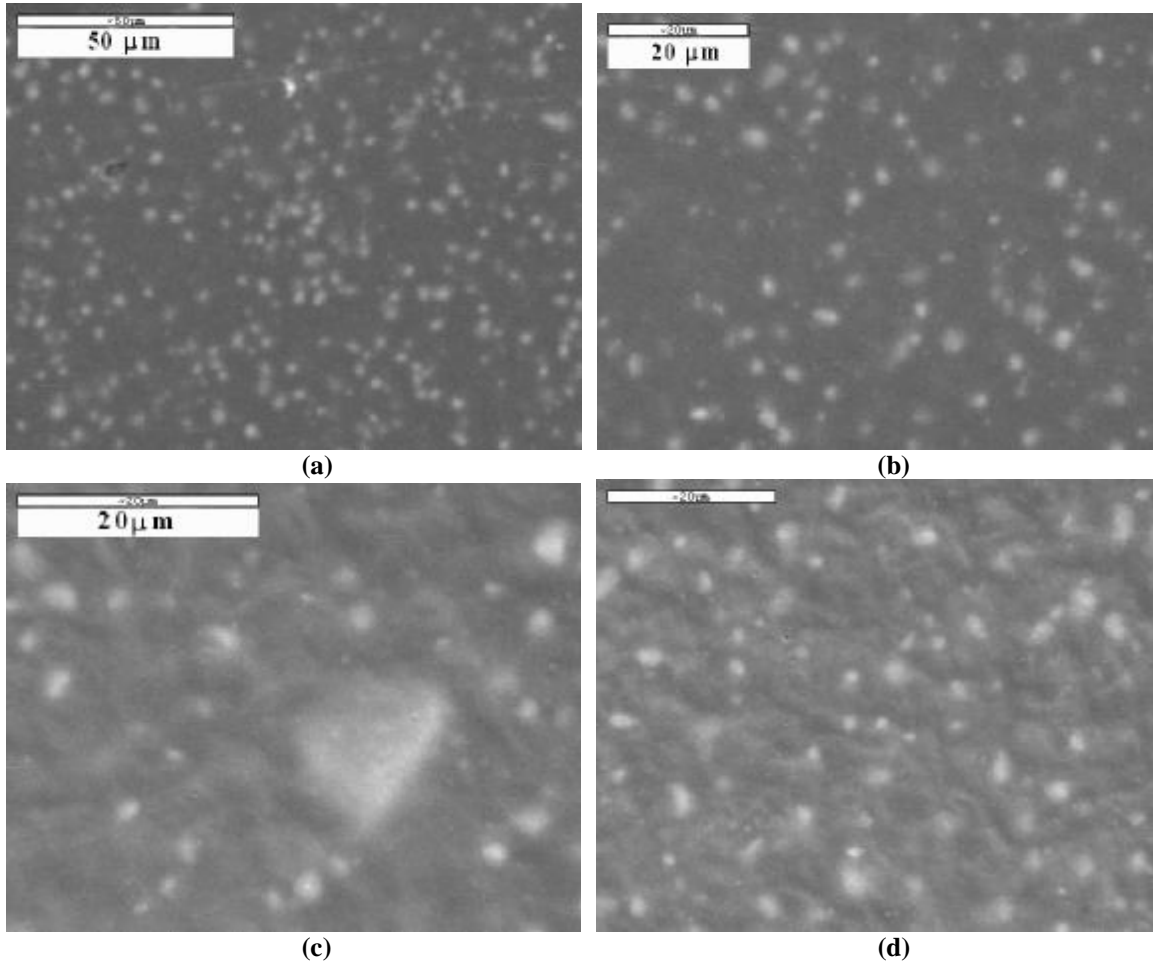


Figure 5.10 (a)-(d) Scanning electron micrographs of masterbatch's smear (mean particle size = 4 mm).

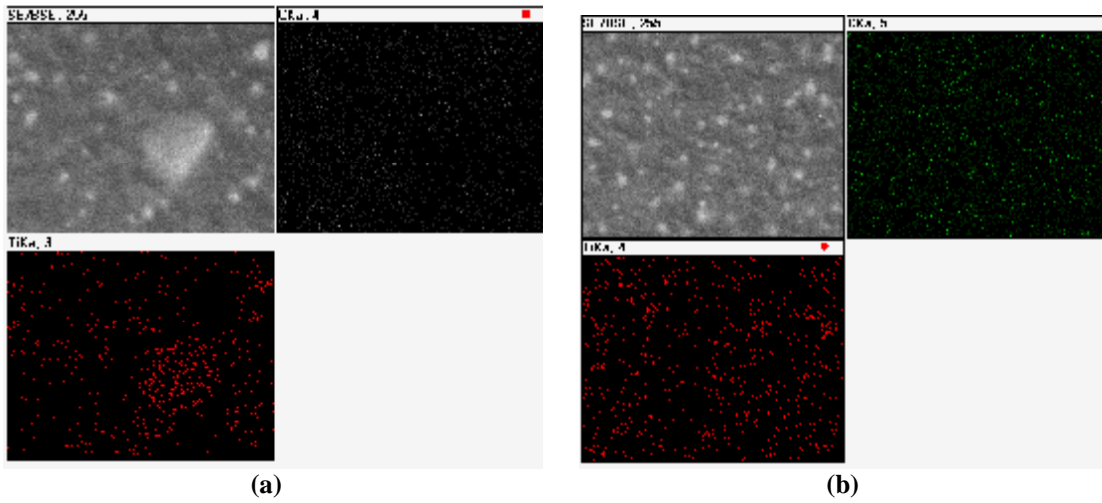


Figure 5.11 (a)-(b) X-ray analysis (EDX) of the smear for carbon and titanium.

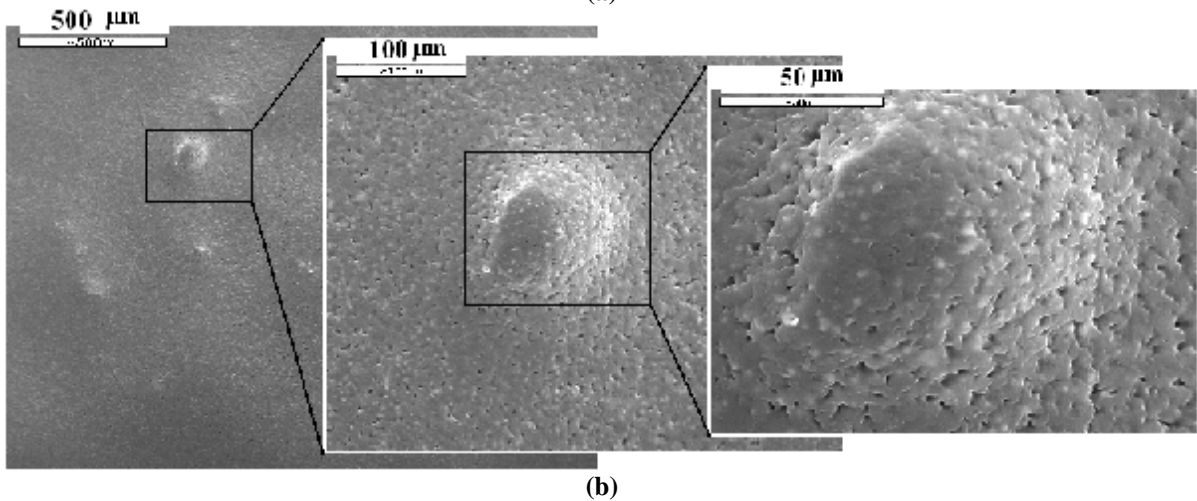
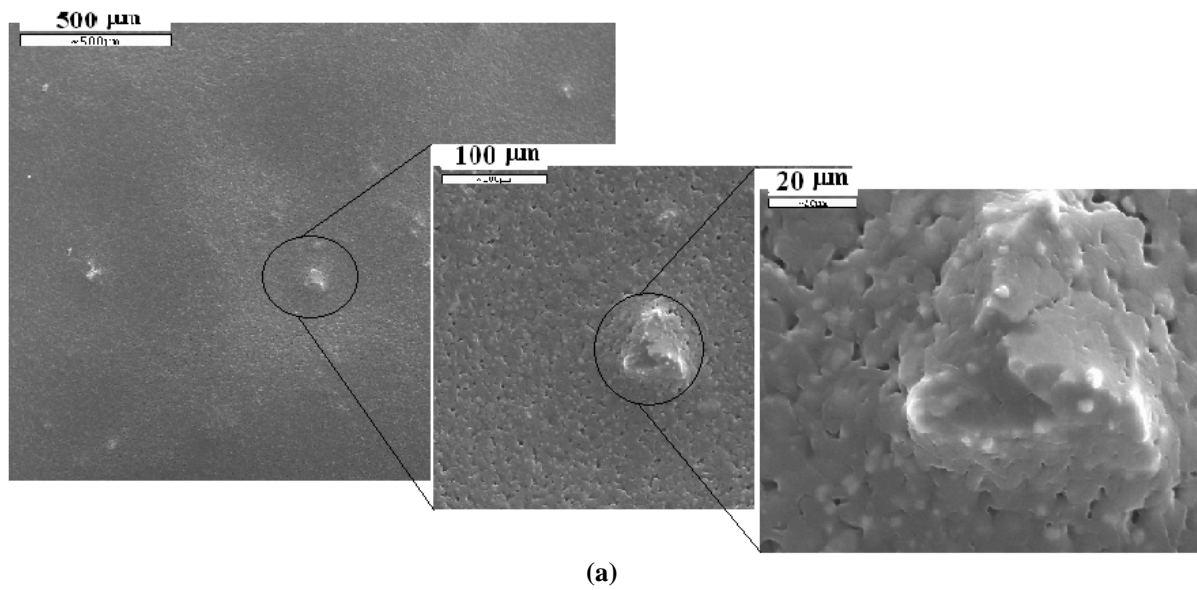


Figure 5.12 (a) – (b) Scanning electron micrographs of the smear at various magnifications highlighting the TiO₂ agglomerates in the melt.

5.2.2 Bicomponent and Biconstituent Structures

Bi-component and biconstituent fibers were meltblown on a pilot scale meltblowing setup¹ with 1200 MFR homopolymer polypropylene as one component and diluted compounded masterbatch as another. Samples of 0.1wt% loading was obtained by sheath-core bicomponent meltblowing. As suspected, meltblowing of compounded polymer with higher than 0.1wt% particle content caused spinning failure due to large number of particle agglomerates in the polymer melt. Shear forces generated in parallel plate die was not enough to break or extrude the particle agglomerates. This problem was compounded by some dead spots in the die acting as collection point of particles resulted in blocking of polymer flow passage leading to spinning failure.

Based on the observations of failure in sheath-core bicomponent extrusion, side-by-side die geometry was tried. In side-by-side geometry, the meltblown die does not have the narrow passage and bends, which acted as points of particle agglomeration eventually leading to spinning failure. In side-by-side die configuration, spinning failure was observed at a slightly higher particle loading, 0.50wt%, as compared to 0.1wt% as observed for sheath-core structures. Also along with die clogging, the fiberweb produced lacked sufficient integrity to be wound as fabric due to formation of large blobs known as ‘drips’. Further analysis of spinning failure is described in later sections. Process parameters for all the samples, made by sheath-core and side-by-side die configurations are listed in **Table A2** in Appendix A. In order to further increase the loading percent biconstituent fiber configuration as shown in **Figure 5.6(c)** was also tried. Samples with slightly higher loading of 0.75wt% was made beyond which spinning failure occurred. This time spinning failure occurred due to weak fiberweb and not due to die clogging. These samples were characterized to study the effect of TiO₂ loading percent.

Web Characterization

Samples made are characterized for loading percent by weight, thermal decomposition temperature and mechanical properties. Also TiO₂ shows photocatalytic activity and can be used as ultraviolet shielding agent, thus ultraviolet transmittance was also measured.

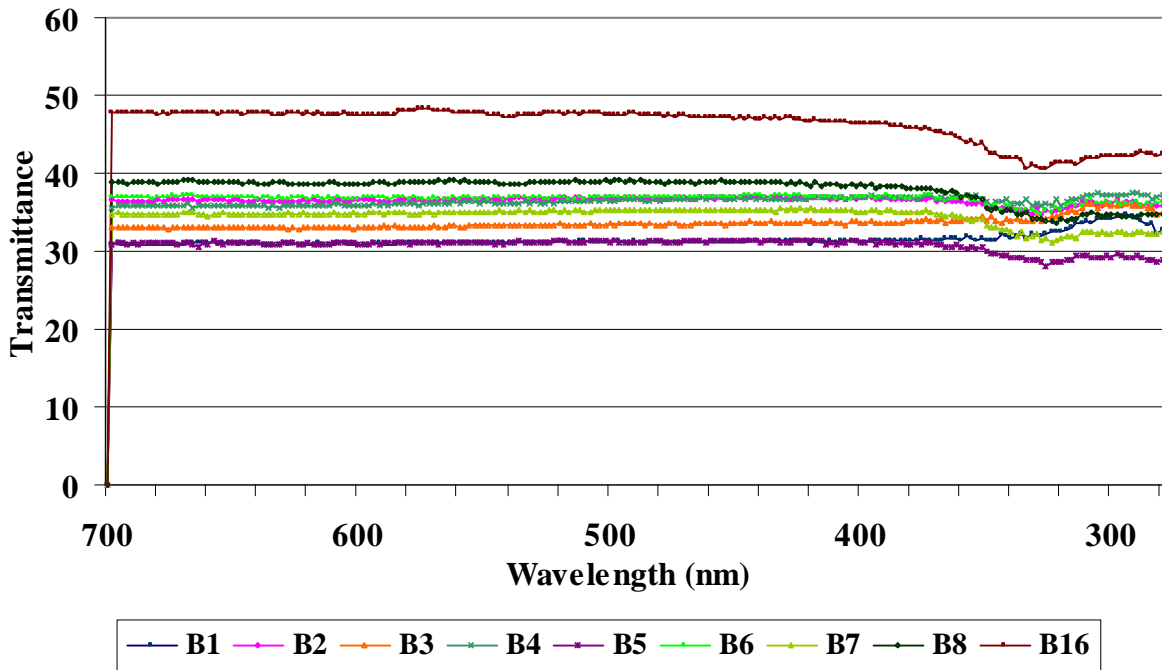
¹ 22” inch wide bicomponent meltblowing setup at NCRC Partner’s Lab (NCSU)

UV-Transmission Testing

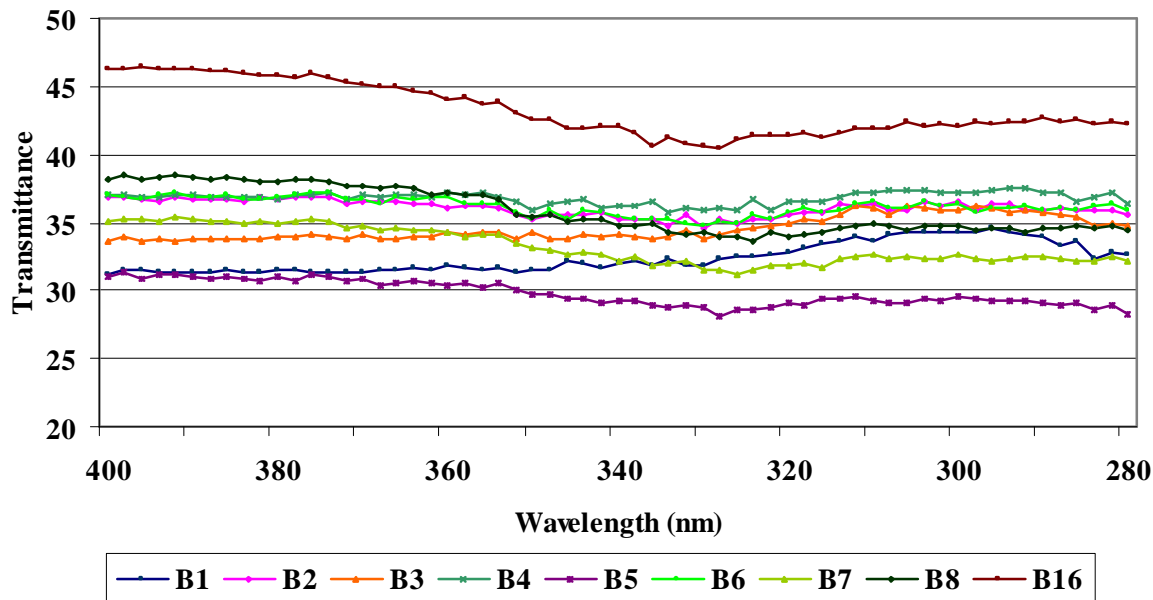
Ultraviolet transmission was measured by procedure mentioned in **section 4.4.2**. **Table 5.5** summarizes the UPF, % Blocking UV-A and % Blocking UV-B values for bicomponent samples. All the samples showed very low UPF values (<3.5) thus, low UV shielding effect. This must be due to the fact that total amount of TiO₂ present in the web was very low (particle loading by weight <1%).

Table 5.5 Summary of UV Transmission testing data for bicomponent samples.

Sample #	B1	B2	B3	B4	B5	B6	B7	B8	B16
% Loading (by wt)	0.0	0.1	0.00	0.10	0.16	0.20	0.24	0.30	0.75
UPF	2.97	2.77	2.81	2.70	3.41	2.77	3.09	2.88	2.38
% Blocking UV-A	68.16	63.96	65.96	63.35	69.94	63.79	66.31	63.54	56.33
% Blocking UV-B	65.20	63.83	64.12	62.78	70.69	63.89	67.64	65.39	56.51



(a)



(b)

Figure 5.13 UV transmission graphs of bicomponent samples B1 – B16 for wavelength (a) 700 nm to 280 nm; (b) 400 nm to 280nm.

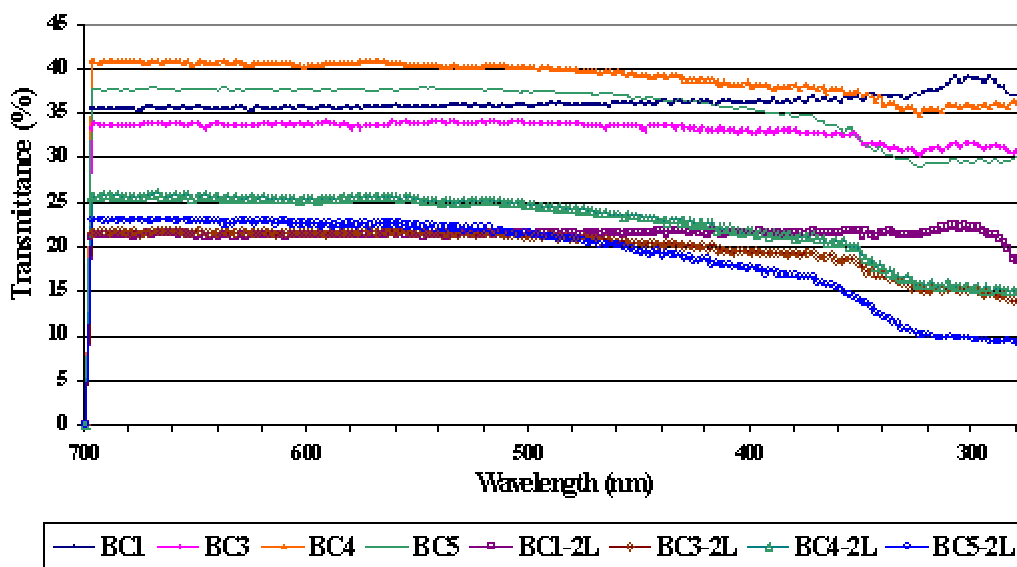


Figure 5.14 UV-transmission graphs for biconstituent samples BC1 – BC5.

Plotting transmittance values of the samples as a function of wavelength ranging from 700nm to 280 nm, **Figure 5.13(a)-(b)**, confirms their high UV transmittance and low protection. As expected all the samples had very low UPF values due to very low TiO₂ loading percent by weight, implying that none of these webs could be used for UV-shielding applications. But significant improvement in UPF values was observed after doubling the web, **Figure 5.14**. The reason for increase might be two folded: firstly, increase in TiO₂

content, and 2) higher aerial density with better uniformity of fiber and TiO₂ particles distribution in web. Thus, the biconstituent webs, BC1-BC5, have low % blocking values for both UV-A and UV-B as single layer but these values improves a lot if these webs are bonded into a stacked 2 layer structure, BC1-2L – BC5-2L. **Table B10** summarizes the UPF value, % Blocking UV-A and % Blocking UV-B of the biconstituent samples, BC1-BC5.

Thermo Gravimetric Analysis (TGA)

Thermal decomposition temperature of the particle loaded meltblown webs was measured using thermo gravimetric analyzer. In case of bicomponent sheath-core structures, B1-B2, addition of 0.1wt% TiO₂ increased the decomposition temperature by 27⁰C as shown in **Figure 5.15**. Similar trends were observed for bicomponent side-by-side structures, B3-B8 where loading of 0.3wt% increased the decomposition temperature by more than 100⁰C, see **Figure 5.16**. As discussed in **section 2.4.2** Chiu [34] reported similar results for TiO₂ filled polypropylene. Rusu and co-workers [39] has seen similar trends for polyethylene filled with zinc particles.

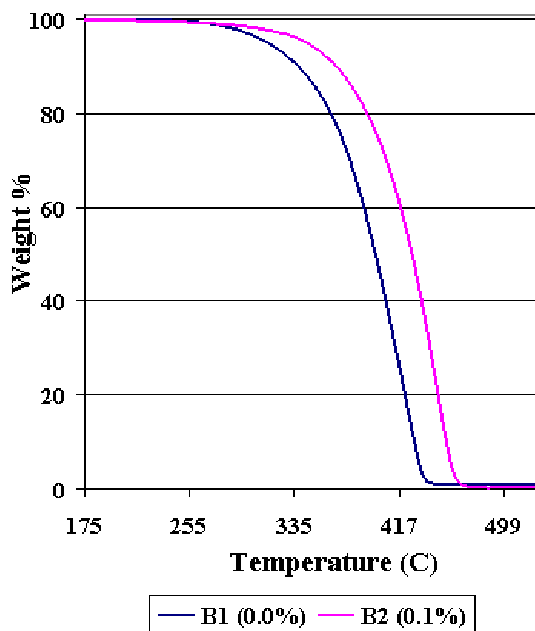


Figure 5.15 Thermo gravimetric analysis graphs of bicomponent sheath-core fiber structures, B1-B2.

Figure 5.17 shows that increase in loading of 0.5wt% of TiO₂ in samples BC5 compared to sample BC3 caused an increase of ~32⁰C in the decomposition temperature. Comparison between biconstituent and bicomponent samples shows that decomposition temperatures are higher for higher loading %, for example, biconstituent sample, BC5 with

0.7wt% loading has decomposition temperature of 493.2 °C while that of bicomponent samples, B8 with 0.3wt% loading was 484.8°C. Published literature explains some of the similar trends based on change in crystal size due to crystal nucleation [32,33,40], change in thermal capacity [41] and enhanced diffusion barrier properties especially when nano-clays are used as fillers [42]. Most probable cause of increase in thermal decomposition temperature for the TiO₂ loaded samples made should be increase in heat capacity of the polymer due to the presence of TiO₂ particles. However, further experimentation is required to find the appropriate explanation of these observed results. **Table B2** and **B3** in Appendix B summarize the thermal decomposition temperature of the bicomponent, B1-B8 and biconstituent samples, BC3-BC5.

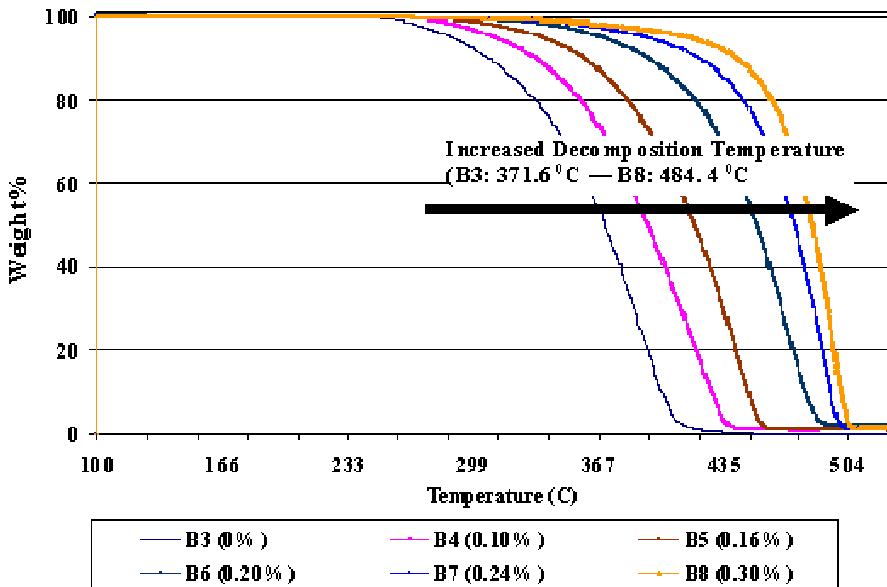


Figure 5.16 Thermo gravimetric analysis graphs of bicomponent side-by-size fiber structures, B3 - B8.

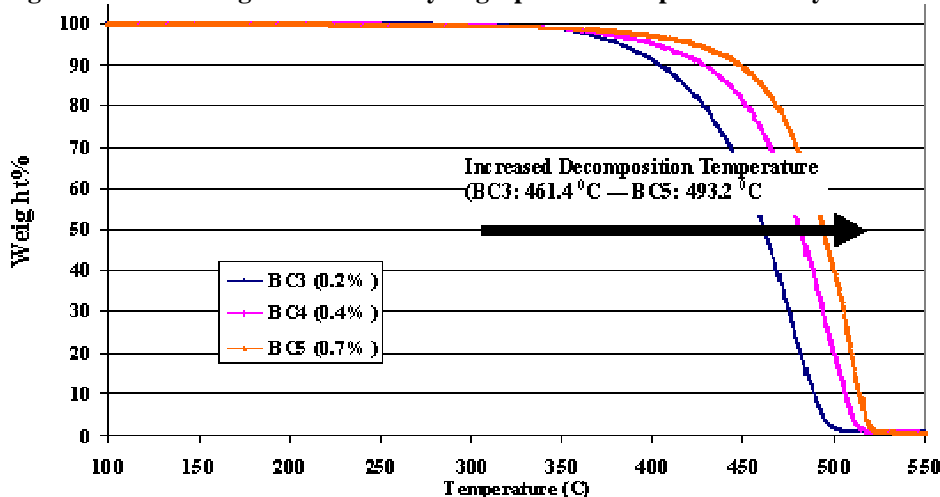
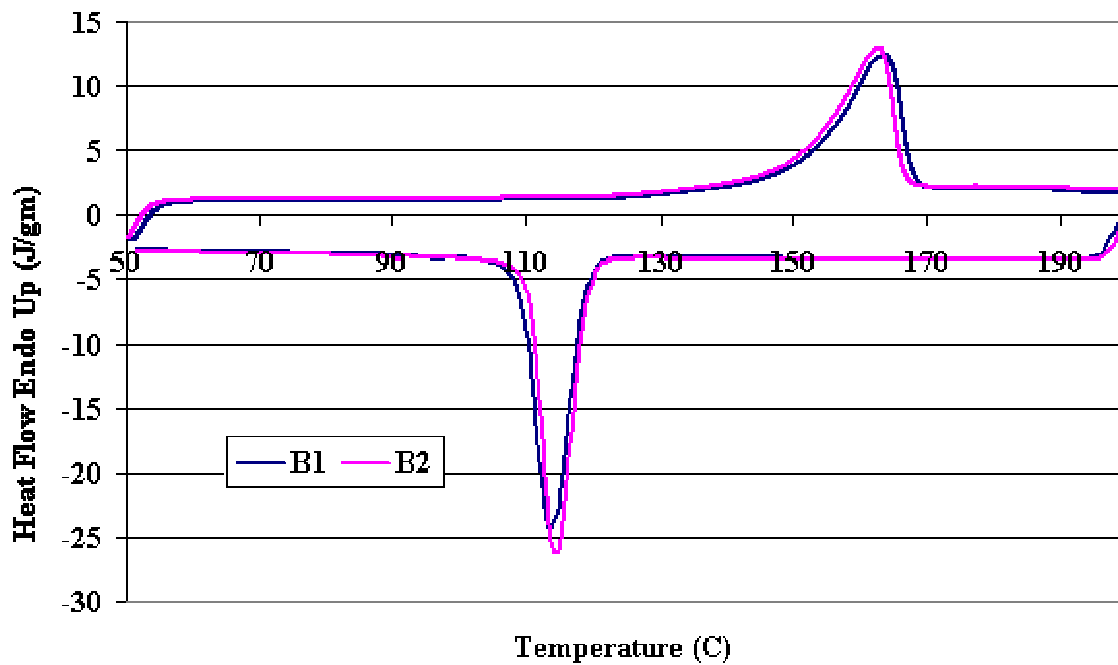


Figure 5.17 Thermo gravimetric analysis graphs of bi-constituent fiber structures, BC3 – BC5.

Differential Scanning Calorimetry (DSC)

Meltblow samples were investigated for their fine structures using differential scanning calorimetry. It has been observed that presence of particles in polypropylene decreases its crystallinity [31]. But results of DSC analysis of the bicomponent samples, B1-B15, shows that the presence of TiO₂ had no effect on crystallinity of the samples as there was no significant change in heat of crystallization, H_f value with various TiO₂ loadings. This may be due to the fact that loading percent of TiO₂ in the melt is very low (<1wt%) to have any significant effect on crystallization. Increase in loading percent to 3-5wt% or higher might be required to have any significant effect. It is also reported in the literature that presence of particles significantly changes crystal size [33], which would be reflected as change in melting point. But in this research no significant change has been observed in onset and peak temperatures of all the samples implying no significant change in crystal size. This could again be due to low loading or large size of TiO₂ particles (diameter : 4-6:μm). Large size particle might not interact with polymer chains in melt to act as nucleating agent. DSC thermograms of the bicomponent samples are shown in **Figures 5.18(a)-(b)**. There is no significant difference in heat of crystallization, H_f for both heating and cooling curves implying that there is no significant change in crystallinity of the samples, as heat of crystallization is directly proportional to crystallinity of the sample.



(a)

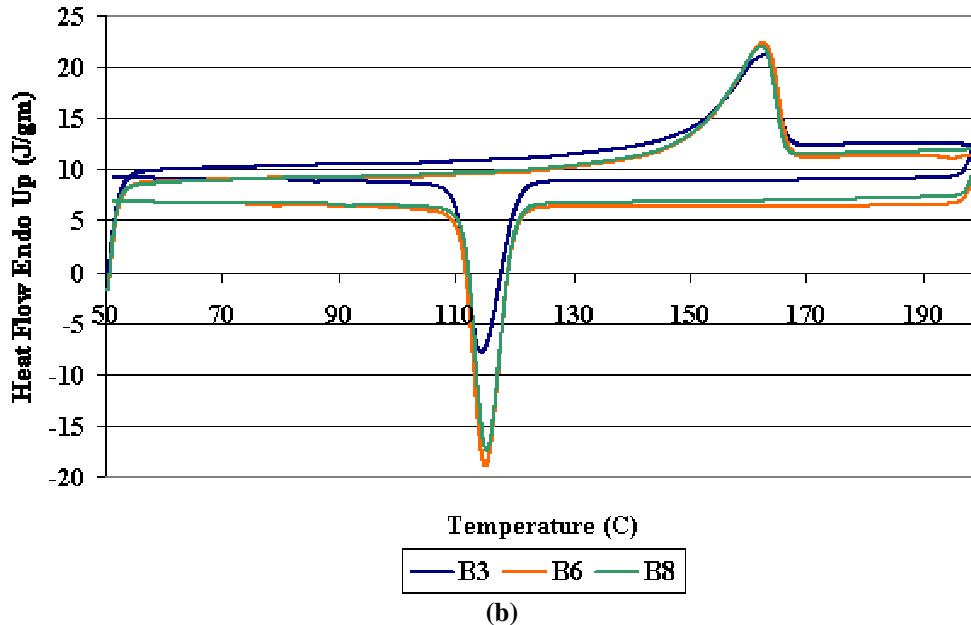


Figure 5.18 DSC thermographs of bicomponent samples (a) B1(0.0wt%-B2(0.1wt%); (b) B3(0.0wt%) , B6(0.24wt%) and B8(0.30wt%).

DSC results of biconstituent samples BC1-BC5, also doesn't show any significant change in f_c value, onset and peak temperature, as shown in **Figure 5.19**, implying that total crystallinity percent is not changing at all due to presence of TiO_2 particles. This may be due to the fact that percent particle loading is still not high enough to have any significant effect on total crystallinity. Further experimentation like X-ray analysis needs to be done to find out more about crystal sizes and structures.

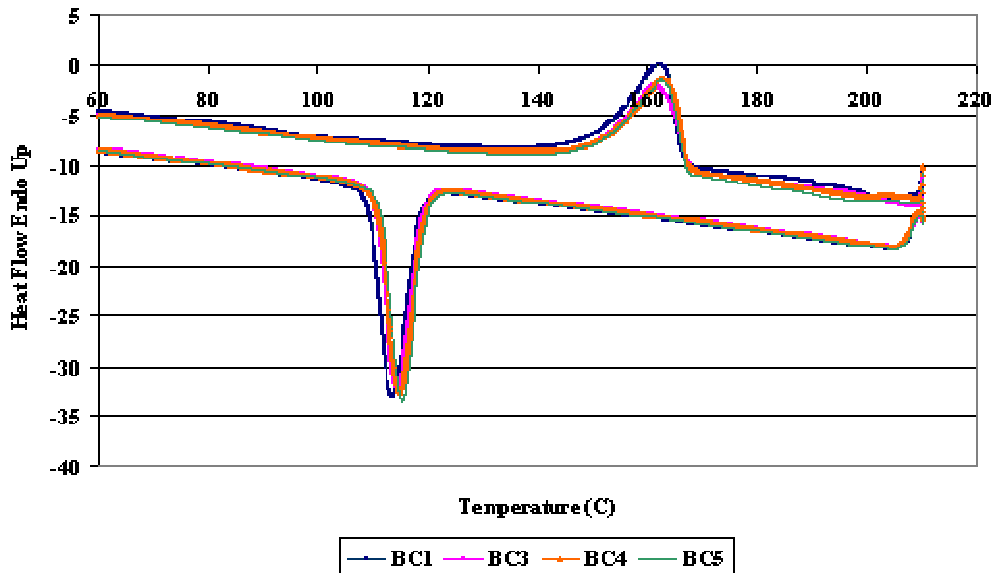
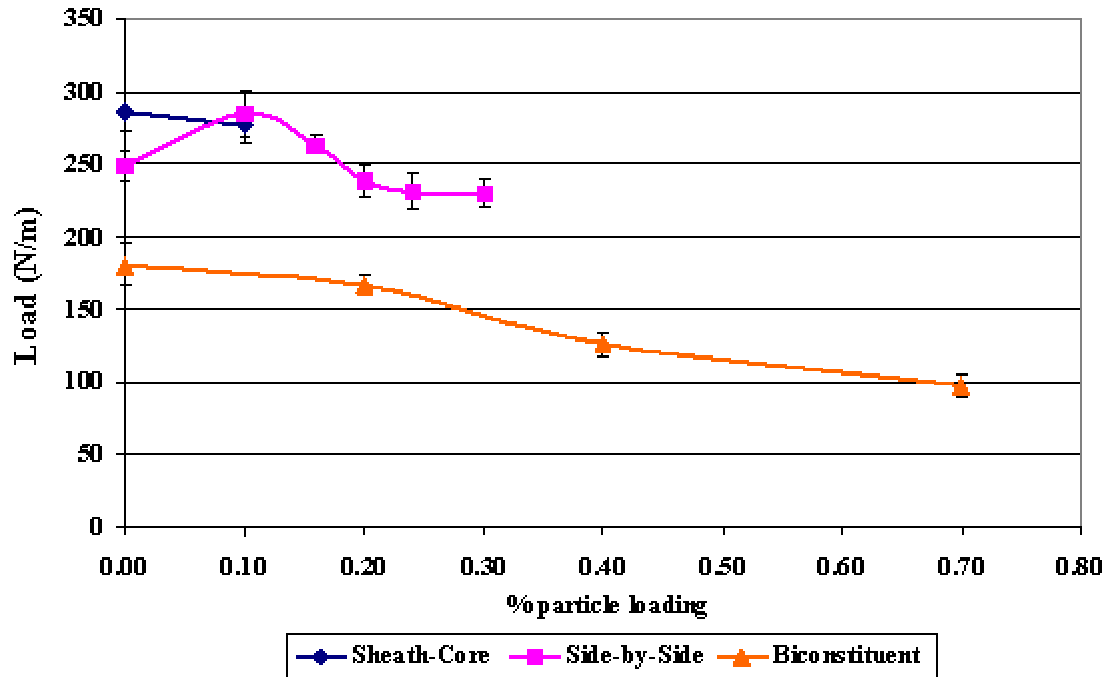


Figure 5.19 DSC thermographs of biconstituent samples, BC1(0.0wt%) – BC5(0.75wt%).

Mechanical Properties

Presence of particle is known to influence mechanical properties of fiber [75-79]. In this study mechanical parameters such as breaking load and strain%, tensile modulus, bending length were measured following ASTM test standards D5035-95 and D5732. **Figures 5.20(a)-(b)** shows the variation of breaking load of various fiberwebs as a function of particle content. As observed the breaking load decreased significantly with increased particle loading for bicomponent as well as biconstituent fiber configuration. Similar results were obtained for change in breaking strain% as a function of particle loading. The decrease in breaking strain % values was significantly more than that of breaking load. Thus, both breaking load and breaking strain% decreased with increase in percent particle loading. Unlike nanoparticles having positive effect on fiber mechanical properties, presence of TiO₂ particles having diameter in the range of 4-6 micron has a negative impact on the mechanical properties. It could be because of the large dimension comparable to that of the fiber size, thus their presence in the fiber bulk or as protrusion outside the fiber surface act as point of stress concentration decreasing the fiber strength and hence, web strength.



(a)

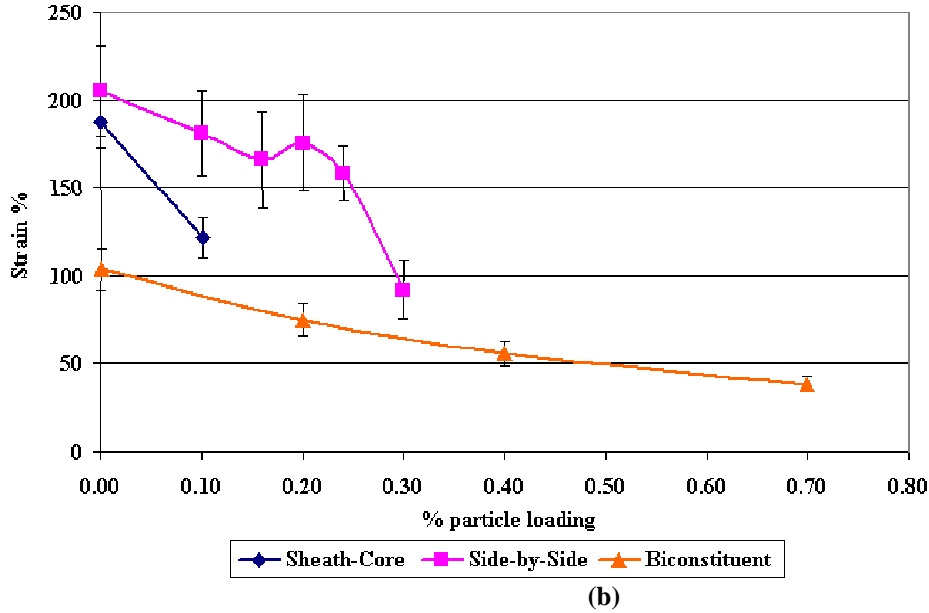


Figure 5.20 Graphs summarizing tensile strip test of bicomponent and biconstituent samples.

Similar results were obtained for bending test of the samples i.e. increase in TiO_2 loading percent leads to slight decrease in bending rigidity, see **Figure 5.21**. Further experimentation needs to be done to find out the possible cause of decrease in bending length with increase in percent particle loading.

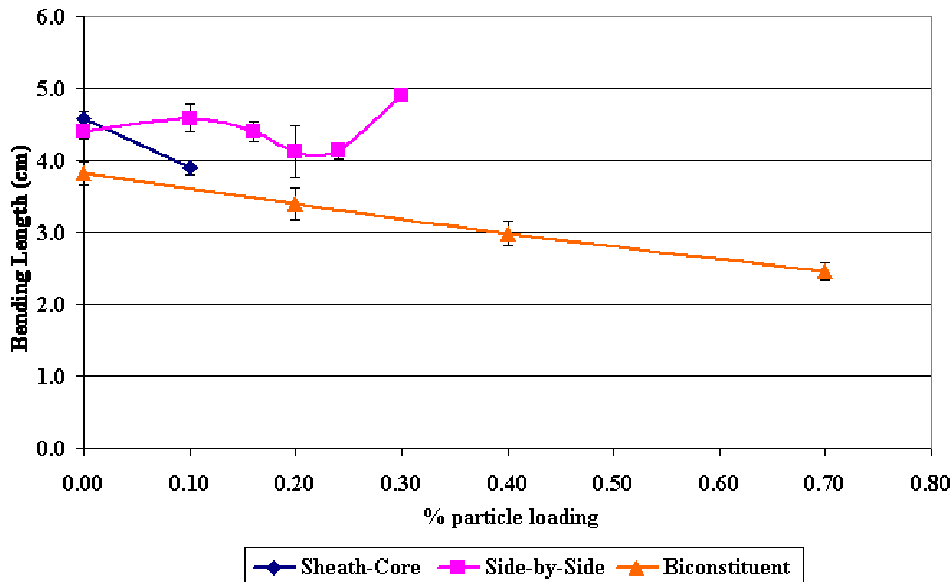


Figure 5.21 Graph summarizing bending length test of bicomponent samples B1 – B14.

Table B6 and **B7** in Appendix B summarize the results of strip test for bicomponent B1-B14 and biconstituent BC1-BC5 webs while **Table B8** and **B9** in Appendix B shows the results of bending length measurement for bicomponent and biconstituent webs.

Surface Characterization

In order to determine the efficacy of the processes utilized in this research in terms of fiber surface coating with the TiO_2 particles the fiberwebs were examined using various microscopy techniques. The bicomponent samples, B1-B20, were characterized for percent surface area covered using optical and scanning electron microscopy. Optical microscopy was done by the procedure mentioned in **section 4.4.5**. For bicomponent samples the highest particle loading being 1wt%, the surface area covered is expected to be very low. Some of the optical micrographs of the samples saturated with refractive index solution were obtained in transmitted light and are shown in **Figures 5.22(a)-(d)**.

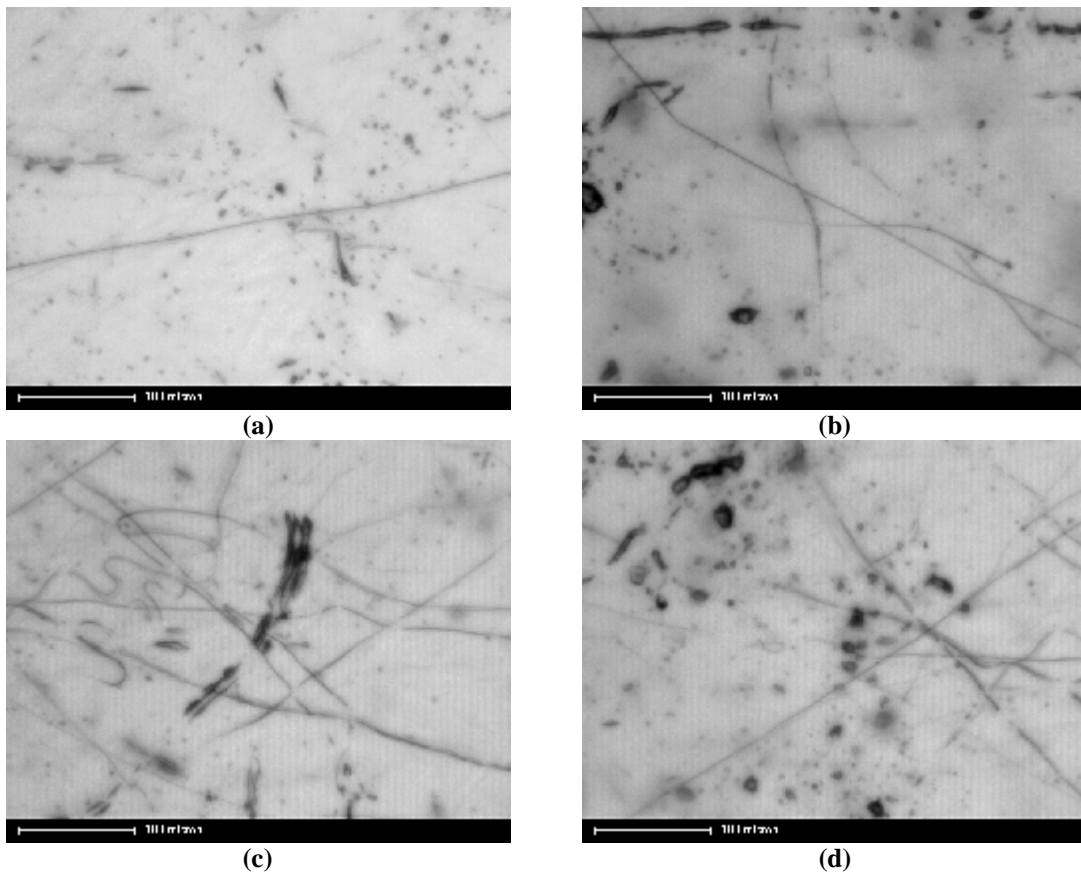


Figure 5.22 Optical micrographs in refractive index solution of some of the bicomponent samples at 10X.

These optical micrographs shows two prominent features: firstly, thick dark spots or short lines. The dark spots seems like voids in fiber bulk and secondly, thin dark lines seemingly TiO_2 particles strung along the fiber surface or in the bulk. Since the samples were saturated with refractive index solution before taking optical micrographs the thick dark spots could be either agglomerates or bubbles trapped in fiber bulk and not voids between two fiber surfaces. To confirm the true nature of dark spots optical microscopy by

stereomicroscope in reflected light was performed. **Figure 5.23** shows some of the optical micrographs taken by stereomicroscope by saturating the samples in refractive index solution for some of these samples. It is evident that most of the samples have small air bubbles trapped in fibers which earlier was appearing to be dark spots that could be interpreted as TiO_2 coating. Also note that amount of bubbles is increasing with amount of TiO_2 loadings from B3 (0.0wt%), **Figure 5.23(a)** to B5 (0.20%), **Figure 5.23(b)**, to B8 (0.3%), **Figure 5.23(c)**. Thus, further studies need to be done to explain the observed voids in optical micrographs as these voids could be the cause of spinning failure.

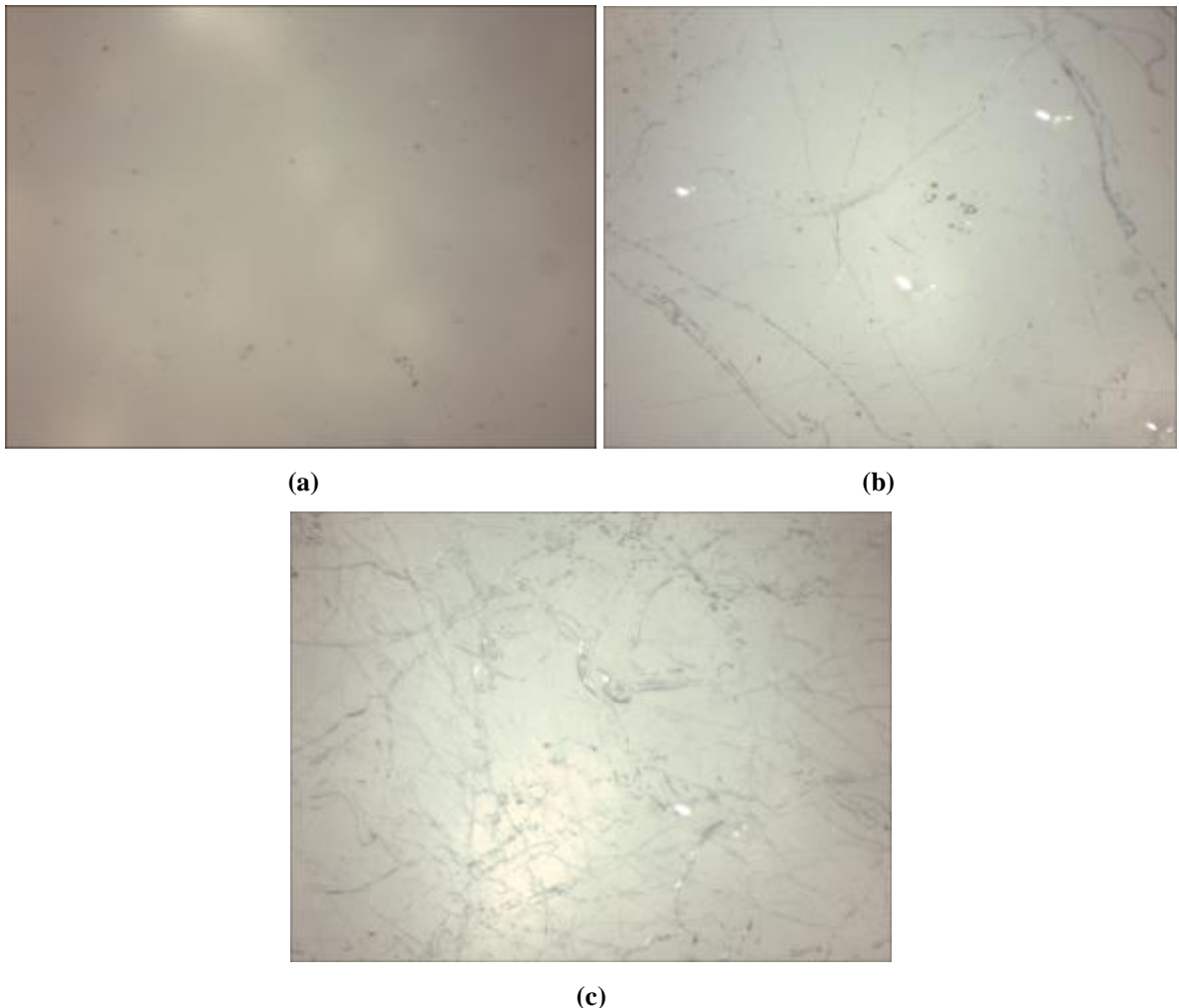


Figure 5.23 Optical micrographs in refractive index solution by stereoscope microscope at 10X (a) B3; (b) B5; (c) B8.

SEM micrographs were also taken at high magnifications to look into more details of the samples. Some of the micrographs as presented in **Figures 5.24(a)-(d)**. It can be seen that significantly low number of TiO_2 particles are on fiber surface. As discussed earlier for the masterbatch pellets, some particles were bigger than 10 micron and some of them were up to

30 microns as agglomerates. However, all the SEM micrographs shows that most of the particles are much less than 10 micron, implying that most of the bigger particles were either filtered out or broken down to smaller particle size or were deposited in the melt flow passage leading to spinning failure. Beyond 0.3wt% loading, test samples have lot of large size shots, also known as blobs, as seen in **Figures 5.25(a)-(b)**. These blobs looks more like dripping melt sputtered on the web after the web has been laid.

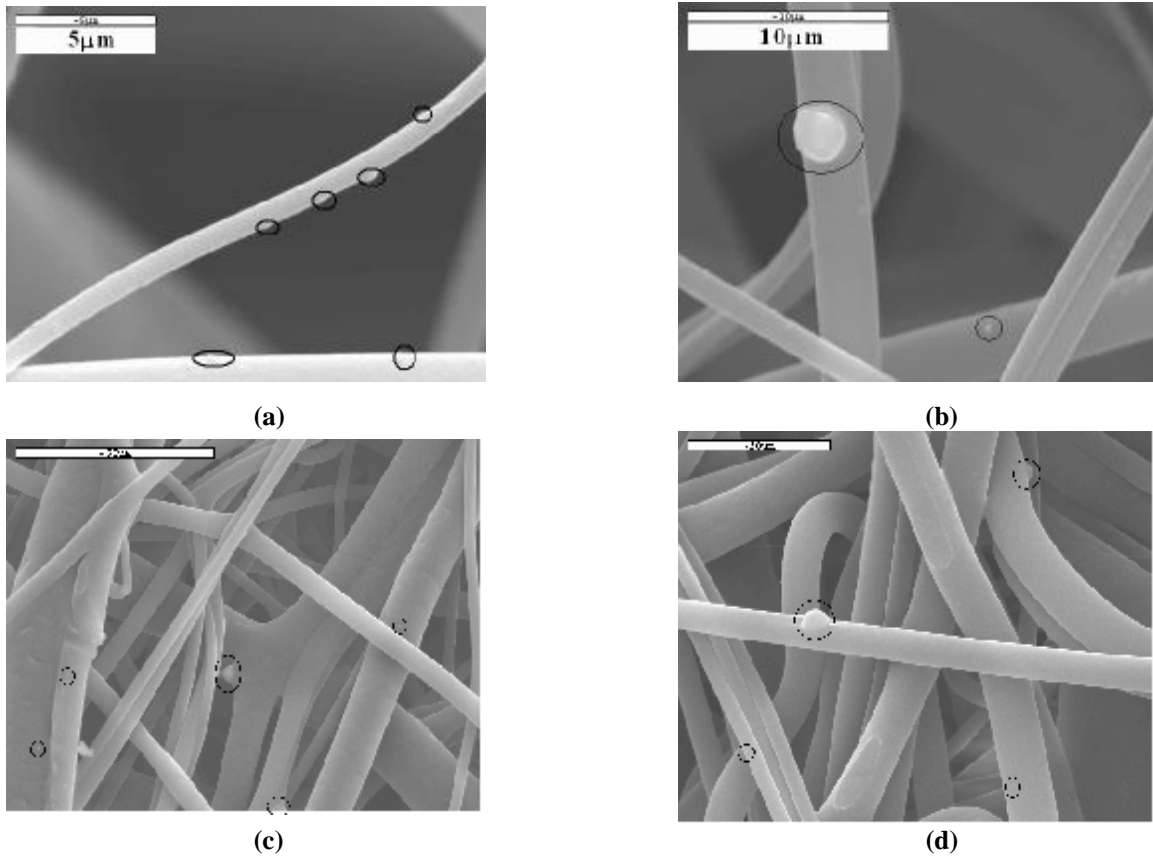


Figure 5.24 SEM micrographs of (a)–(b) bicomponent sample B6; (c)–(d) Bicomponent side-by-side sample B8 at various magnifications.

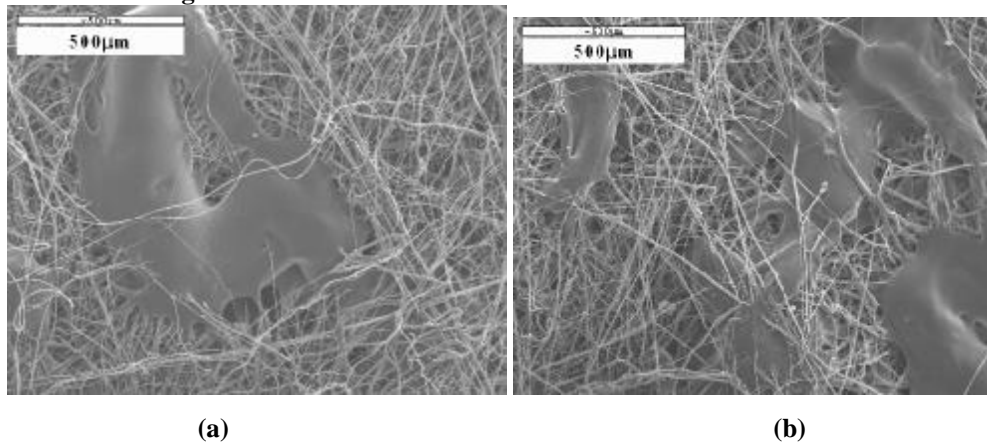


Figure 5.25 (a)–(b) SEM micrographs of sample bicomponent side-by-side sample, B16 showing drips.

Like sheath-core and side-by-side samples, B1-B20, characterization of the samples, BC1-BC5, was also done by procedures mentioned in **section 4.4.5**. Since percent particle loading for the samples was still less than 1wt%, optical micrographs obtained could not be analyzed effectively using image analysis. Some of the optical micrographs obtained are shown in **Figure 5.26**.

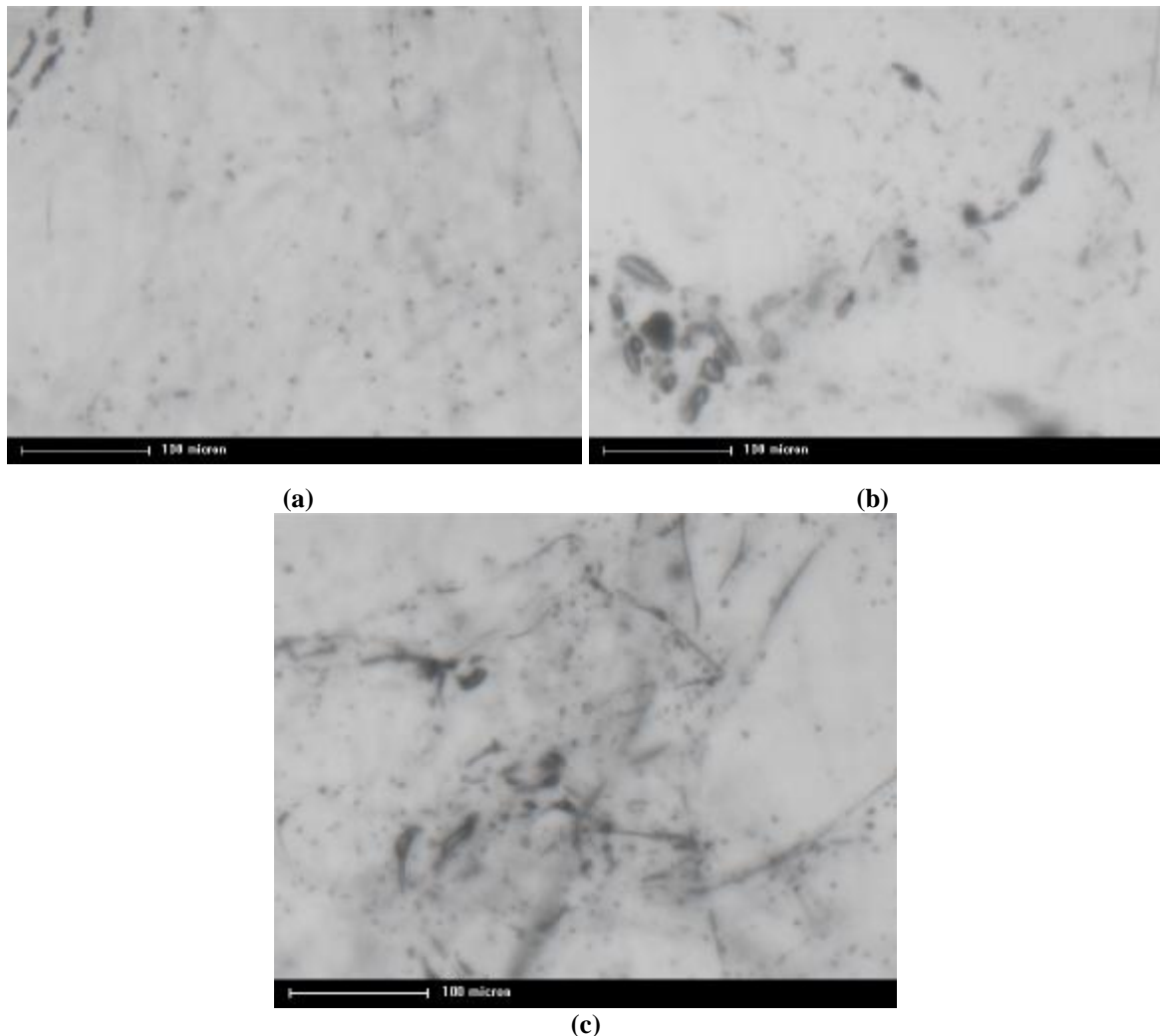


Figure 5.26 Optical micrographs at 10X in refractive index solution a) BC3; b) BC4; c) BC5.

As discussed earlier for bicomponent samples, B1-B20 optical micrographs of biconstituent samples, BC1-BC5, also shows presence of voids in fiber bulk. SEM micrographs, **Figure 5.27(a)-(d)**, shows presence of very few particles on the fiber surface, implying that either they are present in the fiber bulk or have been filtered out or were

deposited somewhere in the melt flow passage in the die forming agglomerates and eventually causing spinning failure.

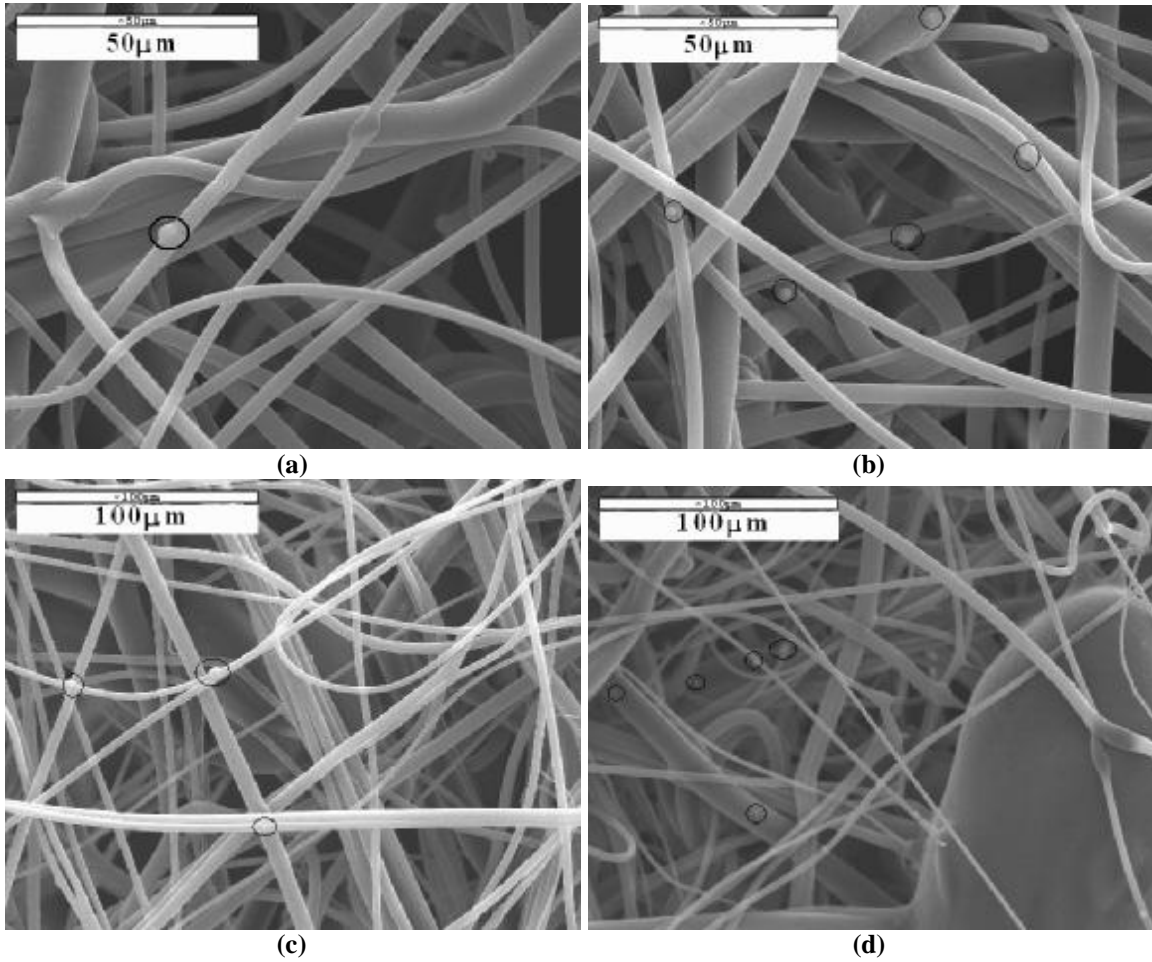


Figure 5.27 SEM micrographs of biconstituent samples (a) BC3 (0.2%); (b) BC4 (0.4%); (c) BC5 (0.7%); (d) BC6 (1.0%).

6 CONCLUSIONS

An integrated set up to incorporate TiO₂ particles in the fiber stream at the die exit in meltblowing has been developed. It has been demonstrated that high particle coating of meltblown fibers with sufficient uniformity can be achieved by spraying charged and heated particles at very low carrying air velocities. It is necessary to spray particles in close proximity to the die. When sprayed at a point farther than 2 inches, amount of TiO₂ particles adhering to the fiber surface decreases. It might be due to the fact that the temperature of fiber surface decreases rapidly with increase in distance from die exit and hence, fibers don't remain tacky to ensure enough particle penetration into soft fiber surface leading to their loss in environment. Also high carrying air pressure of up to 0.8 bars with spraying heights of less than 6cm should be used for the current system to have high particle loading.

It has also been observed that the Ultraviolet Protection Factor (UPF) values of samples made by all the setups is directly proportional to % TiO₂ loading. Samples with high UPF values can be made by the electrostatic spray setup. The UPF value as well as % Blocking for both UV-A and UV-B can be improved significantly by layering the webs into 2 or 4-layered structures.

Spinning of particle filled polymer melt could be used as a potential method for fiber surface modification and to make functional nonwoven webs in a single step. Die geometry, particle size and distribution of particles in polymer melt are critical parameters and govern the spinning behavior percent of the compound.

Regions of high shear in meltblowing die (i.e. bents in polymer melt flow) act as dead points for accumulation of particles. These particles eventually accumulate in small channels between parallel plates of the meltblowing die leading to spinning failure. It has been observed that maximum amount of TiO₂ loading for parallel plate geometry is achieved for configurations with minimum number of high shear regions in the die. TiO₂ particle size distribution is critical in achieving high particle loading in fiber webs. This conclusion is further supported by the observation from another set of experiments not mentioned earlier in the results, that an increase of over 5wt% from ~1wt% particle loading was achieved by lowering the TiO₂ particle size from 4 – 6 μm to 100 – 200 nm.

Amount of particle present in polymer melt affects their rheological and crystallization behavior. Presence of TiO₂ in polypropylene significantly increases its viscosity but doesn't

alter its shear thinning behavior. Also presence of TiO₂ particles in polymer melt decreases the %crystallization of polymer as concluded by significant decrease in heat of crystallization for cooling curve. Similar trends were not observed in meltblown fibers at various loadings. This may be due to low percent TiO₂ loadings in the fibers (<1wt%).

Presence of TiO₂ particles significantly improves the thermal decomposition behavior of the web. An increase of 27⁰C for 0.1wt% loading in sheath core fiber configuration; more than 100⁰C increase for 0.3wt% loading for side-by-side fiber configuration; ~32⁰C increase for loading from 0.2wt% to 0.7wt% for biconstituent web configuration was observed. Thus, increase in thermal decomposition temperature is dependent on % TiO₂ loading as well as fiber configuration.

Further studies need to be done to find out the possible cause of spinning failure at low loadings. Some of the reasons could be formation of large agglomerates leading to formation of large shots and discontinuity in polymer melt flow. The presence of air pockets or voids in fibers with increase in % TiO₂ loading may be due to formation of some volatile materials during spinning. Gaseous substance could have been formed either by thermal degradation of the polypropylene. Increase in bubble formation with increase in TiO₂ loading supports the conclusion that the presence of TiO₂ enhances the formation of gaseous substance. Further investigation is necessary to explain this observation.

7 REFERENCES

- [1] Igor L., (2004) “Ultrahydrophobic Fibers: Lotus Approach”, National Textile Center Annual Report: November, NTC Project: C04-CL06.
- [2] Wang R., Hashimoto K., Fujishima A., (1997) “Light Induced Amphiphilic Surfaces”, *Nature*, **388**, 431-432.
- [3] Braun, D., (1976) United States Patent: 3,971,373, by Minnesota Mining and Manufacturing Company.
- [4] Brooker R. et al., (1989) United States Patent: 4,797,318 by Kimberly-Clark Corporation.
- [5] Riddell et. al, (2002) United States Patent : 6,494,974 by Kimberly-Clark Corporation.
- [6] Cohen B. et. al., (2001) United States Patent : 6,294,222 by Kimberly-Clark Corporation.
- [7] MacLeod, R.B., Mandeville, P.J, (1985) United States Patent: 4,558,537.
- [8] Nakao and Etsuro, (1986) United States Patent: 4,592,815, “Method of manufacturing an electret filter” by Japan Vilene Company Ltd.
- [9] Tatsuo N. et. al., (2005) United States Patent : 6,863,921 B2 by Japan Vilene Company Ltd.
- [10] J.F. Hughes, (1984) “Electrostatic Powder Coating”, Wiley.
- [11] Connor L. A., Maddern P., (1994) United States Patent : 5,366,786 by Kimberly-Clark Corporation.
- [12] McAmish, et. al., (1986) United States Patent : 4,622,259 by Surgikos Inc.
- [13] Currie, K.J.G., Mogel, P.J., (1995) United States Patent : 5,429,854 by Kimberly-Clark Corporation.
- [14] McCulloch, J.W. (2001), “New Opportunities for Bicomponent Meltblown Technology”, *Nonwovens World*, Oct-Nov, 108-115.
- [15] Han C.D., (1973) “A Study of Bicomponent Coextrusion of Molten Polymers”, *J. of App. P. Sc.*, 17, 1289-1303
- [16] Lokamp, D., (1972) United States Patent: 3,841,953.

- [17] Buntin R. and Lohkamp D., (1976) "A one step process for New Nonwovens Products." TAPPI, April, 56:4.
- [18] Bucchsel, A. et al., (2000) "On both sides abrasive single layer meltblown nonwoven cleanup purposes in consumer and industrial applications," 10th annual TANDEC conference, section 3.6.
- [19] Thomas H., Kingsport T., (1971) United States Patent: 3,601,846 by Eastman Kodak Company.
- [20] Krueger, D.L. Dyrud, J.F., (1998) United States Patent: 4,729,371 by Minnesota Mining and Manufacturing Co.
- [21] Berger, R.M., (2000) United States Patent : 6,103,181 by Filtrona Int. Ltd.
- [22] Han C.D., (1974) J. of App. Poly. Sc., 18, 821.
- [23] Jancer J., (1999), Advance in Polymer Science, Springer 67-108, 155-218
- [24] Yeo S.Y and Jeong S.H.(2003) , "Preparation and characterization of polypropylene /silver nanocomposite fibers", Polymer International, 53, 1053-1057.
- [25] Minagawa N. and White J.L., (1976) " The influence of Titanium Dioxide on the Rheological and Extrusion Properties of Polymer Melts", J. of App. Poly. Sc., 20, 501-523.
- [26] Minagawa N. and White J.L., (1975) "Co-Extrusion of Unfilled and TiO₂-Filled Polyethylene: influence of Viscosity and Die Cross-Section on Interface Shape", Poly. Eng. and Sc., Dec., 15:12, 825-830.
- [27] Bond W. B., (1986) United States Patent : 4,610,925 by E. I. Du Pont de Nemours and Co.
- [28] Ghosh K. and Maiti S.N., (1997) "Melt Rheology of Silver-powder-filled polypropylene composites", Poly. Plastic Tech. and Eng., 36:5, 703-722.
- [29] Lin L. and Toshiro M., (1990) "Effect of Dispersion of Particles on Visco-elasticity of CaCO₃ filled Polypropylene Melts", Poly. Eng. and Sc., 30:14, 841-847.
- [30] Hornsby P.R., (1999) " Rheology, Compounding and Processing of Filled Thermoplastics", Springer, 155-218.
- [31] Sang Y.Y. and Sung H. J., (2003) "Preparation and characterization of polypropylene/silver nanocomposite fibers", Poly. Int., 52, 1053–1057.

- [32] Liu C.H. and Lai P.L., (2004) "The development of Nano Zinc Oxide Polyester fiber", *The Journal of China Textile Institute*, 14:3, 217-221.
- [33] Zhang et.al., (2002) "The effect of elastomeric nano-particles on the mechanical properties and crystallization behavior of polypropylene" , *Polymer*, 43:19, 5133–5138.
- [34] Chiu C. W., (2004) "Spinning and Elongational Flow Behavior of Nanoscale TiO₂/PP Fibers", e-thesis, Feng Chia University, China.
- [35] Rochow, T.G. and Tucker, P.A. (1994), "Introduction to Microscopy by means of light, electrons, X-ray or acoustics", Plenum Press, 2nd edition, 23-24, 297-299.
- [36] Dong G.S., Tae J.K., Jae R. Y., (2005), "Rheological characterization of polymer-based nanocomposites with different nanoscale dispersions" *e-Polymers*, 5, ISSN 1618-7229, <http://www.e-polymers.org> (10/10/05), 1-14.
- [37] AATCC-Test Method 183, (2004) "Transmittance or Blocking of Erythemally Weighted Ultraviolet Radiation through Fabrics".
- [38] Curikis J., and Palithrope M., (1996) "Apparel Textiles and Sun Protection", *Textile Magazine* 4, 13-17.
- [39] Rusu M., Sofian N., Rusu D., (2001) "Mechanical and thermal properties of zinc powder filled high-density polyethylene composites", *Material Properties-Polymer Testing* 20, 409–417.
- [40] Hsu S., Chou C.W., Tseng S.M., (2004) "Enhanced Thermal and Mechanical Properties in Polyurethane/Au Nanocomposites", *Macromol. Mater. Eng.* 289, 1096–1101.
- [41] Luyt A.S., Molefi, J.A., Krump, H., (2005) "Thermal, mechanical and electrical properties of copper powder filled low-density and linear low-density polyethylene composites" *Polymer Degradation and Stability*, 1-8
- [42] Chang-Fang O., (2003) "Crystallization Behavior and Thermal Stability of Poly(trimethylene terephthalate)/Clay Nanocomposites", *Journal of Polymer Science: Part B: Polymer Physics*, 41, 2902–2910.
- [43] http://www.sunocochem.com/products/data_sheets/Polypropylene.asp (04/05/2005)
- [44] Fujishima A., Rao T.N., Tryk D.A., (2000) "Titanium Dioxide photocatalysis", *J. of Photochemistry and Photobiology C: Photochemistry Reviews* 1, 1-21.
- [45] Bozzi A., Yuranova T., Kiwi J., (2005) "Self-cleaning of wool-polyamide and polyester textiles by TiO₂-rutile modification under daylight irradiation at ambient temperature", *Journal of Photochemistry and Photobiology A: Chemistry* 172, 27–34.

- [46] Beringer J., Hofer D., (2004) "Nanotechnology and its application", Milland English, September, E107.
- [47] Leodidou T.K., Margraf P., Caseri W., Suter U.W., Walther P., (1997) "Polymer sheets with a thin nanocomposite layer acting as a UV filter", *Polymer for Advanced Technologies* 8:8, 505-512.
- [48] Parkin I.P., Palgrave R.G., (2005) "Self-Cleaning coatings", *J. of Material Chemistry*, 15, 1689-1695
- [49] Reneker D.H., (2005), United States Patent, 6,695,992, "Process and apparatus for the production of nanofibers", University of Akron.
- [50] Editorial, (2005) "New purity" , *Nonwovens Report International*, p92-93.
- [51] Editorial (2005) "Clean future", *Future Materials*, Mar/Apr. 2, 14-15.
- [52] Editorial (2005) "In Brief" *Nonwovens Markets*, 20:2, 2.
- [53] Editorial (2004) "Clearcoat in nonwovens", *Future Materials*, Jul/Aug, 4, 26-26
- [54] Blossey R., (2003) "Self-cleaning Surfaces-virtual realities", *Nature Materials*, 2, May, 301-306]
- [55] Benedix R., Dehn F., Quaas J., Orgass M., (2000) "Application of Titanium Dioxide Photocatalysis to Create Self-Cleaning Building Materials" *Lacer*, 5, 152-168.
- [56] "Nanophase Technologies Corp., (07/11/05) <http://www.nanophase.com>
- [57] Ajayan P.M., Schadler, Buran P.V., (2003) "Nanocomposite Science and Technology", Wiley –VCH, 77-144
- [58] Iskandar Lenggoro, Xia & Okuyama, (2001) "Spherical particle derived from colloidal nanoparticles", *Journal of Nanoparticle Research*, 3:4, 263-270.
- [59] Kearns J.C. and Shambaugh R.L., (2002) "Polypropylene Fibers Reinforced with Carbon Nanotubes", *Journal of Applied Polymer Science*, 86, 2079-2084.
- [60] Blumstein, A., (1965), *Journal of Polymer Science, Part A: Polymer Chemical*, 3, 2665.
- [61] Kojimoto Y.; Usuki A; Kawasumi M; Okada A.; Kuraucki T.; Kamigiato O., (1993) *Journal of Applied Polymer Science*, 49, 1259
- [62] Messersmith P.B.; Giannelis E.P., (1994) *Chemical Materials*, 6, 1719.

- [63] Vysotskii V.V, Pryamova T.D., Roldugin V.I., Shamurina M.V., (1995) “Percolation transition and conductivity mechanisms in metal-filled polymer”, *Kolloidnyi Zhurnal*, Sept-Oct, 649-654.
- [64] Sandler J.K.W., Kirk J.E., Kinloch I.A., Shaffer M.S.P., Windle A.H., “Ultra-low electrical percolation threshold in carbon-nanotube-epoxy composites”, *Polymer*, 44, 5893–5899.
- [65] Catone, D.L., (2004) “Nano-particle additives for PET”, *Chemical Fiber International*, 54, 25-26.
- [66] Kyung W.O., Seong H.K., Eun A.K., (2001) “Improved surface characteristics and the conductivity of polyaniline-nylon 6 fabrics by plasma treatment”, *Journal of Applied Polymer Science*, 81:3, 684 – 694.
- [67] Kim J., Satoh M. Iwasaki T., (2003) “Mechanical-dry coating of wax onto copper powder by ball milling”, *Materials Science and Engineering: A*, 342:1, 258-263.
- [68] Iwasaki T, Satoh M., Ito T., (2004) “Coating of soft metal particles with ceramic fines using a dry mechanical method.”, *Journal of Materials Processing Technology*, 146:3, 330-337.
- [69] Nowarat C., Chang Y., (2003) “Surface modification of Al₂O₃ fiber with binary nanoparticles using a dry-mechanical coating technique.”, *Journal of Nanoparticle Research*, 5, 247–258.
- [70] Huykman W., (1991) United States Patent : 5,066,538, “Nonwoven insulating webs” by Ultrafiber Inc.
- [71] Cohen B., (1994) United States Patent : 5,316,837 “Stretchable metallized nonwoven web of non-elastomeric thermoplastic polymer fibers and process to make the same.” By Kimberlay Clark Inc..
- [72] Cohen B., (1997) United States Patent: 5,656,355 “Multilayer elastic metallized material” by Kimberlay Clark Inc.
- [73] Heikinheimo L; Cavaco P.A., Nousiainen P., Siika-aho M., (1998) “Treatment of cotton fabrics with purified *Trichoderma reesei* cellulases”, *Journal of the Society of Dyers and Colorists*, 114:7/8, 216-220.
- [74] Cai Z., Jiang G., Yang S., (2001) “Chemical finishing of silk fabric”, *Coloration Technology*, 117:3, 161-165.
- [75] Chang C.M., Wu J., Li J.X., Cheung Y.K., (2002) “Polypropylene/Calcium carbonate nanocomposites”, *Polymer*, 4, 2981-2992.

- [76] Wu D., Wang X., Song Y., Jin R., (2004) "Nanocomposites of Poly(vinyl chloride) and Naometric Calcium Carbonate Particles: Effect of Chlorinated Polyethylene on Mechanical Properties, morphology, and Rheology", *Journal of Applied Polymer Science*, 92, 2714-2723.
- [77] Suwanprateeb J., (2000) "Calcium carbonate filled polyethylene: correlation of hardness and yield stress", *Composites Part A: Applied Science and Manufacturing (Incorporating Composites and Composites Manufacturing)*, 31:4, 353-359.
- [78] Ash B.J., Stone J., Rogers D.F., Schandler L.S., Siegel B.C., Benicewicz T., (2000) *Material Research Society Symposium Proc.* 661.
- [79] Mlynarc'kova Z., Borsig E., Lege'n J., Marcinic A., Alexy P., (2005) "Influence of Composition of Polypropylene/Organoclay Nanocomposite Fibers on their Tensile Strength" *Journal of Macromolecular Science, Part A: pure and applied Chemistry*, 42, 543-554.

APPENDIX A : Processing conditions of various samples

Table A1: Processing conditions of samples made by various setups, initial setup, modified setup and final setup.

			Meltblowing Conditions								Gun				Calender		Web		
	Polymer / Particle Type	Sample No.	Zone1	Zone2	Zone3	Flange	Die	Air Hose	Screw RPM	Air Press	Fluid Press	Gun Press	Charging Volt (kV)	Spray Distance	Spray Angle	Temperature	Pressure	GSM	% loading (by weight)
			F	F	F	F	F	F	# of rev	psi	psi	bar	kV	cm	Degree	C	lb/liner inch		
Initial Setup	PP / Al2O3	A20 PW-L 1L I	280	300	320	340	482	557	N.A.	N.A.	65-70	0.2	30	10	90	110	16	30-140	10-12
	PP / Al2O3	A40 PW-H 1L I	280	300	320	340	482	557	N.A.	N.A.	65-70	0.4	30	10	90	110	16	60-150	40-42
Modified Setup	PP / TiO2	M1-2L	280	300	320	340	468	543	150	30	85	0.27	30	5	45	105	25	50	32
	PP / TiO2	M1-4L	280	300	320	340	468	543	150	30	85	0.27	30	5	45	105	25	85	32
	PP / TiO2	M2-2L	280	300	320	340	470	548	200	35	85	0.27	30	5	45	105	25	54	28
	PP / TiO2	M2-4L	280	300	320	340	470	548	200	35	85	0.27	30	5	45	105	25	107	28
	PP / TiO2	M3-2L	280	300	320	340	474	552	250	35	85	0.27	30	5	45	105	25	66	40
	PP / TiO2	M3-4L	280	300	320	340	474	552	250	35	85	0.27	30	5	45	105	25	113	40
	PP / TiO2	M4-2L	280	300	320	340	480	557	300	40	85	0.27	30	5	45	105	25	61	25
	PP / TiO2	M4-2L	280	300	320	340	480	557	300	40	85	0.27	30	5	45	105	25	125	25
	PP / TiO2	M5-2L	280	300	320	340	482	557	350	55	85	0.27	30	5	45	105	25	61	45
Final Setup	PP / TiO2	M6	280	300	320	340	425	425	250	55	80	0.2	40	2	90	50	64	40	9.8
	PP / TiO2	M7	280	300	320	340	425	425	250	55	80	0.4	40	2	90	50	64	40	11.2
	PP / TiO2	M8	280	300	320	340	425	425	250	55	80	0.6	40	2	90	50	64	51	40.8
	PP / TiO2	M9	280	300	320	340	425	425	250	55	80	0.8	40	2	90	50	64	70	94.3

Table A2: List of bi-component webs prepared in various trials

	Sample No.	Polymer Type		Component Ratio		Loading % by weight	
		Side A	Side B	Side A	Side B	in side B	in fiber
				Pure PP	PP+TiO2	%	%
Core / Sheath	B1	Pure PP	Pure PP	50(Core)	50(Sheath)	0.0	0
	B2	Pure PP	PP (2.0%)	75(Core)	25(Sheath)	0.4	0.10
Side – by – Side	B3	Pure PP	Pure PP	75	25	0.0	0
	B4	Pure PP	PP (2.0%)	75	25	0.4	0.10
	B5	Pure PP	PP (2.0%)	60	40	0.4	0.16
	B6	Pure PP	PP (2.0%)	50	50	0.4	0.20
	B7	Pure PP	PP (2.0%)	40	60	0.4	0.24
	B8	Pure PP	PP (2.0%)	25	75	0.4	0.30
	B9	Pure PP	PP (0.5%)	75	25	0.1	0.025
	B10	Pure PP	PP (0.5%)	60	40	0.1	0.040
	B11	Pure PP	PP (0.5%)	50	50	0.1	0.050
	B12	Pure PP	PP (0.5%)	40	60	0.1	0.060
	B13	Pure PP	PP (0.5%)	25	75	0.1	0.075
	B14	Pure PP	PP (5.0%)	75	25	1.0	0.25
	B15	Pure PP	PP (5.0%)	50	50	1.0	0.50
	B16	Pure PP	PP (5.0%)	25	75	1.0	0.75
	B17	Pure PP	PP (10%)	75	25	2.0	0.50
	B18	Pure PP	PP (10%)	90	10	2.0	0.20
	B19	Pure PP	PP (20%)	90	10	4.0	0.40
	B20	Pure PP	PP (20%)	90	10	4.0	0.40

Note: 1. Sample #1 and #2 are sheath/core structures while #3 - #20 are side/side bicomponent structures.

2. Pure PP (1200MFR) refers to the pure homopolymer polypropylene with 1200 Melt Flow Rate.
3. PP (2.0%), PP (0.5%), PP (10%) and PP (20%) refers to the batches prepared by diluting the compounded master batch with homo-polypropylene (1200MFR) to 2%, 0.5%, 5%, 10%, and 20% dilution ratio resp.
4. Sample # 20 has same loading ratios as #19 but is made at higher processing temperature.
5. Loading % in side B = % TiO₂ loading in polymer * dilution ratio
(e.g. in sample # 4 : loading % in side B = 20% * 2.0% = 0.4%)
6. Loading % in fiber = % TiO₂ loading in Side B * side ratio
(e.g. in sample # 4 : loading % in fiber = 0.4% * 0.25 = 0.1%)

Table A3: List of bi-constituent webs prepared in various trials

	Polymer		Component Ratio		Absolute Loading %		
	Side A	Side B	Side A	Side B	Side A	Side B	Web
BC1¹	PP (0.0%)	PP (0.0%)	50	50	0.0	0.0	0.0
BC2¹	PP (0.0%)	PP (0.0%)	75	25	0.0	0.0	0.0
BC3¹	PP (0.0%)	PP (2.0%)	50	50	0.0	0.4	0.2
BC4¹	PP (2.0%)	PP (2.0%)	50	50	0.4	0.4	0.4
BC5¹	PP (2.0%)	PP (5.0%)	50	50	0.4	1.0	0.7
BC6²	PP (5.0%)	PP (5.0%)	50	50	1.0	1.0	1.0
BC7²	PP (0.0%)	PP (5.0%)	50	50	0.0	1.0	0.5
BC8³	PP (0.0%)	PP (5.0%)	50	50	0.0	1.0	0.5

- Note : 1. BC1-BC5 were made at thru-put of 0.25 gms/hole/min.
2. BC6-BC7 were made at thru-put of 0.40 gms/hole/min.
3. BC8 was made at thru-put of 0.5 gms/hole/min.

APPENDIX B : Summary Tables of Characterization

Table B1.1: Summary of viscosity vs. shear rate at 200^oC for TiO₂ loaded polypropylene system

Loading % (by wt)	Screw rpm		
	120	160	200
0%	6.65	7.33	5.97
5%	9.9	9.77	8.95
10%	14.9	13.4	11.9
15%	18.1	15.9	13.9
20%	32	29.2	23.1

Table B1.2: Viscosity of homo-polypropylene and compounded masterbatch at 20wt% loading

(190 ^o C)				(210 ^o C)				(230 ^o C)			
(PP)		(PP/TiO ₂)		(PP)		(PP/TiO ₂)		(PP)		(PP/TiO ₂)	
Shear Rate	0	Shear Rate	0	Shear Rate	0	Shear Rate	0	Shear Rate	0	Shear Rate	0
2.78	13.14	1.29	105.07	1.00	7.59	1.00	46.55	1.00	7.09	1.00	20.64
3.59	12.48	1.67	102.18	1.47	7.45	1.47	49.62	1.47	6.94	1.47	21.36
4.64	12.27	2.15	94.96	2.15	7.41	2.15	49.86	2.15	6.88	2.15	21.68
5.99	12.12	2.78	89.12	3.16	7.26	3.16	51.00	3.16	6.67	3.16	21.70
7.74	12.08	3.59	82.20	4.64	7.23	4.64	50.29	4.64	6.55	4.64	21.85
10.00	11.92	4.64	72.82	6.81	7.15	6.81	48.15	6.81	6.38	6.81	21.35
12.92	11.59	5.99	66.74	10.00	7.10	10.00	43.60	10.00	6.24	10.00	19.19
16.68	10.42	7.74	58.29	14.68	6.99	14.68	38.60	14.68	6.00	14.68	16.18
21.54	9.63	10.00	49.24	21.54	6.89	21.54	31.77	21.54	5.62		
27.83	8.63	12.92	42.01	31.62	6.76			31.62	5.04		
35.94	8.23			46.42	6.51			46.42	5.05		
46.42	8.29			68.13	6.32			68.13	4.68		
59.95	7.91			100.00	5.84			100.00	4.63		
77.43	7.10			146.78	5.31			146.78	4.00		
100.00	6.40			215.44	4.74			215.44	3.64		
129.15	5.92										

Table B2: Summary of decomposition temperature of bicomponent samples B1 – B15

	Sample #	Loading %	Decomposition Temperature
		(by wt.)	^o C
Sheath – Core	B1	0.00 %	398.2
	B2	0.10 %	425.6
Side – by -Side	B3	0.00 %	371.6
	B4	0.10 %	394.9
	B5	0.16 %	418.0
	B6	0.20 %	452.1
	B7	0.24 %	474.5
	B8	0.30 %	484.8
	B9	0.03 %	411.1
	B10	0.04 %	416.2
	B11	0.05 %	416.0
	B12	0.06 %	418.8
	B13	0.08 %	416.4
	B14	0.25 %	481.4
	B15	0.50 %	484.0

Table B3: Summary of thermal decomposition temperatures of biconstituent samples BC3 – BC5

Sample #	Loading %	Decomposition Temperature (^o C)
BC3	0.2%	461.43
BC4	0.4%	480.98
BC5	0.7%	493.24

Table B4: Summary of results H_f , onset values for bicomponent samples, B1 – B15

	Sample #	H_f		Onset		Peak	
		Heating (J/g)	Cooling (J/g)	Heating ($^{\circ}$ C)	Cooling ($^{\circ}$ C)	Heating ($^{\circ}$ C)	Cooling ($^{\circ}$ C)
		+/-3.0	+/-3.0	+/-0.5	+/-0.3	+/-0.5	+/-0.3
Sheath – Core	B1	92.8	-98.2	152.2	118.9	163.2	114.9
	B2	96.2	-99.7	151.3	119.2	162.7	114.5
Side – by – Side	B3	95.7	-98.6	150.3	120.3	162.1	114.7
	B4	87.3	-94.9	150.9	119.9	162.4	115.2
	B5	91.3	-96.5	150.5	119.7	162.1	114.9
	B6	91.9	-96.1	151.3	119.6	162.2	115.1
	B7	92.9	-95.6	151.4	119.6	162.2	115.1
	B8	92.1	-96.3	150	119.9	162.7	115.3
	B9	91.3	-94.6	150.7	119.6	162.2	115.0
	B10	93.7	-96.6	150.5	119.4	162.2	114.8
	B11	96.1	-97.6	151.2	119.4	162.0	114.5
	B12	95.1	-97.9	150.8	119.4	162.3	114.7
	B13	96.3	-97.8	150.5	119.3	162.6	114.3
	B14	92.9	-96.1	150.6	119.7	162.3	114.8
	B15	89.7	-93.5	149.9	119.3	162.4	114.7

Table B5: Summary of results H_f , onset and peak temperatures for biconstituent samples, BC1 – BC5.

Sample #	H_f		Onset		Peak	
	Heating (J/g)	Cooling (J/g)	Heating ($^{\circ}$ C)	Cooling ($^{\circ}$ C)	Heating ($^{\circ}$ C)	Cooling ($^{\circ}$ C)
	+/-3.0	+/-3.0	+/-0.5	+/-0.3	+/-0.5	+/-0.3
BC1	100.91	-101.85	150.41	118.67	162.45	113.59
BC3	98.87	-98.49	151.49	119.15	161.50	114.41
BC4	96.89	-98.29	150.80	119.41	162.88	114.81
BC5	92.55	-97.34	150.62	119.51	162.18	115.00

Table B6: Summary of strip test (ASTM D5035-95) for bicomponent samples B1 – B14

	Sample #	Load (N/m)		Strain (%)		Secant Modulus @ 10% (kPa) (+/- 2.5)
		Avg.	Dev.	Avg.	St. Dev./2	
Sheath – Core	B1	285.6	12.8	187	14.4	32.5
	B2	276.2	11.7	122	11.2	37.0
Side – by – Side	B3	249.3	10.6	205	25.8	29.5
	B4	284.6	16.2	181	24.3	35.5
	B5	263.0	6.3	166	27.1	32.5
	B6	238.2	11.0	176	27.3	30.5
	B7	231.0	12.1	158	15.5	26.0
	B8	230.0	9.9	92	16.6	28.0
	B9	302.5	16.8	204	29.8	35.5
	B10	288.6	21.1	165	30.6	34.0
	B11	258.8	13.6	221	24.7	28.0
	B12	268.3	5.6	200	47.5	32.0
	B13	265.0	7.8	202	26.1	30.0
	B14	204.7	11.4	82	7.5	26.5

Table B7: Summary of strip test (ASTM D5035-95) for biconstituent samples BC1 – BC5

Sample #	Load (N)		Strain (%)		Secant Modulus @ 10% (kPa) (+/- 2.5)
	Average	Dev./2	Average	St.Dev./2	
BC1	180.7	14.6	104	11.9	44.50
BC3	166.6	7.1	82	9.5	43.00
BC4	125.8	8.8	56	6.9	33.50
BC5	97.4	7.9	38	4.5	28.50

Table B8: Summary of bending test (ASTMD5732) for Bicomponent Samples B1-B14

	Sample #	Bending Length, c		Flex Rig
		(cm)	St.Dev./2	Newton.m
Sheath – Core	B1	4.58	0.10	6473168.64
	B2	3.90	0.10	6663723.97
Side – by – Side	B3	4.40	0.10	5880396.12
	B4	4.58	0.19	5707454.54
	B5	4.40	0.13	5537937.43
	B6	4.12	0.35	4468524.09
	B7	4.13	0.10	4915061.51
	B8	4.90	0.05	5822366.31
	B9	4.98	0.10	5577016.62
	B10	4.57	0.16	5317182.39
	B11	4.53	0.26	4919228.93
	B12	4.43	0.03	4919228.93
	B13	4.53	0.13	5155522.55
	B14	4.15	0.05	4415113.09

Table B9: Summary of bending test (ASTMD5732) for Biconstituent Samples BC1-BC5

Sample #	Bending Length, c		Flex Rig
	(cm)	St.Dev./2	Newton.m
BC1	3.82	0.16	6972347.62
BC3	3.40	0.22	7101461.92
BC4	2.99	0.17	5543027.84
BC5	2.46	0.11	6594413.35

Table B10: Summary of UV Transmission testing data for samples BC1-BC5 and BC1-2L – BC5-2L

Sample #	BC1	BC3	BC4	BC5	BC1-2L	BC3-2L	BC4-2L	BC5-2L
UPF	2.56	3.10	2.65	3.16	4.55	6.50	6.34	9.86
T(UV-A)	37.31	32.85	38.93	32.28	21.57	17.78	19.20	14.16
% Blocking UV-A	62.69	67.15	61.07	67.72	78.43	82.22	80.80	85.84
T(UV-B)	39.29	32.26	37.83	29.30	21.86	14.95	15.35	9.66
% Blocking UV-B	60.71	67.74	62.17	70.70	78.14	85.05	84.65	90.34

APPENDIX C : List of figures of setups used for samples fabrication

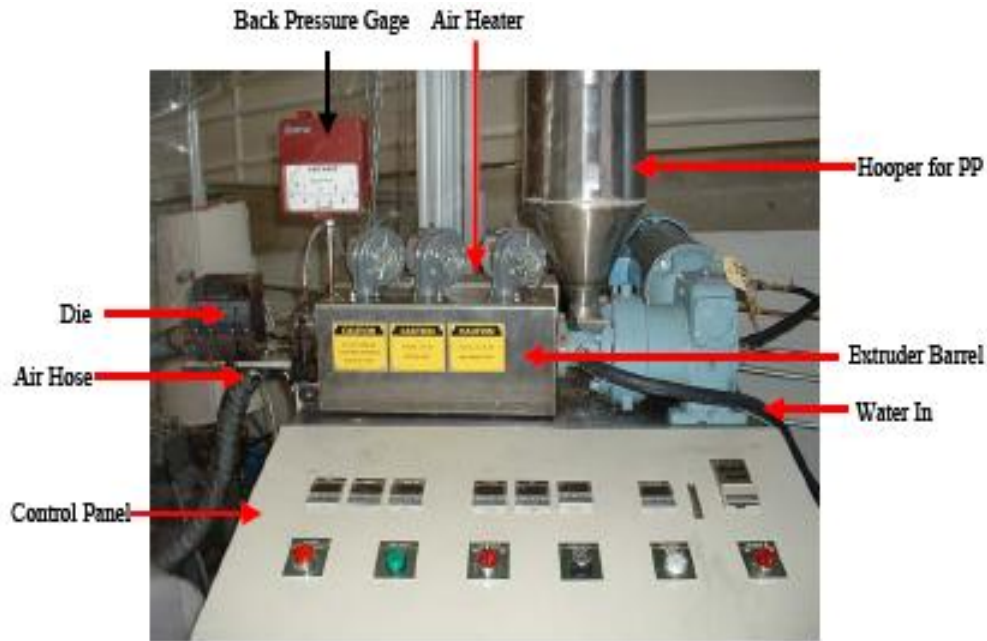


Figure C1: 3" laboratory scale meltblown setup

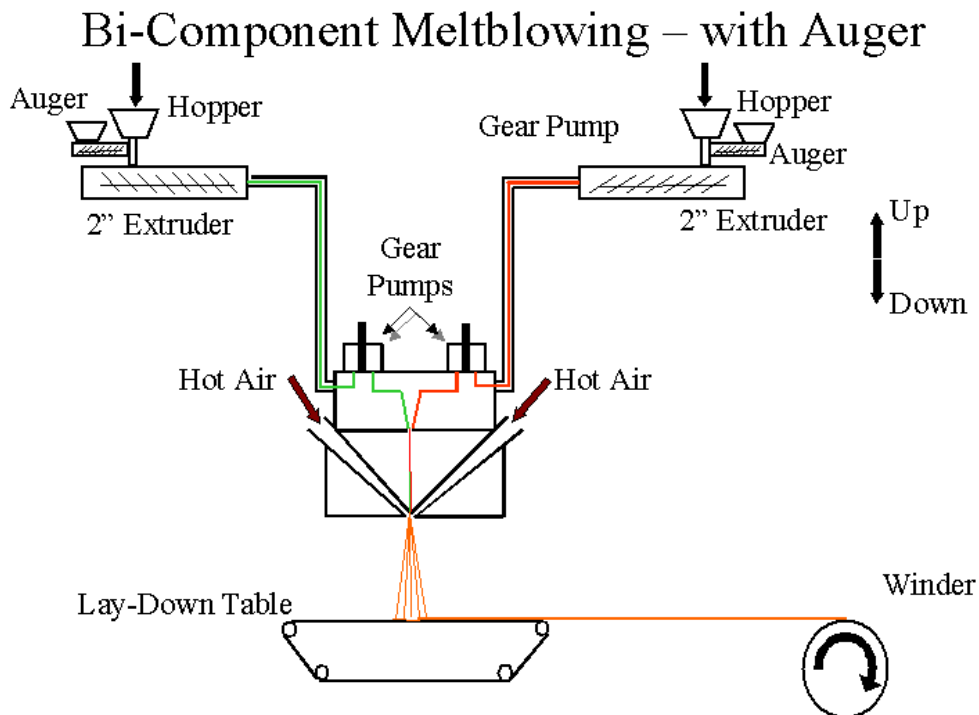


Figure C2: Schematic of bicomponent meltblown setup at NCRC Partner's Lab.

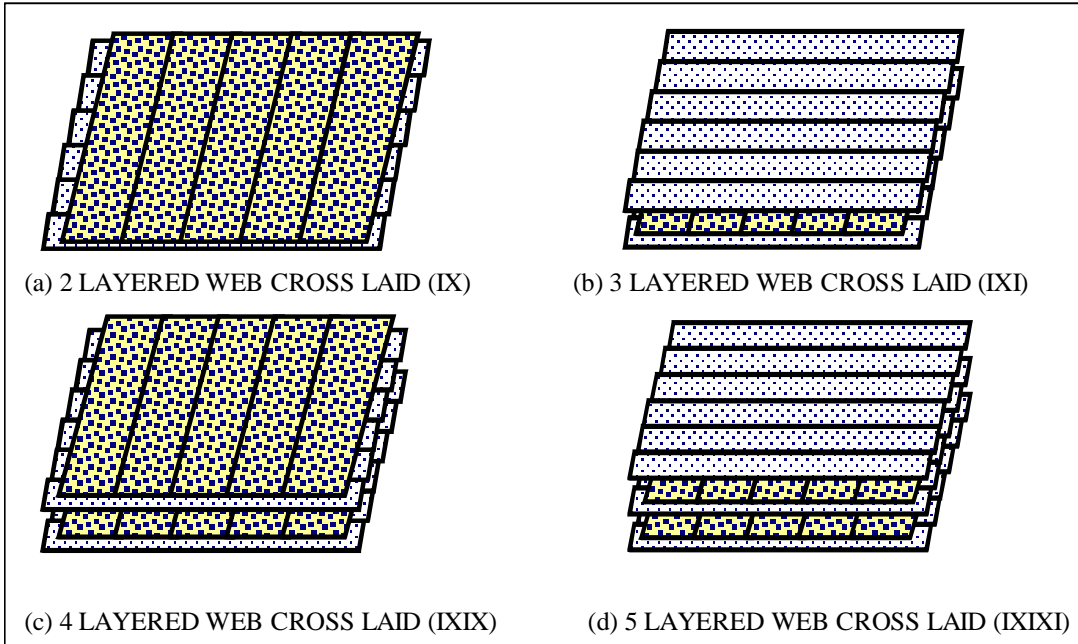


Figure C3: Cross laid web (IX) made by perpendicularly orienting particle loaded meltblown web by thermal point bonding.

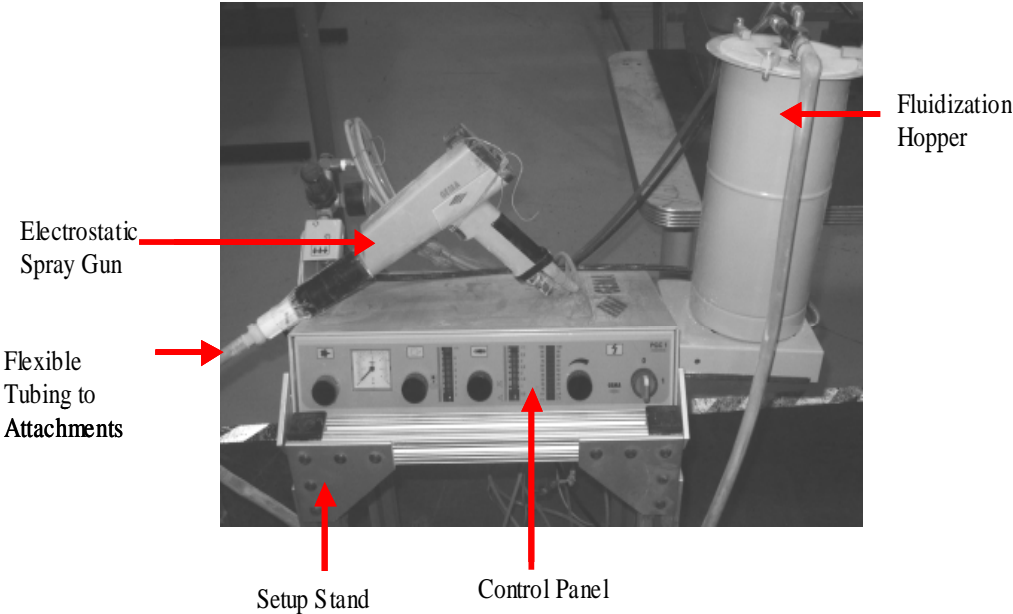


Figure C4: Electrostatic spray gun.